



CHALMERS
UNIVERSITY OF TECHNOLOGY



Characteristics of Fifth Wheel and its Influence on handling and maneuvering of Articulated Heavy vehicles

Master thesis

RISHABH NIGAM

Department of Mechanics and Maritime Sciences
CHALMERS UNIVERSITY OF TECHNOLOGY
Gothenburg, Sweden 2018

MASTER THESIS

Characteristics of Fifth Wheel and its Influence on
handling and maneuvering of Articulated Heavy vehicles

RISHABH NIGAM

Department of Mechanics and Maritime Sciences
Division of Vehicle Engineering and Autonomous Systems
CHALMERS UNIVERSITY OF TECHNOLOGY
Göteborg, Sweden 2018

Characteristics of Fifth Wheel and its Influence on handling and maneuvering of
Articulated Heavy vehicles

RISHABH NIGAM

© RISHABH NIGAM, 2018-01-01

Master's Thesis 2018:41
Department of Mechanics and Maritime Sciences
Division of Vehicle Engineering and Autonomous Systems
Chalmers University of Technology
SE-412 96 Göteborg
Sweden
Telephone: + 46 (0)31-772 1000

Supervisor:

Niklas Fröjd (Volvo GTT)
Toheed Ghandriz (Chalmers University)
Karel Kural (HAN University)

Examiner:

Bengt Jacobson (Chalmers University)
Karel Kural (HAN University)

Cover:

Experimental Setup for friction measurement on the dolly.

Chalmers Reproservice/ Department of Applied Mechanics
Göteborg, Sweden 2018-01-01

Characteristics of Fifth Wheel and its Influence on handling and maneuvering of Articulated Heavy vehicles

Master thesis

RISHABH NIGAM

Department of Mechanics and Maritime Sciences

Division of Vehicle Engineering and Autonomous Systems

Chalmers University of Technology

Abstract

Articulated vehicles have been the subject of study for long. The risks entailed with every mistake and accident involving these vehicles, dwarf any other mode of road transport. Since, articulated vehicles are used for transporting everything, or nearly everything on land, not only are they significant for economic concerns, they also impact human safety on the road. These risks escalate with the increasing vehicle length and amount of cargo carried.

Fifth-wheels are an important component of articulated vehicles. Their behaviour has been often simplified in the existing literature. In this study, a fifth-wheel model is developed to represent its influence on the vehicle behaviour. Tests are conducted to capture the interactions at the fifth-wheel under different conditions, commonly encountered during everyday driving. These test results are then analysed and a fifth-wheel model is proposed based on the observations. It is then validated and generalized in applicability using two different vehicle models replicating the test scenarios.

Furthermore, the proposed model is used to simulate the maneuvers commonly encountered and the behaviour is compared. It was observed that the articulation angle achieved during these maneuvers shows significant difference from their counterparts. This in turn effects the lateral acceleration of the vehicle combination, which can be seen in its overall trajectory during the maneuver.

Key words: Articulated Vehicles, Fifth-Wheel, Friction Model, Roll compliance

ACKNOWLEDGEMENTS

I would like to thank and acknowledge the contributions of Niklas Frojd, my supervisor at VGTT, Bengt Jacobson, Toheed Ghandriz, supervisors at Chalmers University, Karel Kural, supervisor at HAN University for their continuous support, patience, motivation, immense knowledge, and guidance during my thesis work.

I will be forever grateful to Niklas for clarifying my queries, even the frustratingly silly ones, and for providing me the opportunity to work in a stimulating environment at VGTT.

Thanks to my batchmates, Shammy, Aman, Nitesh, Rishabh, Sanjal, Santosh, Gokul, Ashrith for the helpful discussions and occasional distractions. Their support and encouragement during this whole journey was worth more than I can express on paper.

I dedicate this thesis to my parents, it will be a futile attempt to thank them for everything they have done, so I am not going to try.

My brother Puneet and his family for being my North Star. Yash, Rohan and Sarvesh for sticking by my side through good, bad and the ugly.

And finally, this work couldn't have been completed without the help of staff members at Chalmers, VGTT and HAN.

Gothenburg, May, 2018
Rishabh Nigam

Contents

Abstract.....	I
ACKNOWLEDGEMENTS.....	III
Contents.....	IV
1 Introduction.....	1
1.1 Problem motivating the Project.....	2
1.2 Objective	2
1.3 Deliverables	2
1.4 Limitations	3
1.5 Report Structure	3
2 Literature Review.....	4
2.1 Vehicle Models.....	4
2.1.1 VTM (Volvo Transport Model)	4
2.1.2 One Track model.....	5
2.1.3 Two Track Model	5
2.1.4 Roll plane model.....	5
2.2 Tire Models.....	6
2.2.1 Magic Formula (Pacejka Model)	6
2.2.2 The Brush model.....	6
2.2.3 Burckhardt model.....	7
2.2.4 Dugoff's Tire model.....	7
2.3 Friction Models.....	8
2.3.1 Coulomb Model.....	8
2.3.2 Coulomb Model with Viscous Friction.....	9
2.3.3 Coulomb Model with Stiction and Viscous Friction	9
2.3.4 Model with Stribeck Effect.....	10
2.3.5 Karnopp Model	11
2.3.6 Threlfall Model.....	11
2.3.7 Bengisu and Akay Model.....	12
2.3.8 Ambrósio Model	12
2.3.9 Awrejcewicz Model.....	13
3 Methodology.....	15
4 Strategy Overview.....	16

5	Representative Vehicle Model.....	17
5.1	Model Assumptions	17
5.2	Coordinate Systems	17
5.3	Equation of Motion	18
5.3.1	Equations in Yaw Plane	18
5.4	Constraint Relations.....	21
5.4.1	Force and Moments Constraints.....	21
5.4.2	Velocity and Acceleration Constraints	21
5.5	Tire Forces	23
5.6	Vertical Load and Load Transfer	24
5.6.1	Static Loading.....	24
5.6.2	Semi-Static Load Transfer	25
5.7	State Space Form	26
6	Design of experiments.....	27
6.1	Experimental Setup	28
6.1.1	Working.....	28
7	Fifth-Wheel Model.....	29
7.1	Physical model of the fifth-wheel.....	29
7.2	Preliminary Analysis	29
7.2.1	Fifth-wheel effective diameter	30
7.2.2	Bushing Stiffness.....	31
7.3	Observations and Overall behavior.....	32
a.)	Nature of friction	32
b.)	Impact of normal load: same lubrication with different stages of kingpin loads	33
c.)	Impact of extent of lubrication: same kingpin load with different stages of lubrication	34
7.4	Friction Model.....	34
7.4.1	Explanation and Physical interpretation.....	35
7.4.2	Parameter Estimation Methodology	35
7.5	Fifth Wheel Roll Model	36
8.	Validation	41
8.1	Validation of RVM	41
8.1.1	Static Validation	41
8.1.2	Dynamic Validation.....	41
8.2	Fifth-wheel Model Validation.....	42
8.2.1	Influence of Bushing compliance on Vehicle behavior	42
8.2.2	Procedure	45

9. Case Studies	47
9.1 Different Fifth-wheel friction level	47
9.2 Different road friction level with constant fifth-wheel friction	49
9.3 Slow ramp steer	50
9.4 J-turn	52
9.5 Lane change	54
9.6 Driving on ice.....	58
9.7 Roll Behavior	59
9.7.1 Medium Load Height.....	59
9.7.2 High Load Height	60
10. Conclusion	62
References	63
Appendix A	66
Appendix B	67
Scenario 1	67
Scenario 3	67
Scenario 4.....	68
Scenario 5.....	69
Scenario 6.....	69
Scenario 7	70
Appendix C.....	72
Scenario 1	72
Scenario 3	72
Scenario 4.....	73
Scenario 5.....	73
Scenario 6.....	74
Scenario 7	75

List of Figures

Figure 1 (a) Coupling a Converter dolly with semi-trailer, (b) Coupling a (fixed) dolly with Full-trailer and (c) Coupling a Tractor with semi-trailer.....	1
Figure 2 Schematic representation of Tractor-Semitrailer Multi-body Model in VTM	4
Figure 3 Single Track or Bicycle Model [13].....	5
Figure 4 Coulomb Friction+ Viscous Friction	9
Figure 5 Coulomb friction+ Viscous friction+ Static friction	10
Figure 6 Coulomb Friction+ Viscous Friction+ Static Friction+ Stribeck Effect.....	10
Figure 7 Karnopp Model.....	11
Figure 8 Threlfall Model	12
Figure 9 Bengisu and Akay Model	12
Figure 10 Ambrósio Model	13
Figure 11 Awrejcewicz Model.....	14
Figure 12 Truck FBD in Yaw Plane.....	19
Figure 13 A-Dolly FBD in Yaw Plane.....	20
Figure 14 Semi-Trailer FBD in Yaw Plane.....	20
Figure 15 Velocities at coupling point in Truck CS.....	22
Figure 16 Velocities at coupling point in Dolly CS	22
Figure 17 Static Loading.....	24
Figure 18 Free Body Diagram of i^{th} axle of cornering vehicle.....	25
Figure 19 Experimental Setup.....	28
Figure 20 Physical Model for fifth-wheel in yaw plane.....	29
Figure 21 Friction Moment vs. Angular Velocity (including bushing compliance).....	29
Figure 22 Wear on Fifth-wheel	31
Figure 23 Wear on Fifth-wheel	31
Figure 24 Friction Moment vs. Angular Velocity (adjusted for bushing compliance)	32
Figure 25 Friction Moment vs. Angular Velocity generic behavior	32
Figure 26 Friction Moment with new lubrication at stages of kingpin load.....	33
Figure 27 Friction Moment with different stages of lubrication.....	34
Figure 28 Friction Moment vs. Angular Velocity	36
Figure 29 Fifth wheel Static Loading.....	37
Figure 30 Theoretical roll characteristic of fifth-wheel [34].....	38
Figure 31 Practical Approximated roll characteristic of fifth-wheel	38
Figure 32 FBD For Stage 1 Load Transfer	39
Figure 33 FBD in Roll Plane for after Trailer Separation	40
Figure 34 Steering Inputs for tests.....	43
Figure 35 Lateral acceleration under sinusoidal input.....	43
Figure 36 Lateral acceleration under J-turn.....	44
Figure 37 Articulation Angle under Sinusoidal Input.....	44
Figure 38 Articulation Angle under J-turn	45
Figure 39 Maximum Articulation Angle (deg).....	45
Figure 40 Friction moment vs. Angular velocity (Measured and Simulated).....	46
Figure 41 Articulation Angle for different levels of fifth-wheel friction.....	48
Figure 42 Lateral Acceleration for different levels of fifth-wheel friction.....	48
Figure 43 Lateral acceleration and articulation angle for $\mu_c=0.26$	48
Figure 44 Articulation Angle as a function of time for different levels of road friction	49

Figure 45 Lateral Acceleration as a function of time for different levels of road friction	50
Figure 46 Tractor and trailer path under ramp steer.....	50
Figure 47 Tractor and trailer path under ramp steer.....	51
Figure 48 Articulation Angle as a function of time for ramp steer.....	51
Figure 49 Lateral Acceleration as a function of time for ramp steer	51
Figure 50 Tractor and trailer path under J-turn.....	52
Figure 51 Tractor and trailer path under J-turn.....	53
Figure 52 Articulation Angle as a function of time for J-turn.....	53
Figure 53 Lateral Acceleration as a function of time for J-turn.....	53
Figure 54 Tractor and trailer path under lane change for fifth-wheel load=11500 kg.....	55
Figure 55 Tractor and trailer path under lane change for fifth-wheel load=16500 kg.....	55
Figure 56 Lateral Acceleration as a function of time for lane change @ 50 kmph.....	55
Figure 57 Articulation Angle as a function of time for lane change @ 50 kmph.....	56
Figure 58 Tractor and trailer path under lane change for fifth-wheel load=11500 kg.....	56
Figure 59 Tractor and trailer path under lane change for fifth-wheel load=16500 kg.....	57
Figure 60 Lateral Acceleration as a function of time for lane change @ 80 kmph.....	57
Figure 61 Articulation Angle as a function of time for lane change @ 80 kmph.....	57
Figure 62 Tractor and yaw rate driving over ice.....	58
Figure 63 Lateral Acceleration as a function of time driving over ice.....	58
Figure 64 Articulation Angle as a function of time driving over ice.....	59
Figure 65 Tractor and Trailer roll behavior, medium load height.....	59
Figure 66 Lateral Acceleration at Tractor front axle for Medium Load Height.....	60
Figure 67 Tractor and Trailer roll behavior, high load height.....	60
Figure 68 Lateral Acceleration at Tractor front axle for High Load Height	61

List of Tables

Table 1 Nomenclature for force and moments.....	18
Table 2 Design of Experiments	27
Table 3 Static Load.....	41
Table 4 Peak Yaw Rate RVM vs. VTM	42
Table 5 Peak Lateral Acceleration (m/s ²)	44

1 Introduction

Articulated Vehicles serve to transport everything: from solids to liquids to gases, from one point to another, in bulk. Owing to the economies of scale, this reduces the costs involved by 23%, can lead to fuel savings of up to 15% and reduce the number of trips by 32%; minimizing the prices for customers [1], and making them a lucrative option for the manufacturers. According to a study done in Alberta, Canada, it is estimated that use of longer combination vehicles (LCVs) showed 40% decrease in road wear, 29% reduction in transportation costs, 32% reduction in fuel consumption and emissions [2]. This prompts countries like Australia, Canada, Brazil to employ long and heavy vehicle combinations (HCV's), with lengths exceeding 50 m and gross weight in excess of 100 tons, on designated roads [3].

In Europe, however, the situation is different. The regulations are based in length and weight, instead of performance. For the most part, only the conventional combination of maximum length 18.75 m is allowed with maximum weight capped at 40 ton (44 ton with an ISO container). The exceptions are found in Sweden and Finland where LCVs up to 25.25 m in length and weighing 60 ton are permitted.

Concerns regarding the safety issues associated with the LCVs are primary inhibitors in their widespread use. Nonetheless, in light of the expected increase in the amount of transported goods by 55%, by 2020, organizations are bolstering their support for European Modular System (EMS). EMS suggests usage of existing load carrying units coupled together, to form LCVs, as a possible solution to meet the increasing demand. Apart from Sweden and Finland, Netherlands, since 2000, has been carrying out trials with LHV's according to EMS [4]. Sweden, currently, is testing even longer and heavier combinations, to serve, for instance, the timber haulage industry [5].

Under EMS, and in general operation, the number of articulation units can be increased or decreased, depending on the requirement and regulations, by using either full-trailers or semi-trailers. Semi-trailers come with the added advantage of being compatible to a variety of towing units; tractors and trucks both, via a convertor dolly.

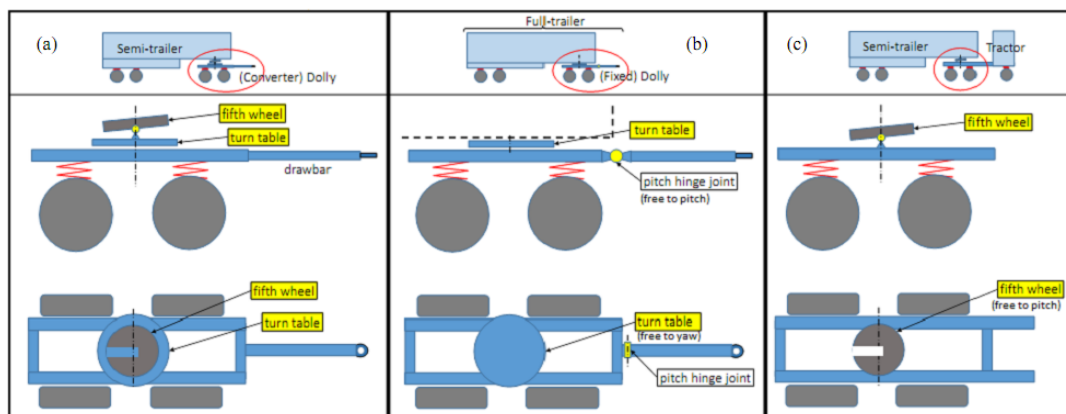


Figure 1 (a) Coupling a Converter dolly with semi-trailer, (b) Coupling a (fixed) dolly with Full-trailer and (c) Coupling a Tractor with semi-trailer.

Whether it is the convertor dolly, or a direct connection to the tractor, a fifth wheel and/or turntable is employed to connect the towing units (tractor/truck) and the towed units (full-trailer or semi-trailer). The behavior of these coupling devices greatly influences that of the resulting combination vehicle. Unfortunately, these devices have not been studied in depth and are often considered in their simplified form, while the attention is diverted to stabilizing or improving the vehicle performance as a whole, which remains incomplete without in-depth understanding of these coupling devices.

1.1 Problem motivating the Project

Converter dollies, in Sweden and Norway, are equipped with a turntable and/or a fifth wheel depending on the requirement of the customer.

- **Convertor Dolly:** A vehicle designed for the specific purpose of connecting trailers (semi-trailer and full) to a towing unit. It may have one or two axles depending on the configuration, which may or may not have steering capability. If the dolly can be detached from its trailer it is called a convertor dolly, else, a fixed dolly.
- **Fifth wheel:** A mechanical coupling mechanism primarily used for connecting semi-trailers to towing units (Tractors/Trucks) through a kingpin connection. It may be directly mounted on the towing unit (as in a tractor semi-trailer configuration) or on the rear of the lead trailer (as in a B-double configuration) or used on convertor dolly (as in an A-double configuration). The fifth wheel introduces degrees of freedom in yaw and pitch between the trailer and dolly.
- **Turntable:** A mechanical coupling mechanism primarily used for connecting the body of a full-trailer to its (fixed) dolly. They are inherently different from the fifth-wheels due to the presence of a large rolling element bearing and the absence of kingpin connection. The turntable introduces degrees of freedom in yaw only, all other movements are restricted between the trailer and dolly.

Turntable is selected because it ensures that there is very small resistance yaw torques between the dolly and semi-trailer, allowing for the trailer to articulate more easily during tight turns or high speed maneuvers at low road friction. The fifth wheel is needed for the standardized kingpin connection to the semi-trailer.

Having only fifth wheel increases the coupling yaw friction, significant contact area between trailer and fifth wheel provides resistance to yaw motion, negatively impacting the low speed maneuverability. Using only the turntable, reduces yaw friction, the bearings with rolling elements (ball or roller) provide virtually no resistance in yaw motion. Also, compatibility between units with varying coupling heights is affected.

In contrast to what is found in most of the literature, where vehicle behavior is estimated by simplifying the fifth-wheel as frictionless articulation point, on the contrary, this coupling does influence the dynamics of the complete vehicle combination and hence, such simplification is not a complete representation of the vehicle behavior. Previous researches, ex. [6] [7] [8] [9] [10] [11], have modeled the fifth wheel connection as being frictionless and having resistance free yawing motion in simulations, experimental results are not presented in most of these works and, hence, their validity and repeatability needs further investigation, which is the purpose of this study. In practical fifth-wheel couplings, there exists a significant friction between the fifth wheel and the trailer at the kingpin connection, which is why lubrication at the interface plays an important role in proper operation of the vehicle.

In brief, the problem motivating this research is to understand the behavior of fifth-wheel and find its influence, if any, on overall lateral and roll behavior of the vehicle.

1.2 Objective

The aim of this work is, to be able to estimate the forces/torques and moments acting on the fifth wheel of the combination vehicle and their effects of the dynamics on the vehicle in yaw and roll motion.

1.3 Deliverables

1. Vehicle model which includes fifth-wheel: yaw-friction, roll compliance and roll lash.

2. Factor affecting friction at the fifth-wheel and kingpin interface. The effects of the following factors are to be studied:

- Force/torque levels (F_{xy} , F_z , M_y)
- Temperature
- Velocity
- Lubrication
- Surface Roughness and unevenness
- Surface Wear

3. Theoretical and simulated analysis of the influence of the elements in compliant fifth wheel to the roll-over performance of:

- Tractor + Semi-Trailer

1.4 Limitations

The rollover calculation is dealing with vehicle units ‘decoupled’ in roll motion and is not applicable to the coupled ones.

1.5 Report Structure

Chapter 2 presents, in brief, literature review of the relevant previous work done in the field. In this chapter, different vehicle models, brief review of several friction models, to be used for fifth-wheel friction modeling, is presented.

Chapter 3 contains the detailed methodology for the development of the model and an overview of the strategy to be followed is given Chapter 4.

The details of the vehicle model developed are introduced in chapter 5. Chapter 6 details the experimental setup used in the study. The proposed fifth-wheel model is developed and validated in Chapter 7 and Chapter 8 respectively.

Chapter 9 uses the validated model to analyze the influence of introduction of fifth-wheel in the vehicle model through simulation studies.

2 Literature Review

The literature review is divided into the following main parts:

1. Vehicle models
2. Tire Models
3. Friction models

The review provided here will serve as the basis on which the vehicle and friction model (potentially) will be subsequently developed. The vehicle models are discussed in section 2.1 along with tire models, in brief, in 2.2, the existing friction models are described in section 2.3.

2.1 Vehicle Models

There are numerous methods available in the literature to represent a vehicle. Some may use Newtonian equations or Lagrangian equations to describe the motion of the vehicle. Others may use quarter car, half car or full car representation. The models may have a 2-D or a 3-D approach. The section introduces vehicle models used for analysis of vehicle behavior.

2.1.1 VTM (Volvo Transport Model)

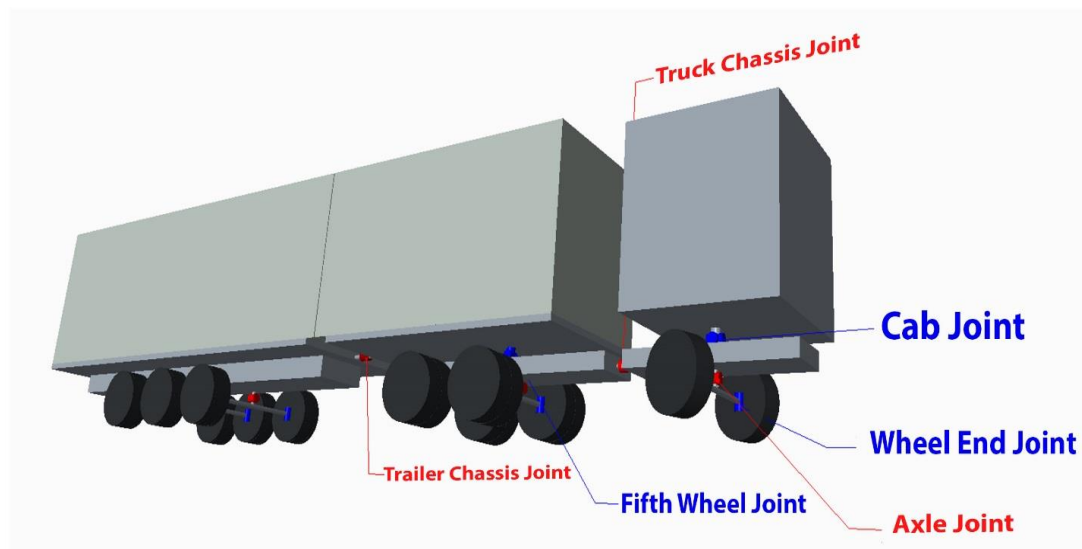


Figure 2 Schematic representation of Tractor-Semitrailer Multi-body Model in VTM

VTM is the in-house two-track multi-body modelling platform used by VOLVO GTT, to simulate articulated vehicles and buses. The model is based on MATLAB[®] and uses Simulink[™] SimMechanics for representing vehicle bodies. Flexibility of the frame is included in the model by torsional joints. Vehicle parameters like mass, inertia come from existing VOLVO truck designs. Simulink is used for wheel rotation, torque and steering actuation. Wheels are connected to the bodies and are capable simulating wheel lift-off, essential for simulating roll over scenarios. Pacejka tire model is employed for representing tire forces. The axle suspensions are included in the model. The system is modular in nature and units (e.g. dollies, semi-trailer) can be attached or detached from the existing vehicle combinations.

2.1.2 One Track model

A one-track model (bicycle model) is a simplified model, used to describe the lateral vehicle dynamic behavior, used primarily when studying sideslip angles and axle characteristics is the prime objective. It is also known as the single-track model [12]. It can be represented as in Fig. 1

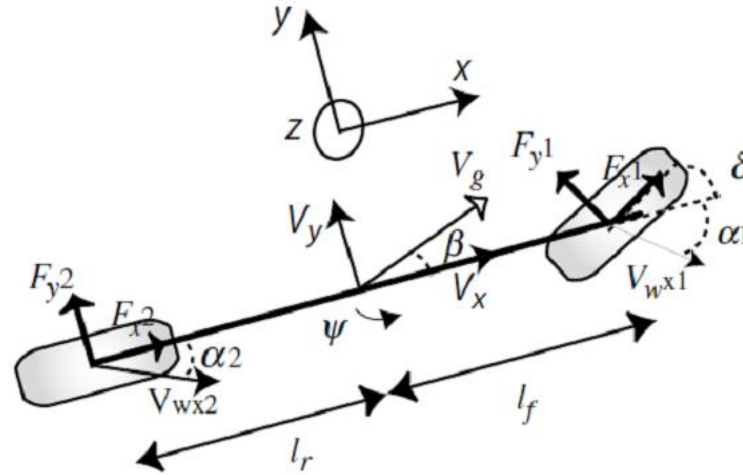


Figure 3 Single Track or Bicycle Model [13]

The model can be represented mathematically by the following equations:

$$m(\dot{v}_y + v_x \cdot r) = F_{y1} + F_{y2} + F_{ye} \quad (1)$$

$$J_r \cdot \dot{r} = l_f \cdot F_{y1} - l_r \cdot F_{y2} + M_{ze} \quad (2)$$

where,

\dot{r} – Yaw acceleration

J_r – Yaw moment of inertia

l_f – Front base

l_r – Rear base

F_{y1} – Front axle lateral force

F_{y2} – Rear axle lateral force

δ – Wheel steering angle

m – Mass of vehicle

v_x – Longitudinal Velocity

\dot{v}_y – Lateral acceleration

2.1.3 Two Track Model

Unlike the single track model, two track model does not lump together the left and right wheel of the axle and, hence, the behavior of each wheel during a maneuver can be studied separately. This is especially useful in case of maneuvers with high lateral acceleration which may eventually lead to wheel lift-off. The assumptions and other details of the model can be found in Chapter 5. As this is the chosen model for extension to include friction at the fifth wheel and turntable.

2.1.4 Roll plane model

The roll plane (y-z plane) is used for studying the lateral load transfer due to the roll motion. During handling maneuvers on smooth roads, vehicle roll motion is primarily induced by centrifugal forces caused by lateral accelerations. The roll motion of the vehicle body can be presented by a roll model including the roll angle. For more

explanation regarding this model, refer to section 5.3.3.2 as it is being used in estimating the lateral load transfer of the vehicle.

2.2 Tire Models

Tires are an important part of any vehicle model as they responsible for generating almost all the controlling forces imposed on the vehicle, primarily longitudinal and lateral forces.

Tire models are developed to understand how the tire behaves and consequently affects vehicle performance. The tire forces are results of '*slip*' existing in longitudinal and lateral direction. The '*slip*' for longitudinal forces is the difference between the velocity of the tire and the velocity of the ground at the point of contact, which is dimensionless when normalized with either wheel or wheel hub velocity, then called the longitudinal slip. For lateral force as well as for the aligning torque the '*slip*' is the slip angle, which is the angle between the velocity vector of the tire and the wheel plane.

“Physical tire models are more complex and are applied to derive quantitatively correct tire performance based on the detailed description of tire structure and material properties while the empirical tire models are based on an approach in which experimental results are used to find parameters to tune a certain mathematical description.” [12]

2.2.1 Magic Formula (Pacejka Model)

The Magic Formula is an empirical tire model that uses a mathematical relation to define forces and moments accurately. It is called the magic formula because there is no physical explanation for the model but, nevertheless, it agrees with the experimental data to a high degree. The underlying principle behind the magic formula is that the evolution of longitudinal and lateral force with respect to '*slip*' both follows a general relation that can be expressed by:

$$y(x) = D \cdot \sin[C \cdot \arctan\{B \cdot x - E \cdot (Bx - \arctan Bx)\}] + S_{vy} \quad (3)$$

Where $y(x)$ then represents longitudinal force and lateral force for longitudinal slip and slip angles respectively. Coefficients B , C , D , and E describe the tire characteristics [14]:

1. B : It determines the slope at the origin and is also called the stiffness factor
2. C : shape factor, which controls the limits of the range of the sine function and thereby determines the shape of the resulting curve
3. D : peak factor
4. E : the curvature factor, it regulates the value of the slip at which the peak of the curve occurs
5. BCD : the product corresponds to the slope at the origin ($x = y = 0$). For lateral force, this factor corresponds to the cornering stiffness.
6. S_{vy} =horizontal shift

These coefficients are further dependent on sub-coefficients which are extracted directly from tire testing.

2.2.2 The Brush model

In the brush model [15], the tire treads are approximated by the brush made of tread elements. The carcass is assumed to be rigid, and the forces are generated by the

deformation of the brush elements. The deflection range of the brushes is limited, depending on the coefficient of friction μ , vertical force distribution and the stiffness of the element. This model is further categorized into three more categories:

1. Pure lateral slip = For this case, the brush elements deflect in the direction perpendicular to the wheel plane
2. Pure longitudinal slip = For pure longitudinal slip the tread elements are deflected in the longitudinal direction.
3. Combined slip = In this case, when the tire is subjected to both longitudinal load and lateral load, then the combined slip situation occurs.

2.2.3 Burckhardt model

Burckhardt model defines slips in the direction of wheel velocity vector (longitudinal slip s_l) and perpendicular to this direction (side slip s_s). The resultant of both the slips (s_{res}) gives the direction of the resultant force. The tire model contains five empirical parameters:

$$F = (c_1 \cdot (1 - e^{-c_2 s_{res}}) - c_3 \cdot s_{res}) e^{-c_4 \cdot s_{res} \cdot v} (1 - c_5 \cdot F_{ZT}^2) \quad (4)$$

But can be simplified to:

$$F = (c_1 \cdot (1 - e^{-c_2 \cdot s_{res}}) - c_3 \cdot s_{res}) \quad (5)$$

The model assumes equal tire characteristics in both directions which influences its accuracy [4].

2.2.4 Dugoff's Tire model

It is a simple model capable of describing forces under pure cornering, pure (acceleration/braking) and combined (acceleration/braking) cornering maneuvers. The simplicity of the model is its ability to include all the tire properties in just two constants, known as the longitudinal and lateral stiffness of the tire. A simplified and robust Dugoff's tire model has been presented assuming pure slip conditions with negligible longitudinal slip to estimate the lateral tire forces. This model is as follows:

$$\bar{F}_y = -C_\alpha \cdot \tan(\alpha) \cdot f(\lambda) \quad (6)$$

Where $f(\lambda)$ is given by:

$$f(\lambda) = \begin{cases} (2 - \lambda), & \text{if } \lambda < 1 \\ 1 & \text{if } \lambda \geq 1 \end{cases} \quad (7)$$

$$\lambda = \frac{\mu_y \cdot F_z}{2 \cdot C_\alpha \cdot |\tan(\alpha)|} \quad (8)$$

Where,

C_α – Cornering stiffness

μ_y – Coefficient of friction

α – Tire slip angle

F_z – Normal tire load

The assumption of keeping the longitudinal slip negligible reduces the accuracy of the model for the current study; hence this model will not be used.

2.3 Friction Models

Friction refers to the resistance to the relative motion between contacting surfaces. It is nearly omnipresent in all physical phenomena. In most of the cases, the presence of friction forces is not desirable as it causes loss of power, undesired increase in temperature, wear etc. This warrants a detailed study into friction existing in the system, its influence and possible control.

Several studies have been conducted to study and model friction occurring in different fields but, so far, there exists no single model which can explain friction in its entirety. The earliest works date back to Leonardo Da Vinci and since then many different models have been suggested and are used by the industry based on what satisfies their needs the best.

Coulomb's friction law was a milestone of the evolution of the friction force models and still forms the basis, in one way or the other, of nearly all the friction models. However, the model is not continuous, resulting in numerical instability during a dynamic simulation and several other models have been developed to better explain the experimental observations.

The existing models for friction in the literature can be broadly classified into [16]:

1. Static models: They describe the steady state behavior of friction
2. Dynamics Models: They use extra state variables making the model not only more complex but also more flexible in representing friction.

Most of the dynamic friction models are based on the physical interaction between the surfaces asperities, such as the Dahl model [17], bristle model [18], the reset integrator [18], the LuGre [19], among others. Generally, these approaches consider an extra state variable related to the bristle deflection and very small displacements between contacting surfaces. For practical purposes, the measurement of bristle deflection on the test track, on a truck-trailer, is a little impractical for this study and such models will not be considered further.

2.3.1 Coulomb Model

Probably, the most well-known model is the so-called Coulomb friction model. Even though it greatly over simplifies the frictional phenomena, it is widely used, when dynamic effects are not considered. Also, the Coulomb model forms the foundation of all (or nearly all) more advanced models. The Coulomb friction force is a force (F) of constant magnitude, acting in the direction opposite to motion, independent of the relative velocity (v).

$$F = \begin{cases} F_C \cdot \text{sgn}(v) & \text{if } v \neq 0 \\ \min(F_{ext}, F_C) \text{sgn}(F_{ext}), & \text{if } v = 0 \end{cases} \quad (9)$$

where,

$$F_C = \mu_k \cdot F_N \quad (10)$$

in which F_N is the normal force, F_C is the magnitude of Coulomb friction, μ_k is the kinetic coefficient of friction, F_{ext} is the external tangential force, and v is the relative velocity of the contacting bodies. Coulomb friction is often referred to as dry friction, but the model is used for dry contacts as well as boundary and mixed lubricated contacts.

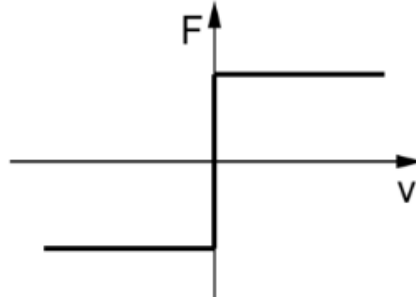


Figure 2: Coulomb Friction Model

2.3.2 Coulomb Model with Viscous Friction

The model in its essence is the modification of Coulomb's friction model by adding a viscous friction component. The viscous friction component models the friction force as a force proportional to the relative velocity, although there may be other approaches. It, too, poses the same problem as that of coulomb model; inability to handle zero velocity. It can be represented as:

$$F = \begin{cases} F_C \cdot \text{sgn}(v) + F_v \cdot v & \text{if } v \neq 0 \\ \min(F_{ext}, F_C) \text{sgn}(F_{ext}), & \text{if } v = 0 \end{cases} \quad (11)$$

where, F_v is the viscous friction coefficient

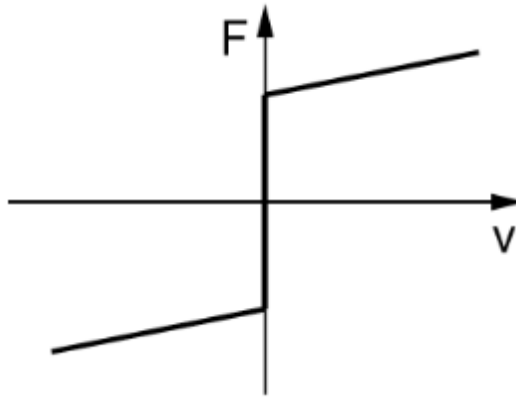


Figure 4 Coulomb Friction+ Viscous Friction

2.3.3 Coulomb Model with Stiction and Viscous Friction

Studies have shown that the friction force at zero velocity is higher than the kinetic friction, and hence presented the necessity of introducing a friction model, which includes two friction coefficients. This modification in Coulomb's approach has a similar behavior except in the vicinity of zero velocity. It is also a multivalued function, but is capable of representing the higher friction force, and can be described as follows [20]:

$$F = \begin{cases} F_C \cdot \text{sgn}(v) + F_v \cdot v & \text{if } v \neq 0 \\ \min(F_{ext}, F_S) \text{sgn}(F_{ext}), & \text{if } v = 0 \end{cases} \quad (12)$$

where,

$$F_S = \mu_S \cdot F_N \quad (13)$$

Where, F_C is the magnitude of Coulomb friction given by (10), F_S is the magnitude of static friction, and μ_S is the static friction coefficient which is higher than the kinetic coefficient, μ_k .

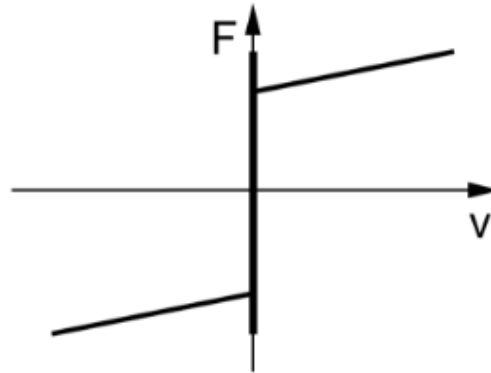


Figure 5 Coulomb friction+ Viscous friction+ Static friction

2.3.4 Model with Stribeck Effect

The above mentioned models have a discontinuity when the nature of friction changes from static to kinetic friction. The friction force will vary with the sliding speed depending on the extent to which the interacting contact surfaces are running under a given extent of lubrication (ranging from boundary, mixed to full film).

Even dry contacts show some behavior similar to that of lubricated surfaces in that they have a higher μ_S than μ_k . In lubricated sliding contacts, the friction decreases with increased sliding speed until a mixed or full film situation is obtained, after which the friction in the contact can either be constant, increase, or decrease somewhat with increased relative velocity due to viscous and thermal effects, see figure 6, this is called Stribeck effect [21] and ensures that the transition from static to kinetic friction is continuous function. Thus, the friction force during relative motion is expressed as a continuous function of velocity as:

$$F = \begin{cases} F(v) & \text{if } v \neq 0 \\ \min(F_{ext}, F_S) \operatorname{sgn}(F_{ext}), & \text{if } v = 0 \end{cases} \quad (14)$$

where, $F(v)$ is an arbitrary function that depends on the relative velocity. It is generally accepted as defined by Bo and Pavelescu [22]:

$$F(v) = \left(F_C + (F_S - F_C) e^{-(|v|/v_s)^\delta} \right) \operatorname{sgn}(v) + F_v \cdot v \quad (14.1)$$

where v_s is the Stribeck velocity and δ is a factor that relies on the geometry of the contacting surfaces, which is often considered 2 as suggested by Armstrong-Hélouvy [23] but may be different for different applications.

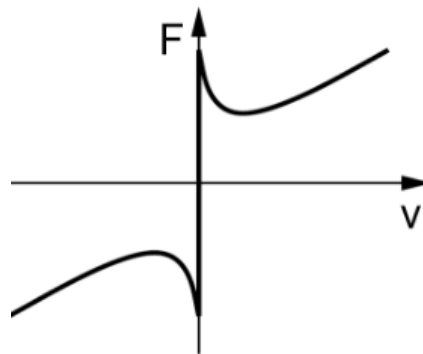


Figure 6 Coulomb Friction+ Viscous Friction+ Static Friction+ Stribeck Effect

2.3.5 Karnopp Model

Previous models are all having multivalued functions for zero velocity, presenting difficulties with capturing their static behavior in a simulation. Karnopp [24] proposed a model where the velocity is considered zero, for a specified range, to eliminate this difficulty. Thus, when the velocities are within this interval, the system's state can change and the model's response will be the same as when the relative velocity is zero.

$$F = \begin{cases} F(v) & \text{if } |v| > D_v \\ \min(F_{ext}, F_S) \operatorname{sgn}(F_{ext}), & \text{if } |v| \leq D_v \end{cases} \quad (15)$$

where, D_v is the tolerance range for null velocity. $F(v)$ is defined as in (14.1). The accuracy and validity of the model is highly dependent on the appropriate selection of a suitable range of the null velocity. Nevertheless, this null velocity range does not represent the real behavior.

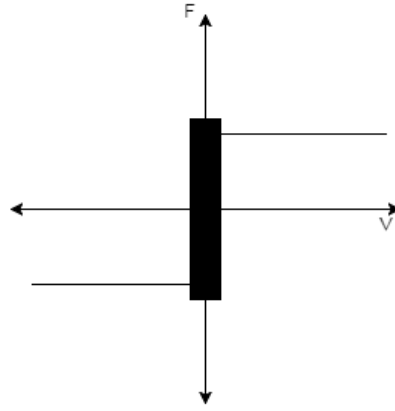


Figure 7 Karnopp Model

2.3.6 Threlfall Model

In static models described above, friction force at zero velocity is multivalued, and is a function of the external tangential force. In order to simplify and ensure computational efficiency, the discontinuity at zero velocity is replaced by a finite slope model (figure 8). Threlfall in [25] presented a model that avoids the discontinuity associated with the Coulomb's law, and is written as

$$F = \begin{cases} F_c (1 - e^{-k|v|/v_0}) \operatorname{sgn}(v) & \text{if } |v| \leq v_0 \\ F_c \operatorname{sgn}(v) & \text{if } |v| > v_0 \end{cases} \quad (16)$$

where, v_0 is the velocity at which friction is to be velocity independent.

and $k = 3$, a factor to ensure that at $v = v_0$:

$$F \sim \pm 0.95 F_S.$$

Threlfall argues that unlike other static models, where the instantaneous change in the friction force from $+F$ to $-F$, or vice versa, causes the integration routine some 'distress'. A simple linear transition of finite gradient will aid in the computational process. He also claimed that the model will not "self-jam" rather "creep through the jamming position at very low velocity."

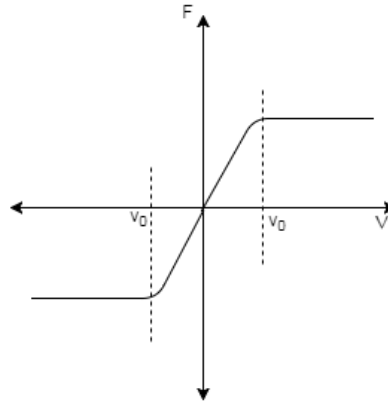


Figure 8 Threlfall Model

2.3.7 Bengisu and Akay Model

Bengisu and Akay [26] proposed an approach capable of modeling the Coulomb friction as well as Stribeck effect, and is defined as:

$$F = \begin{cases} \left(-\frac{F_s}{v_0^2}(|v| - v_0)^2 + F_s\right) \operatorname{sgn}(v) & \text{if } |v| < v_0 \\ (F_c + (F_s - F_c)e^{-\xi(|v|-v_0)}) \operatorname{sgn}(v) & \text{if } |v| \geq v_0 \end{cases} \quad (17)$$

in which ξ is be a positive parameter representing the negative slope of the sliding state (figure 9). They demonstrated using a three mass system with one frictionless contact surface and contact with friction, that the model could eliminate the discontinuity at zero relative velocity. However, when the slope at zero velocity is too large, a small step size is needed, which slows down the simulation.

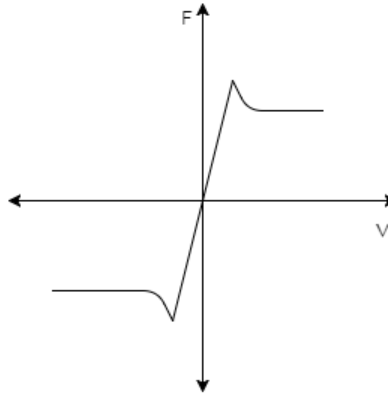


Figure 9 Bengisu and Akay Model

2.3.8 Ambrósio Model

Ambrósio suggested the use of models where a compromise between accuracy and computational efficiency has to be reached. In light of the above mentioned limitations he proposed a modified Coulomb friction law defined as:

$$F = \begin{cases} 0 & \text{if } |v| < v_0 \\ \frac{|v|-v_0}{v_1-v_0} F_c \cdot \operatorname{sgn}(v) & v_0 < |v| < v_1 \\ F_c \cdot \operatorname{sgn}(v) & |v| \geq v_1 \end{cases} \quad (18)$$

Where, v_0 and v_1 are the tolerances for the velocity.

This prevents the friction force from reversing when the relative velocity is close to zero eliminating the numerical instability. However, it does not describe the stick-slip motion and the null velocity range does not represent the real behavior.

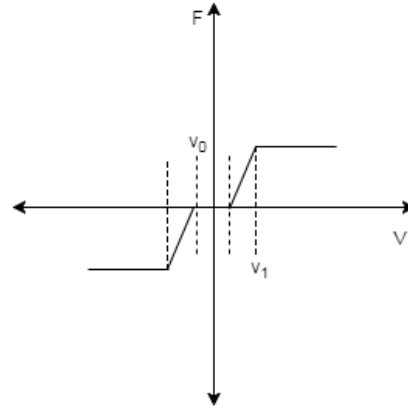


Figure 10 Ambrósio Model

2.3.9 Awrejcewicz Model

The previously mentioned friction models are either dependent on sliding velocity (relative velocity between the contact surfaces) or on the externally applied force (tangential to the moving surface). Awrejcewicz et al. [27] developed a more complete and complex static friction model for dry contact which takes into account both tangential force and relative velocity. They suggest that during the stick phase the friction force will depend on v but may not depend on F_{ext} . The model has 4 equations, one for sliding, two for the transition from stick to slip, and one for sticking mode and are defined as:

$$F = \begin{cases} F(|v|)sgn(v) & \text{for } V1 \\ F_S \cdot sgn(F_{ext}) & \text{for } V2 \\ (2A - 1) \cdot F_S \cdot sgn(v) & \text{for } V3 \\ A(-F_{ext} + F_S \cdot sgn(v)) + F_{ext} & \text{for } V4 \end{cases} \quad (19)$$

where,

$$\begin{aligned} V1: & |v| > \epsilon; \\ V2: & [(0 \leq v \leq \epsilon) \cap (F_{ext} > F_S)] \cup [(-\epsilon \leq v \leq 0) \cap (F_{ext} < -F_S)], \\ V3: & [(0 \leq v \leq \epsilon) \cap (F_{ext} < -F_S)] \cup [(-\epsilon \leq v \leq 0) \cap (F_{ext} > F_S)], \\ V4: & [(|v| \leq \epsilon) \cap (|F_{ext}| < F_S)] \end{aligned}$$

$$F(|v|) = F_C \quad [28]$$

and, $A = \frac{v}{\epsilon^2} (3 - 2 \frac{|v|}{\epsilon})$
 ϵ – velocity tolerance

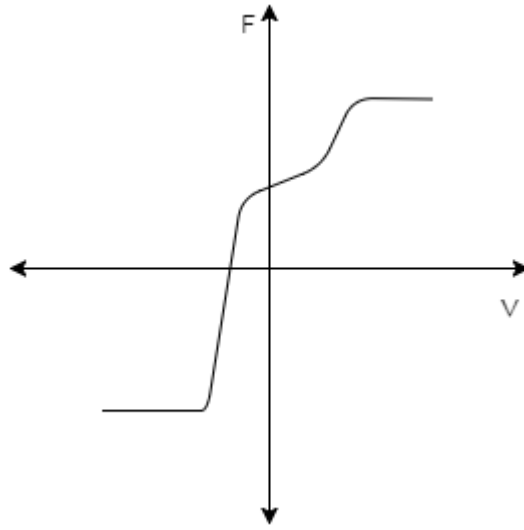


Figure 11 Awrejcewicz Model

The tolerance velocity defines the limit for sliding state. Below this tolerance, the friction force is also calculated as a function of the external tangential force.

3 Methodology

In this project, following steps are taken to achieve the objectives:

- **Defining the problem**
The first step in modeling a dynamic system is to describe the system adequately. Since the aims of the project are itself vast, it would be easier to divide the work into activities. Then, after modeling all the activities, one can integrate them into a complete model of the system.
- **Identifying System Components**
The second step in the modeling process is to identify the system components. The focus here is mainly to identify the components to be considered like bushing, fifth-wheel, turntable etc..
- **Modeling the System with Equations**
The third step in modeling a system is to formulate the mathematical equations that describe the system. For each phase, the model equations are selected which goes hand in hand with the estimation techniques.
- **Implementation**
Once the decided strategies are theoretically proved from the literature research, then only it is worth to implement. After the analytical validation of the chosen models and estimation techniques, the implementation of the selected strategies is performed in MATLAB/Simulink.
- **Validation**
Once the model has been successfully implemented, its validity can be measured against experimental results and the model can be tuned till the desired level of accuracy is achieved.

4 Strategy Overview

To achieve the above mentioned objectives the following strategy will be followed:

Step-1: Selection of Vehicle Model

- The primary objective is to include a fifth-wheel model in the VTM. Since, VTM is Volvo's internal platform and is not available for public access, a simplified representative vehicle model (RVM) will also be developed to represent these effects and to generalize the applicability of the fifth wheel model. For this purpose, after literature review, a non-linear two track model has been selected to represent VTM.
- Both vehicle models take into account the effects of combined slip and load transfer (due to roll).
- In RVM, tires will be modeled using the magic formula (Pacejka Model). It has been selected due to the availability of the data required for the model and to keep the tire forces and moments same as in case of VTM.

Step-2: Selection of Friction Model

- Due to the empirical nature of the friction, no initial selection for friction model is being made. It can be assumed to resemble Coulomb Friction+ Viscous Friction+ Static Friction± Stribeck Effect, but in the absence of measurements a different model may be selected, should the measurement warrant it.
- The assumed model is the most descriptive friction model and will present a comprehensive representation of the interaction.
- The model will be validated against test results using both RVM and VTM.
- The friction model will be generalized in its application using the vehicle model from RVM and VTM.

Step-3: Modelling fifth-wheel roll compliance

- The model will be extended to account for roll compliance. This step will be solely performed in VTM and the vehicle model from Step-1 will not undergo any extension.
- Fifth wheel compliance and roll lash at the fifth-wheel and kingpin interface will be taken into account.
- The model will be validated against results previously obtained.

Step-4: Comparative analysis using the extended model

- When the model is validated in Step-2, it will be able to represent vehicle behavior taking into account the friction at fifth wheel and trailer interface.
- This model will now to be used to compare the performance of selected vehicle combination by analyzing their behavior under the selected maneuvers (simulated in VTM).
- Effects of factors influencing friction will be studied by varying their values and analyzing its effects on the vehicle performance (sensitivity analysis).

5 Representative Vehicle Model

The chapter details the representative vehicle model (called RVM hereafter) for a Nordic Combination which is: Rigid Truck-Trailer, convertor dolly, and semi-trailer. All the vehicle models used in the study can be derived from this combination. The assumptions of the models are listed in section 5.1, reference frames are detailed in 5.2. In section 5.3 equations of motion for each vehicle unit are derived. Section 5.4 details the constraint between units. Tire forces for the detailed in 5.5. Section 5.6 presents the load transfer calculations. Vehicle states of interest are listed in 5.7.

5.1 Model Assumptions

The model developed in the following section is a non-linear two-dimensional model, which is extended to include the effects of roll through changes in vertical loads on the tires. Equation of motions will be developed for the Nordic combination from which the equations for tractor-semitrailer (used later in Chapter 9) can be derived by suitable manipulation of parameters.

As with any other real system, certain assumptions have been made to facilitate with the formulation of the equations of motion. Following assumptions have been made for the purpose of this study:

1. Steering inputs are applied through the tractor front axle tires only.
2. System parameters such as masses and inertias are always taken as constant.
3. No steering compliance is considered, steering for the tractor wheels is given through direct values of steering angle.
4. Suspension compliance is not considered.
5. There is no bending of bodies along the vehicle's length, i.e. they are rigid.
6. Significant angular motion occurs in yaw plane only, such that pitch and roll motion will not dominate the vehicle behavior at any point in the analysis, and allow for semi-static load transfer to account for the effects of roll.
7. Aerodynamic effects have not been considered.
8. The motion is considered on a flat road, i.e. no banking grade.
9. The vehicle is not subject to hard braking and acceleration and as such load transfer due to pitch motion is neglected.
10. The mass of the fifth-wheel is neglected.

5.2 Coordinate Systems

Nordic combination has a large number of degrees of freedom and, hence, choosing of coordinate systems, for easy formulation of equations of motion, is of great importance. The approach taken here is similar to that of Mikulcic [29].

Each unit in the combination will have two co-ordinate systems (ISO). First, an inertial reference frame with the origin positioned at the center of tractor front axle. The second frame (local frame) is attached to the center of mass of each unit and can both translate as well as rotate with the respective unit. Euler rotation angles will be used to relate the local and inertial frame of reference through a transformation matrix. Also, it has been assumed that significant angular motion is in yaw only the transformation matrix can be reduced to:

$$\begin{bmatrix} X_i \\ Y_i \end{bmatrix} = \begin{bmatrix} \cos(\phi_i) & -\sin(\phi_i) \\ \sin(\phi_i) & \cos(\phi_i) \end{bmatrix} \begin{bmatrix} x_i \\ y_i \end{bmatrix}$$

$[X_i, Y_i]^T$ are inertial co-ordinates, $[x_i, y_i]^T$ are local coordinates, ϕ_i is the yaw angle of the i^{th} unit as seen from the inertial frame.

5.3 Equation of Motion

Equation of motion for each unit of the combination will be derived separately, and then related through the coupling points in the combination. Truck will be considered as the first unit in the combination and the trailer as the last unit and the numbering will represent the same. **Twin tires have been reduced to single tire. Their effect is, however, included.** Unless stated otherwise, the subscripts x, y, z will represent standard ISO directions. The nomenclature, shown in Table 1, follows the same pattern as [29]. So, F_{2x} represent force on tractor front left tire in x-direction of the local frame.

Number	Location
1	Truck, left front
2	Truck, right front
3	Truck, left rear-axle 1
4	Truck, right rear-axle 1
5	Truck, left rear-axle 2
6	Truck, right rear-axle 2
7	A-dolly, left front
8	A-dolly, right front
9	A-dolly, left rear
10	A-dolly, right rear
11	Trailer, left front
12	Trailer, right front
13	Trailer, left middle
14	Trailer, right middle
15	Trailer, left rear
16	Trailer, right rear
17	Truck, pintle hook
18	Dolly, pintle hook
19	Dolly, kingpin
20	Trailer, kingpin

Table 1 Nomenclature for force and moments

5.3.1 Equations in Yaw Plane

For each vehicle unit Newtonian equations of motion will be derived based on its free body diagram, called FBD hereafter.

5.3.1.1 Truck

From figure 12, applying force and moment balancing we get:

$$m_1(\dot{v}_{x1} - v_{y1}\omega_1) = F_{1x}\cos\delta - F_{1y}\sin\delta + F_{2x}\cos\delta - F_{2y}\sin\delta + F_{3x} + F_{4x} + F_{5x} + F_{6x} + F_{17x} \quad (20)$$

$$m_1(\dot{v}_{y1} + v_{x1}\omega_1) = F_{1y}\cos\delta + F_{1x}\sin\delta + F_{2y}\cos\delta + F_{2x}\sin\delta + F_{3y} + F_{4y} + F_{5y} + F_{6y} + F_{17y} \quad (21)$$

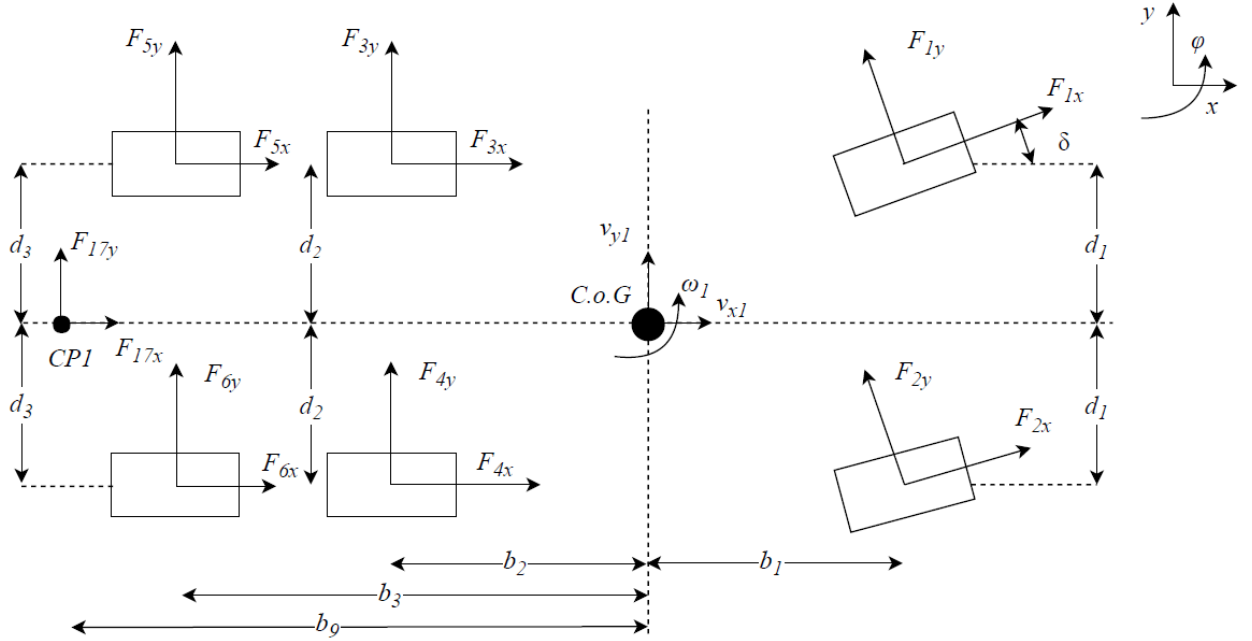


Figure 12 Truck FBD in Yaw Plane

$$I_1\dot{\omega}_1 = (F_{1y}\cos\delta + F_{1x}\sin\delta + F_{2y}\cos\delta + F_{2x}\sin\delta)b_1 - (F_{1x}\cos\delta F_{1y}\sin\delta - F_{2x}\cos\delta + F_{2y}\sin\delta)d_1 - (F_{3x} - F_{4x})d_2 - (F_{3y} + F_{4y})b_2 - (F_{5x} - F_{6x})d_3 - (F_{5y} + F_{6y})b_3 - F_{17y}b_9 + M_{1z} + M_{4z} + M_{3z} + M_{4z} + M_{5z} + M_{6z} \quad (22)$$

where, M_{iz} (for $i=1,2..16$) is the restoring moment arising from the tires at the i^{th} position.

5.3.1.2 Dolly

Proceeding as above in Figure 13:

$$m_2(\dot{v}_{x2} - v_{y2}\omega_2) = F_{7x} + F_{8x} + F_{9x} + F_{10x} + F_{18x} + F_{19x} \quad (23)$$

$$m_2(\dot{v}_{y2} + v_{x2}\omega_2) = F_{7y} + F_{8y} + F_{9y} + F_{10y} + F_{18y} + F_{19y} \quad (24)$$

$$I_2\dot{\omega}_2 = -(F_{7x} - F_{8x})d_4 + (F_{7y} + F_{8y})b_4 - (F_{9x} - F_{10x})d_5 - (F_{9y} + F_{10y})b_5 + F_{18y}b_{10} - F_{19y}b_{11} + M_{7z} + M_{8z} + M_{9z} + M_{10z} + M_{19} \quad (25)$$

M_{19} , is the frictional moment at the kingpin position

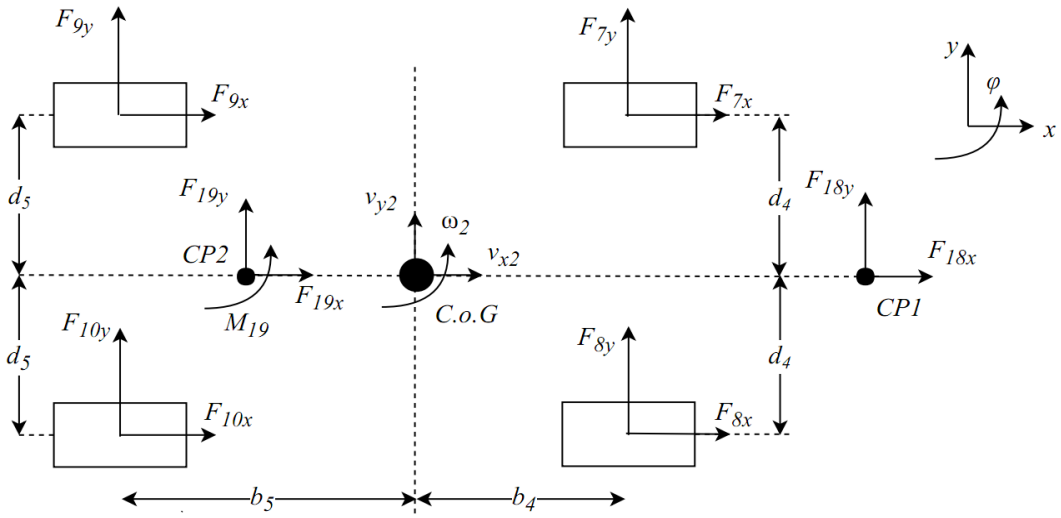


Figure 13 A-Dolly FBD in Yaw Plane

5.3.1.3 Semi-Trailer

From Figure 14, we get:

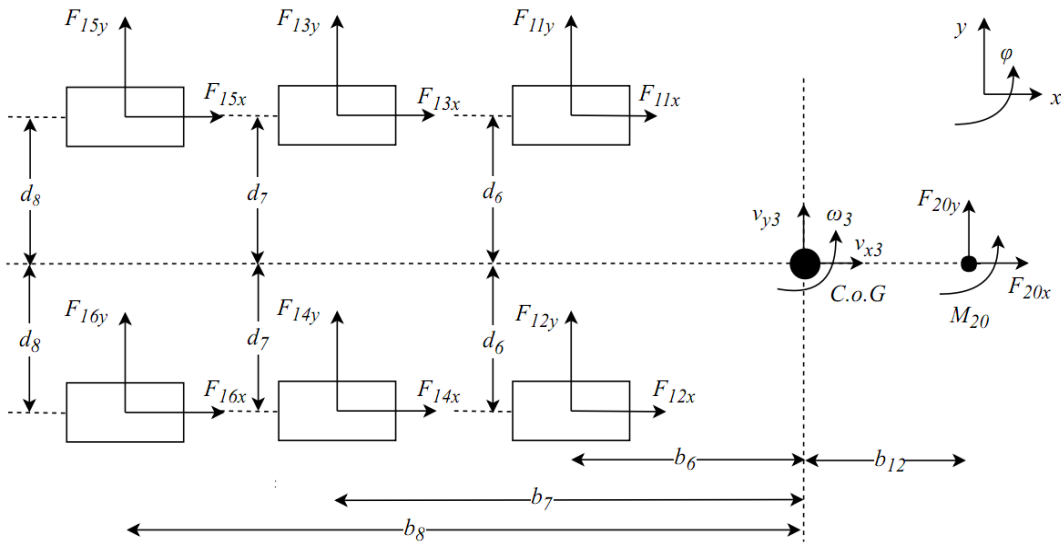


Figure 14 Semi-Trailer FBD in Yaw Plane

$$m_3(\dot{v}_{x3} - v_{y3}\omega_3) = F_{11x} + F_{12x} + F_{13x} + F_{14x} + F_{15x} + F_{16x} + F_{20x} \quad (26)$$

$$m_3(\dot{v}_{y3} + v_{x3}\omega_3) = F_{11y} + F_{12y} + F_{13y} + F_{14y} + F_{15y} + F_{16y} + F_{20y} \quad (27)$$

$$I_3\dot{\omega}_3 = -(F_{11x} - F_{12x})d_6 - (F_{11y} + F_{12y})b_6 - (F_{13x} - F_{14x})d_7 - (F_{13y} + F_{14y}) - (F_{15x} - F_{16x})d_8 - (F_{15y} + F_{16y})b_8 + F_{20y}b_{12} + M_{11z} + M_{12z} + M_{13z} + M_{14z} + M_{15z} + M_{16z} + M_{20} \quad (28)$$

M_{20} , is the frictional moment at the kingpin connection.

5.4 Constraint Relations

The equations of motion derived for the individual units need to be related to represent the vehicle as a whole. For this purpose the velocity and acceleration constraints will be derived using angular transformations to allow for transfer from one frame (local) to another.

The articulation angles between two units is defined as:

$$\angle \text{ between truck and dolly: } \phi_{12} = (\phi_1 - \phi_2) \quad (29)$$

$$\angle \text{ between dolly and trailer: } \phi_{23} = (\phi_2 - \phi_3) \quad (30)$$

5.4.1 Force and Moments Constraints

These articulation angles will be used to form the transformation matrices.

1. Transformation matrix from the truck to the dolly will be:

$$T_1 = \begin{bmatrix} \cos\phi_{12} & -\sin\phi_{12} \\ \sin\phi_{12} & \cos\phi_{12} \end{bmatrix} \quad (31.1)$$

The forces at the coupling point can be related as

$$\begin{bmatrix} F_{18x} \\ F_{18y} \end{bmatrix} = -T_1 \begin{bmatrix} F_{17x} \\ F_{17y} \end{bmatrix} \quad (31.2)$$

2. Transformation matrix from the dolly to the trailer will be:

$$T_2 = \begin{bmatrix} \cos\phi_{23} & -\sin\phi_{23} \\ \sin\phi_{23} & \cos\phi_{23} \end{bmatrix} \quad (32.1)$$

The forces at the fifth wheel and first trailer kingpin can be related as

$$\begin{bmatrix} F_{20x} \\ F_{20y} \end{bmatrix} = -T_2 \begin{bmatrix} F_{19x} \\ F_{19y} \end{bmatrix} \quad (32.2)$$

Moments at coupling positions are assumed to be equal and opposite in nature. Therefore:

$$M_{20} = -M_{19} \quad (33)$$

5.4.2 Velocity and Acceleration Constraints

The velocity and acceleration constraints are obtained by equating the velocities and accelerations of the coupling points. This approach is proposed and shown to work by Hibbeler in [30], and the same has been adopted here. Using the transformation matrix derived above the following constraints can be derived:

1. Truck and dolly: The velocity of the coupling point between truck and dolly, in their respective coordinate system is shown in Fig. 15 and Fig. 16 respectively.

The velocity at the coupling point can be found using:

$$v_{CP1} = v_{C.o.G} + v_{CP1/CG_i} \quad (i)$$

where v_{CP1} is the absolute velocity at the coupling point in the respective axis and v_{CP1/CG_i} is the relative velocity of the coupling point w.r.t C.o.G of the i^{th} unit. Using (i) with regards to truck and dolly, the following relation can be derived.

$$\begin{bmatrix} \dot{v}_{x2} \\ \dot{v}_{y2} \end{bmatrix} = T_1 \begin{bmatrix} \dot{v}_{x1} - v_{y1}\omega_1 + \omega_1^2 b_9 \\ \dot{v}_{y1} + v_{x1}\omega_1 - \dot{\omega}_1 b_9 \end{bmatrix} - \begin{bmatrix} -\omega_2^2 b_{10} - \omega_2 v_{y2} \\ \dot{\omega}_2 b_{10} + \omega_2 v_{x2} \end{bmatrix} \quad (34.2)$$

2. Dolly and Semi-Trailer: Proceeding as above

$$\begin{bmatrix} v_{x3} \\ v_{y3} \end{bmatrix} = T_2 \begin{bmatrix} v_{x2} \\ v_{y2} - b_{11}\omega_2 \end{bmatrix} + \begin{bmatrix} 0 \\ -b_{12}\omega_3 \end{bmatrix} \quad (35.1)$$

$$\begin{bmatrix} \dot{v}_{x3} \\ \dot{v}_{y3} \end{bmatrix} = T_2 \begin{bmatrix} \dot{v}_{x2} - v_{y2}\omega_2 + \omega_2^2 b_{11} \\ \dot{v}_{y2} + v_{x2}\omega_2 - \dot{\omega}_2 b_{11} \end{bmatrix} - \begin{bmatrix} -\omega_3^2 b_{12} - \omega_3 v_{y3} \\ \dot{\omega}_3 b_{12} + \omega_3 v_{x3} \end{bmatrix} \quad (35.2)$$

5.5 Tire Forces

Tire forces will be modeled using the Magic Formula (Pacejka Tire model). It allows the tire forces to be modeled, nonlinearly, as a function of vertical load (see 5.6), longitudinal slip (κ), slip angle (α), camber (γ), and longitudinal velocity (v_{xi}). The model is selected to closely represent the tire forces generated by VTM and provide a common ground for comparison.

$$F_{i,x} = f(F_{iz}, \kappa, \alpha, \gamma, v_{xi}) \quad (36)$$

$$F_{i,y} = f(F_{iz}, \kappa, \alpha, \gamma, v_{xi}) \quad (37)$$

$$M_{i,z} = f(F_{iz}, \kappa, \alpha, \gamma, v_{xi}) \quad (38)$$

In the current study the model is given an initial velocity which is then kept constant, i.e. $\kappa = 0$, also camber angle is set to zero. The tire model will operate under the condition of combined slip. The slip angles for the tires are derived as:

$$\alpha_i = \frac{v_{yi}}{v_{xi}}$$

which gives the following relations for the slip angles at the wheels:

$$\alpha_{1,2} = \tan^{-1} \frac{v_{y1} + b_1 \omega_1}{v_{x1} \pm d_1 \omega_1} - \delta \quad (39)$$

$$\alpha_{3,4} = \tan^{-1} \frac{v_{y1} - b_2 \omega_1}{v_{x1} \pm d_2 \omega_1} \quad (40)$$

$$\alpha_{5,6} = \tan^{-1} \frac{v_{y1} - b_3 \omega_1}{v_{x1} \pm d_3 \omega_1} \quad (41)$$

$$\alpha_{7,8} = \tan^{-1} \frac{v_{y2} + b_4 \omega_2}{v_{x2} \pm d_4 \omega_2} \quad (42)$$

$$\alpha_{9,10} = \tan^{-1} \frac{v_{y2} - b_5 \omega_2}{v_{x2} \pm d_5 \omega_2} \quad (43)$$

$$\alpha_{11,12} = \tan^{-1} \frac{v_{y3} - b_6 \omega_3}{v_{x3} \pm d_6 \omega_3} \quad (44)$$

$$\alpha_{13,14} = \tan^{-1} \frac{v_{y3} - b_7 \omega_3}{v_{x3} \pm d_7 \omega_3} \quad (45)$$

$$\alpha_{15,16} = \tan^{-1} \frac{v_{y3} - b_8 \omega_3}{v_{x3} \pm d_8 \omega_3} \quad (46)$$

5.6 Vertical Load and Load Transfer

The determination of vertical load on the tires at any time during a maneuver is of great importance. As discussed earlier, tires are responsible for nearly all the controlling forces of interest for vehicle control, these forces are predominantly effected by the vertical loads acting on them.

Two types of loading conditions is considered for this study:

1. Static Loading
2. Semi-static load transfer

Static load will determine the load acting on each tire at standstill condition. While the latter shall account for the effects of roll motion. Hence, the total load acting on the tire will be the sum of both these loads. It should be noted that, though there is indeed load transfer due to pitching of the vehicle it is neglected here as we are focused more on the investigation of lateral behavior which permits the omission of effects of pitch.

5.6.1 Static Loading

To calculate the static loads the vehicle is assumed to be at standstill on a plane surface. Also, loading on left and right sides is taken to be equal.

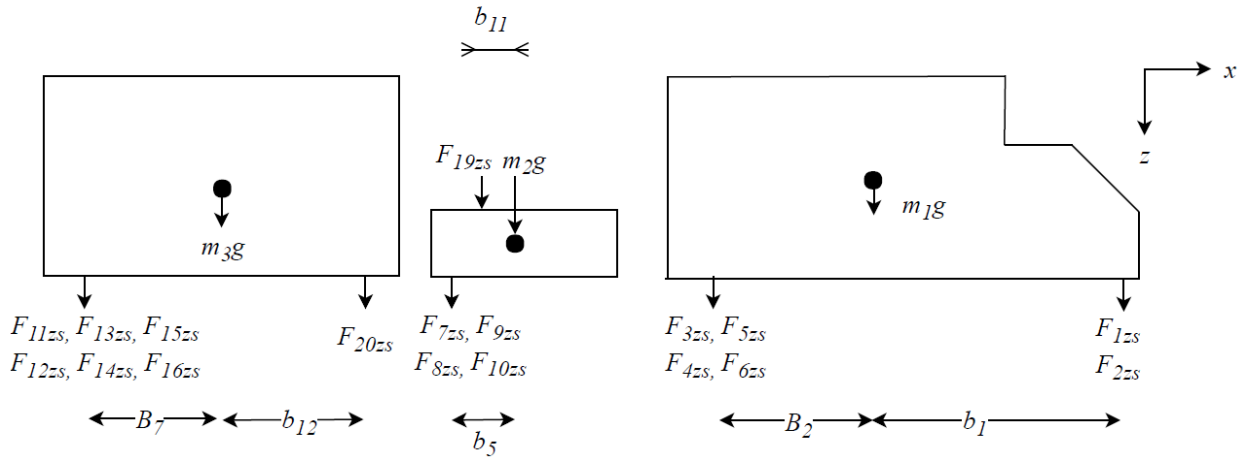


Figure 17 Static Loading

where, B_7 and B_2 are the distances of equivalent axle from respective C.o.G for the axle groups.

Applying force and moment balancing on the forces as shown in the figure above.

The following relations can be derived:

$$F_{1zs} = F_{2zs} = \frac{-1}{2} \left[\frac{B_2 m_1 g}{b_1 + B_2} \right] \quad (47)$$

$$F_{3zs} = F_{4zs} = \frac{-1}{2} * load\ ratio * \left[\frac{b_1 m_1 g}{b_1 + B_2} \right] \quad (48)$$

$$F_{5zs} = F_{6zs} = \frac{-1}{2} * (1 - load\ ratio) * \left[\frac{b_1 m_1 g}{b_1 + B_2} \right] \quad (49)$$

$$F_{7zs} = F_{8zs} = F_{9zs} = -F_{10zs} = \frac{-1}{4} \left[\frac{B_7(m_2 + m_3)g + b_{12}m_2g}{(B_7 + b_{12})} \right] \quad (50)$$

$$F_{11zs} = F_{12zs} = F_{13zs} = F_{14zs} = F_{15zs} = F_{16zs} = -\frac{1}{6} \left[\frac{b_{12}m_3g}{b_{12} + B_7} \right] \quad (51)$$

$$F_{19zs} = -F_{20zs} = \left[\frac{b_7 m_3 g}{b_{12} + B_7} \right] \quad (52)$$

For detailed derivation, refer Appendix A.

(Note: In static conditions, the load sharing between truck rear axles is not equal and is biased towards front-rear axle represented by *load ratio*. The trailer axles, however, share equal load.)

5.6.2 Semi-Static Load Transfer

Fancher [31] [32], has shown that the pintle hook-eye mechanism cannot transmit roll moments and ‘decouples’ the two units in roll. For purpose of load transfer due to roll, semi-static load transfer is used to account for load transfer, between vehicle sides.

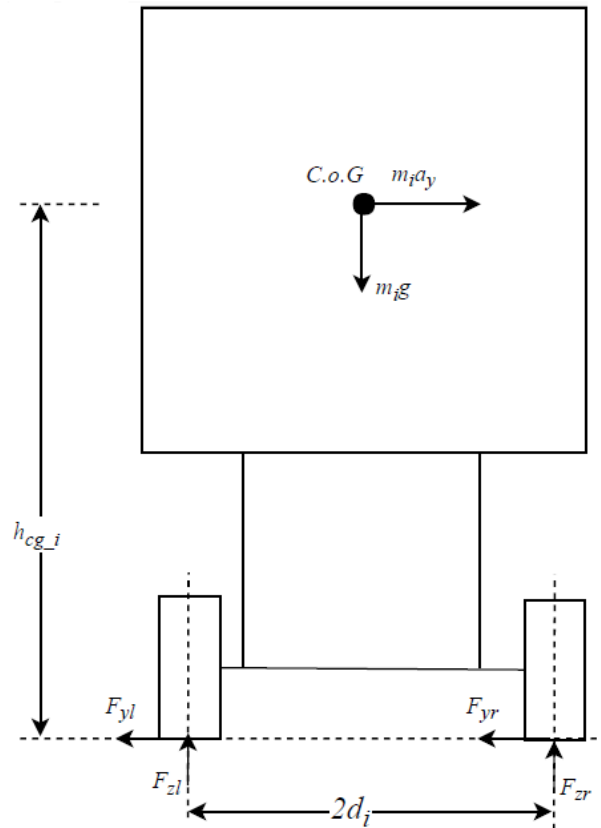


Figure 18 Free Body Diagram of i^{th} axle of cornering vehicle

As shown in the figure above, for any axle during a turn, at lateral acceleration level a_y , moment equilibrium around left contact with ground:

$$\begin{aligned} m_i g d_i + m_i a_y h_{cg_i} &= F_{zri} * 2d_i \\ F_{zri} &= m_i \frac{g}{2} + m_i a_y \frac{h_{cg_i}}{w_i} \end{aligned} \quad (53)$$

Similarly, from moment equilibrium around right contact with ground:

$$F_{zli} = m_i \frac{g}{2} - m_i a_{yi} \frac{2 * h_{cg,i}}{d_i}$$

As, $m_i \frac{g}{2}$ =static load on sides

$$F_{zri} = F_{zrsi} + F_{zrsi} \frac{a_{yi} h_{cg,i}}{g d_i} \quad (54)$$

$$F_{zli} = F_{zlsi} - F_{zlsi} \frac{a_{yi} h_{cg,i}}{g d_i} \quad (55)$$

These equations confirm what we know from experience, inner side to the curve is off-loaded (if we disregard the pendulum effect).

5.7 State Space Form

The equations of motion from 5.3 can be manipulated, using the constraint relations from 5.4 to eliminate the coupling forces, and give five independent non-linear equations of the form:

$$\dot{\underline{y}} = f(\underline{y})$$

where, \underline{y} is the vector representing vehicle states and $\dot{\underline{y}}$ is the vector of states derivatives.

The resulting state vector and its derivative are:

$$\underline{y} = \begin{bmatrix} v_{x1} \\ v_{y1} \\ \omega_2 \\ \omega_2 \\ \omega_3 \end{bmatrix} \quad \dot{\underline{y}} = \begin{bmatrix} \dot{v}_{x1} \\ \dot{v}_{y1} \\ \dot{\omega}_2 \\ \dot{\omega}_2 \\ \dot{\omega}_3 \end{bmatrix}$$

6 Design of experiments

As mentioned earlier, based on the literature survey, the following factors were selected to be studied:

- Force/torque levels (F_{xy} , F_z , M_y)
- Temperature
- Velocity (angular and longitudinal)
- Lubrication
- Surface Roughness
- Surface Wear

* **Note:** 1. No significant change in fifth-wheel temperature was measured before and after the test and hence, the parameter was neglected during further analysis.
 2. Due to the complexity in quantification of surface roughness and surface wear without sophisticated measuring equipment, general classification of ‘base’ and ‘worn’ were used.

Table 2 Design of Experiments

Design of Experiments				
Factor/Range				No. of Combinations
Normal Force	9 tons	11.5 tons	16.5 tons	3
Longitudinal Velocity	10 km/hr	80 km/hr		2
Lubricant	base	new	dry	3
Surface wear	base	worn		2
Total				36

As can be seen from Table 2, the selected choice of factors result in 36 possible combinations to test, measure and analyze. In an ideal world with ideal resources and ideal time availability, all the combinations can be tested, measured and analyzed but based on the priority and time constraint for the project, the following scenarios were considered:

1. Normal force=9 tons, longitudinal velocity=10km/hr, lubricant=base, surface wear=base
2. Normal force=11.5 tons, longitudinal velocity=10 km/hr, lubricant=new, surface wear=worn
3. Normal force=16.5 tons, longitudinal velocity=10 km/hr, lubricant=new, surface wear=worn
4. Normal force=9 tons, longitudinal velocity=10km/hr, lubricant=dry , surface wear=base
5. Normal force=9 tons, longitudinal velocity=80km/hr, lubricant=base, surface wear=base
6. Normal force=11.5 tons, longitudinal velocity=80 km/hr, lubricant=new, surface wear=worn
7. Normal force=16.5 tons, longitudinal velocity=80 km/hr, lubricant=new, surface wear=worn

8. Normal force=9 tons, longitudinal velocity=80km/hr, lubricant=base, surface wear=base

6.1 Experimental Setup

For measurement of friction, the approach recommended by American Society for Testing and Materials (ASTM) for pin on disc test (ASTM G99-17) in [33] was adapted to the meet the requirements.

According to ASTM G99-17, the disc and pin, the surfaces between which friction is to measured, are brought into contact and the disc is rotated. The resistive force measured on the pin is the measure of friction force against the relative velocity of contact surface. The pin is held stationary.

In the adapted system, the fifth-wheel represented the pin and the trailer surface (not shown in the figure) was taken as the disc in our system. The fifth-wheel on the dolly was mounted on turntable. A force sensor was fixed to the turntable, in order to be able to use the force sensor, the turntable had to be unlocked.

The test setup shown in figure 19, was used to replicate similar conditions.



Figure 19 Experimental Setup

6.1.1 Working

When the trailer rotates over the surface of fifth-wheel, it applies a moment on the fifth-wheel, trying to turn the fifth-wheel. Since, the fifth-wheel is fixed either to the dolly surface or mounted on a turntable, a resistive moment will develop between the two surfaces. If the applied moment is greater than the resistive moment, there will be relative motion between the two surfaces. This will in turn cause the turntable to rotate, applying the resistive moment on the force sensor, which can be measured, keeping the turntable in place.

For relative velocity a displacement sensor was fixed between the trailer and dolly and the relative velocity was calculated using the displacement sensor readings.

7 Fifth-Wheel Model

7.1 Physical model of the fifth-wheel

The fifth-wheel model can be represented as below:

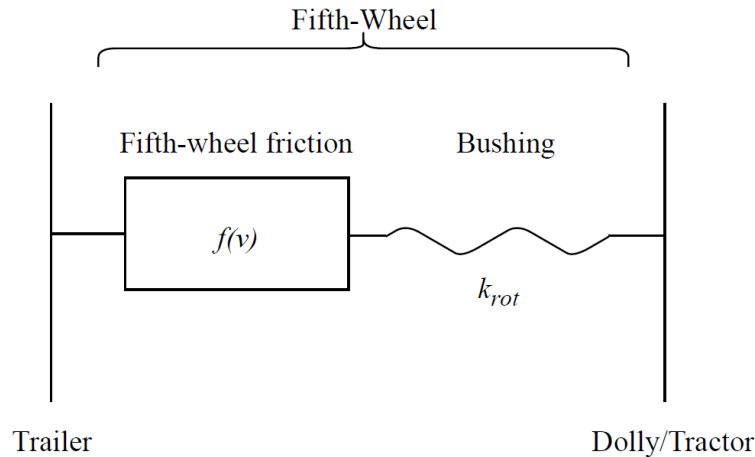


Figure 20 Physical Model for fifth-wheel in yaw plane

Explanation: A fifth-wheel serves to connect trailer to the towing unit via the kingpin. The forces and moments due to the rotation of trailer, in the yaw plane, are transmitted through the fifth-wheel and vice-versa, as shown above. The interactions of fifth-wheel can be broken down into two components: friction at the trailer-fifth-wheel interface, and bushing compliance at the fifth-wheel-dolly (or tractor) connection.

The experimental setup, shown in Figure 19, allows for inclusion of both the components to be included in the measurements. However, care should be taken when considering the measurement data for parameter identification and validation.

The friction model is taken to be a function of relative rotational velocity between the fifth-wheel and trailer surface. The bushing between the fifth-wheel and the trailer can be seen as a spring, with rotational stiffness k_{rot} .

7.2 Preliminary Analysis

Unadjusted measurements for friction moment vs. rate of change of articulation angle (referred to as angular velocity hereafter) for fifth-wheel load=11500 kg with vehicle longitudinal velocity= 10 km/hr, under sinusoidal input is shown below.

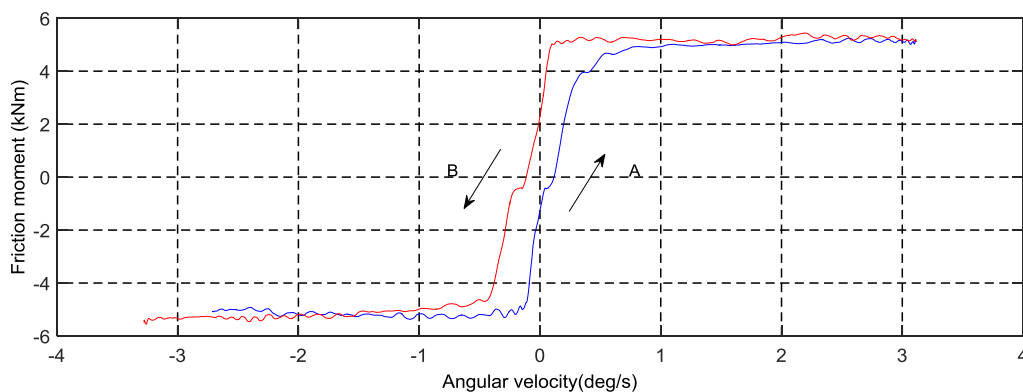


Figure 21 Friction Moment vs. Angular Velocity (including bushing compliance)

The curve shows two separate curves for increasing angular velocity (curve A) and decreasing velocity (curve B); intersecting x-axis at +0.114 deg/s and -0.114 deg/s

respectively. From the literature it is known that, friction moment should follow the same path with increasing and decreasing angular velocity, may not be applicable in the case of articulation angle (referred to as angle hereafter), due to presence of hysteresis.

In order to isolate the friction behavior, the measurements are to be adjusted to remove the influence of bushing compliance, using the following equation:

$$angle_{w/o\ bushing} = angle_{w/bushing} - \frac{moment}{k_{rot}} \quad (56)$$

where, k_{rot} is the rotational stiffness of the bushing and is given by:

$$k_{rot} = \frac{1}{2} d_{fw}^2 \cdot k_{linear} \quad (57)$$

where,

d_{fw} - effective diameter of the fifth-wheel

k_{linear} - linear stiffness of the bushing

To proceed further with the determination of friction parameters and bushing stiffness, effective diameter of the fifth-wheel needs to be determined first.

7.2.1 Fifth-wheel effective diameter

For calculating effective radius, at which the normal load will act, three approaches were considered depending on load (pressure) distribution:

1. Constant load (pressure) distribution on the fifth-wheel :

$$r_{fw_eff} = \frac{2(R_o^3 - R_i^3)}{3(R_o^2 - R_i^2)}$$

R_o - outer radius of the fifth-wheel

R_i - radius of kingpin

2. Hyperbolic pressure distribution on the fifth-wheel :

$$r_{fw_eff} = \frac{(R_o + R_i)}{2}$$

3. Two point approach:

The approach considers the load to be concentrated on two ends (same as used for roll modeling), situated at the mounting/pivoting points of the fifth wheel.

$$r_{fw_eff} = \frac{(D_{tp})}{2}$$

D_{tp} = distance between the mounting/pivoting points

From practical observations, this approach is supported by the fact that, maximum wear was observed, figure 22 and figure 23, at these points and, therefore, will be selected for further calculations.

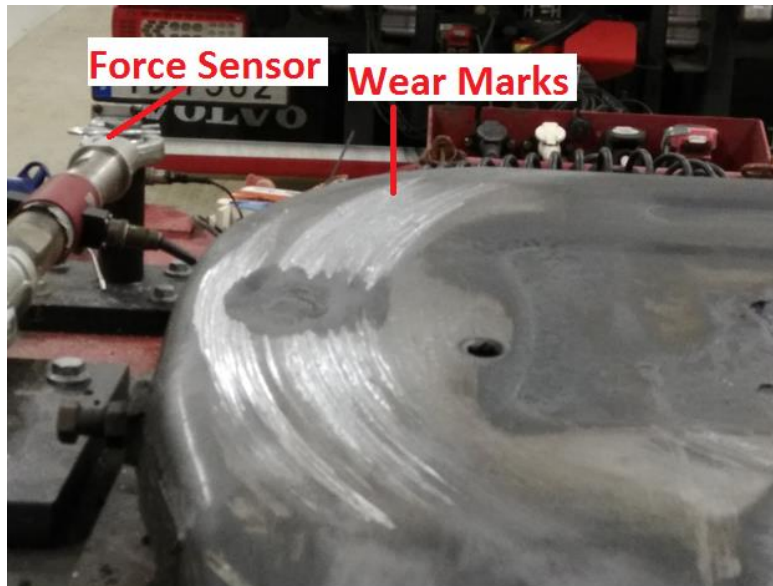


Figure 22 Wear on Fifth-wheel



Figure 23 Wear on Fifth-wheel

The distance between the pivoting points was measured to be 770 mm.

i.e. $d_{fw} = 2 * r_{fw_eff} = 770 \text{ mm}$

7.2.2 Bushing Stiffness

For determining the bushing stiffness, the measurements will be adjusted using (56) and (57). The adjustment will be stopped when either the intersections of curve A and B come closer to origin and show reversal in intersection points upon further increment of bushing stiffness, i.e. in figure 19, curve A intersects negative x-axis and curve B intersects positive x-axis. With $k_{linear} = 30 \text{ kN/mm}$ measurement data after adjustment for bushing compliance is shown in figure 24.

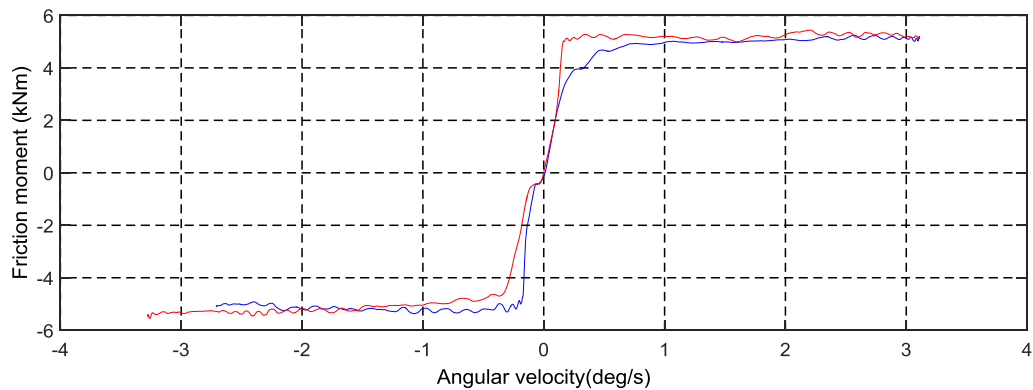


Figure 24 Friction Moment vs. Angular Velocity (adjusted for bushing compliance)

Upon further increment in k_{linear} reversal in intersection with x-axis was observed. The behavior seen is in agreement with that found in literature and, hence, moving forward these adjusted measurements will be used for friction model and its parameter estimation.

7.3 Observations and Overall behavior

Overall Behavior

From the above scenarios the following key results can be summarized:

a.) Nature of friction

Observations from one of the scenarios (Scenario-2) is shown below. Case-by-case analysis for the rest of the scenarios is presented in Appendix B.

The test was conducted with normal load at fifth wheel =11500 kg, at low longitudinal vehicle velocity of 10 km/hr while giving small sinusoidal input. The existing lubrication at the fifth-wheel was removed and fresh lubrication was applied.

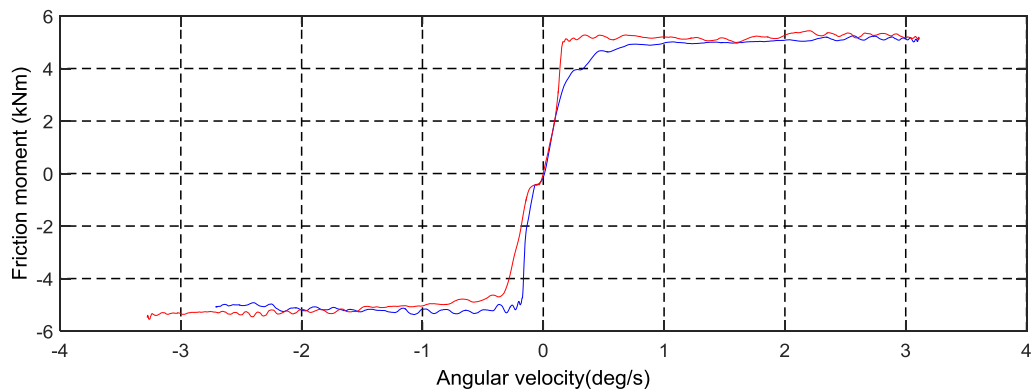


Figure 25 Friction Moment vs. Angular Velocity generic behavior

The friction moment can be seen to increase with velocity, the dependence is not constant rather showing two distinct components. The friction moment rapidly increases at low velocities and then at a comparatively lower rate at higher velocities. From the figure, it can be seen that, the friction moment increases with angular velocity, reaching the maximum values of ± 5 kN-m.

The first part, exponential rise with angular velocity is attributed to coulomb friction. The low linear rate of increment seen after ± 2 deg/s, indicates the impact of viscosity.

b.) Impact of normal load: same lubrication with different stages of kingpin loads

The time plot of friction moment represent the behavior of friction moment for corresponding sinusoidal input and fresh lubrication.

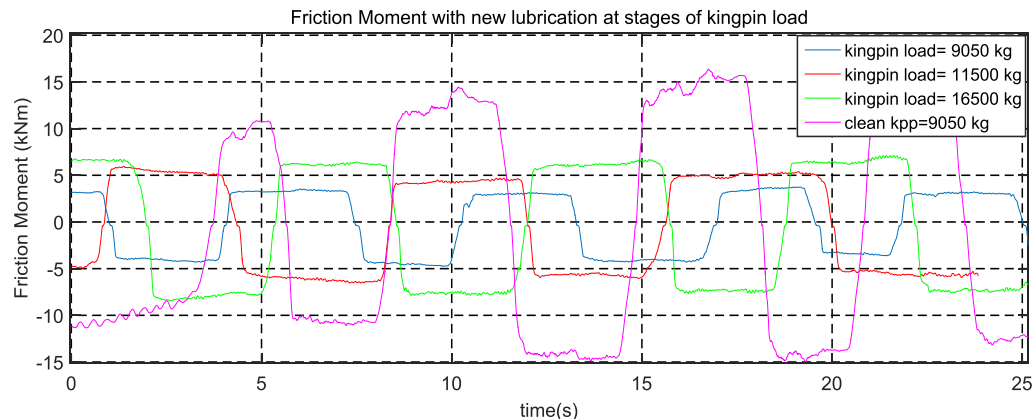


Figure 26 Friction Moment with new lubrication at stages of kingpin load

(*the curve for 'clean kpp=9050 kg' represents the friction moment without any lubrication at the fifth-wheel and is added for comparison)

Observations:

a.) Friction force increases with vertical load.

Reason: It is directly proportional to vertical load.

b.) The moment shows a rapid increase to an extent and, then increases very slowly before reversing its sign and repeating the behavior.

Reason: The sharp increase is attributed to coulomb friction while the slow increase is due to the presence of a viscous component.

c.) The slow increase of moment before sign reversal becomes negligible with increasing normal load/kingpin pressure.

Reason: As the normal load increases, it reduces the effective thickness of the layer of lubrication at the interface and the interaction moves from hydrodynamic lubrication to mixed or even boundary lubrication. It can be corroborated by an increase in friction coefficient for increasing loads.

d.) The friction for the curve: 'clean kpp=9050 kg' is significantly higher than the rest.

Reason: When the lubrication is removed there is direct metal to metal contact, which results in a high friction coefficient and hence a higher force. But it still follows the same pattern and, hence, has the same underlying model.

c.) Impact of extent of lubrication: same kingpin load with different stages of lubrication

The time plot of friction moment represent the behavior of friction moment for corresponding sinusoidal input and kingpin load=9050 kg.

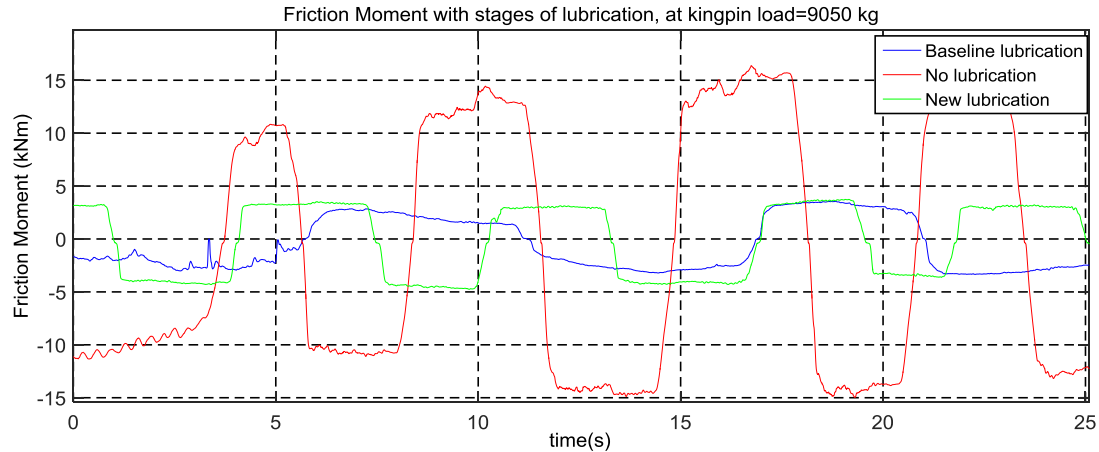


Figure 27 Friction Moment with different stages of lubrication

Observations:

a.) The frequency of friction moment for all the cases are different.

Reason: Open road tests were performed to simulate all the scenarios, encountered in real world driving, making the constant frequency aspect of the steering more difficult than longitudinal velocity. Also, the frequency of friction moment is directly influenced by the frequency of angular velocity, which is the input to the model. It does not provide meaningful insights into the behavior and can be overlooked.

b.) The curve for 'no lubrication' shows sudden increases, even though the velocity shows no such change, between sign reversals.

Reason: The absence of lubrication is resulting in repeated 'stick-slip' behavior between the metal contact surfaces. So, the friction force builds up in the stick phase, due to increasing/decreasing velocity, and changes suddenly as it transitions into slip phase.

7.4 Friction Model

From the analysis of the behavior under different scenarios, the following friction model is proposed:

$$M_{fric} = \text{Coulomb friction} + \text{Viscous friction}$$

Mathematically:

$$M_{fric} = \begin{cases} N \cdot r_{fweff} \cdot \mu_{sat} (1 - e^{-k(v_T)}) + b \cdot v_T & v_T \geq 0 \\ -N \cdot r_{fweff} \cdot \mu_{sat} (1 - e^{k(v_T)}) + b \cdot v_T & v_T < 0 \end{cases}$$

where,

M_{fric} –Friction Moment

v_T – Angular velocity

- μ_{sat} – Saturated friction co-efficient
- N – Vertical load on fifth-wheel (Newton)
- r_{fw_eff} – Effective radius (m)
- b – Effective Viscosity coefficient (N-m.s/deg)
- k – Relaxation factor (s/deg)

7.4.1 Explanation and Physical interpretation

- a.) From the observations it was clear that there are two regions. This is represented in the model by using two components to generate the resulting friction.

Exponential region: In this region the coulomb friction dominates and a rapid increase in friction moment is seen. The coulomb friction coefficient increases with velocity and reaches a saturated or steady state value at the boundaries of this region. The angular velocity is low, hence, the contribution of viscous effect is minimal.

Linear Region: Once, the coulomb friction coefficient has reached saturation (μ_{sat}), its contribution will remain constant (almost) and viscous effects will be dominate any change in resulting friction.

- b.) The low linear rate of increment at higher velocities is governed by the viscosity coefficient b and depends upon the extent of lubrication and the type of lubricant used on fifth-wheel trailer interface.
- c.) The rate of rise of frictional moment in the exponential region is influenced by the relaxation factor: k .
- d.) It is known that the friction force is directly dependent on the normal force. However, friction moment is not only dependent on the normal load but also on the effective moment arm, i.e. the distance between the axis of rotation and point of application of force. With the axis of rotation as the vertical axis at the center of the fifth-wheel. The moment arm is represented by effective radius ' r_{fw_eff}' . The expression for the effective radius has already been established in 7.2.1 and the same has been used here.

7.4.2 Parameter Estimation Methodology

The proposed friction model needs five parameters along with angular velocity as an input to determine the resulting friction moment. The estimation of these parameters can be done as explained below:

- a.) N : Based on the loading condition, the approach described in section 5.3.3 is used to determine the vertical load.
- b.) r_{fw_eff} : See 7.2.1
- c.) μ_{sat}, b, k : Curve fitting of the measurement data

The fitted curve and the resulting parameters obtained from one of the scenario (Scenario-2) are shown in figure 28. Case-by-case analysis for the rest is presented in Appendix B.

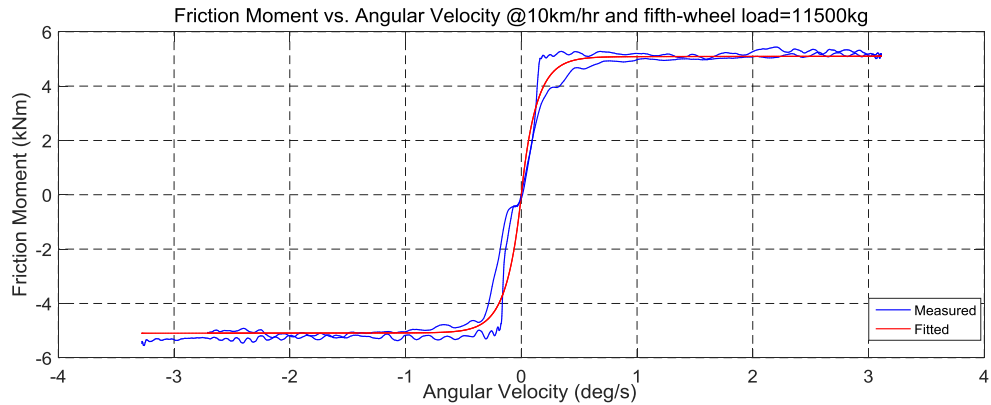


Figure 28 Friction Moment vs. Angular Velocity

Fitted parameters:

μ_{sat}	0.112
b (N.m.s/deg)	5
k (deg/s)	8

7.5 Fifth Wheel Roll Model

Practical vehicles are almost never rigid, hence, it is necessary to understand the compliance in their constituting units and its effect on roll behavior of the vehicle. Fifth wheel compliance greatly influences the roll behavior of the combination [34].

Studying compliance in fifth wheel also aligns with one aspect of the objective of the thesis work and, as stated earlier, the study will solely be performed on VTM and RVM will not be extended to include the roll behavior. Law [35] has modeled the fifth wheel “by two knife-edges located at the edges of the tractor fifth-wheel”, making it easier to model and analyze the behavior.

A similar approach has been used when calculating effective diameter for fifth-wheel and the same will be followed here, wherein, the fifth wheel will be reduced to ‘two knife-edges’, at the lateral extremities of the fifth wheel supports. Their roll stiffness represented by virtual springs at their connection to the tractor.

The discussion below is for the fifth-wheel in a tractor-semi-trailer combination but is equally applicable for the Nordic combination (by replacing tractor with dolly parameters)

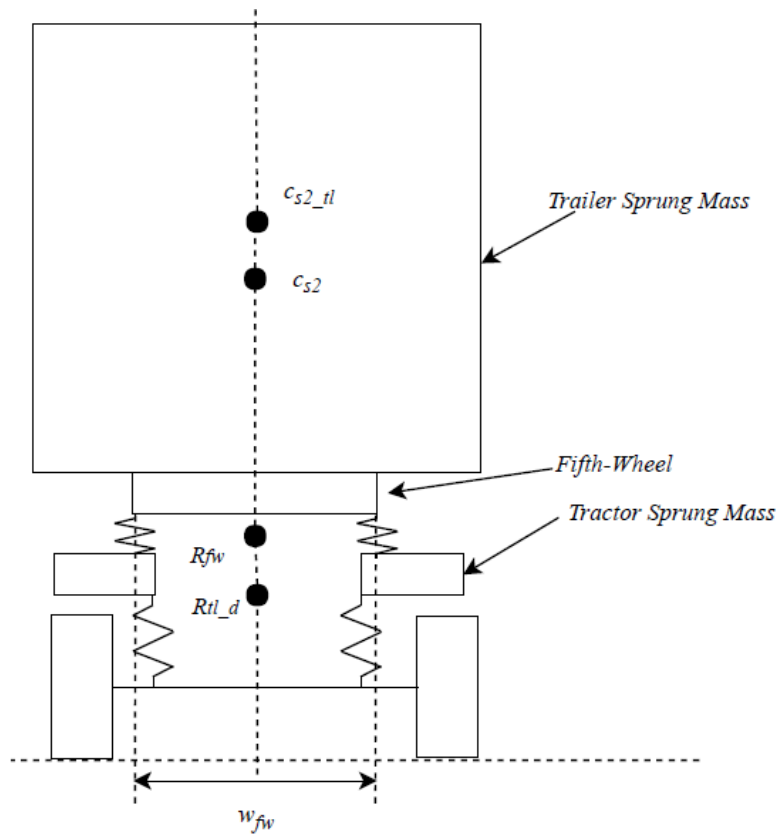


Figure 29 Fifth wheel Static Loading

Under static equilibrium the left and the right edges will share the load equally and is given by:

$$F_{fwl} = F_{fwr} = \frac{F_{fw}}{2} \quad (58)$$

where, F_{fw} is the load on fifth wheel and is given by (52) for the dolly fifth wheel.

When a roll moment acting on the fifth-wheel, results in a 3-stage process until rollover:

Stage 1: Load transfer occurs between the edges of fifth wheel, shifting load from the right to the left edge to the right (or vice versa). When this load is completely transferred to one of the edges the trailer lifts-off other edge, referred to as trailer separation.

Stage 2: After trailer separation, fifth-wheel can no longer synchronize the roll motion between tractor and trailer units. Fifth-wheel has its own roll degree of freedom, therefore, it rolls relative to tractor and follows the trailer roll motion until bump stops make contact. This angular freedom, after trailer separation to bump stop contact, is called fifth-wheel lash.

Stage 3: After the bump stop contact, the connection between the tractor and trailer is rigid. After this point they roll together as one lumped mass.

The theoretical behavior of roll angle at the fifth-wheel is shown in the figure below:

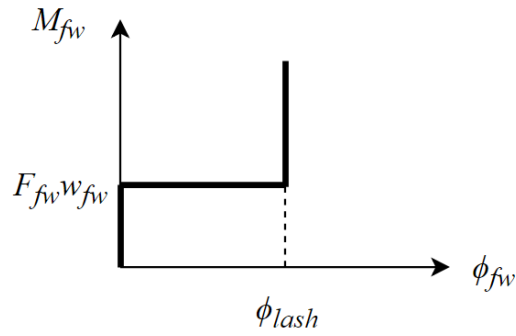


Figure 30 Theoretical roll characteristic of fifth-wheel [34]

The pitfall associated with the theoretical model is the extremely high roll stiffness introduced in Stage-1 and Stage-3. This creates high frequency oscillations before the final lift-off and slow down the simulation. For practically viable model, i.e. capable of being simulated, a compromise is struck and the following behavior is modelled:

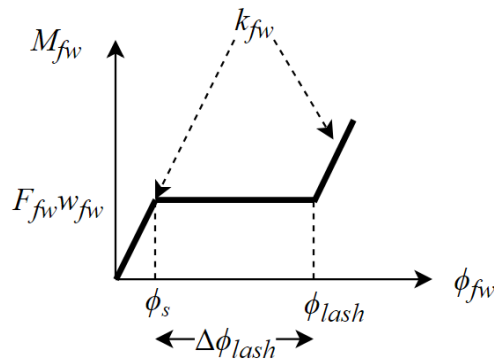


Figure 31 Practical Approximated roll characteristic of fifth-wheel

Stage 1: Load Transfer at fifth wheel:

For simplicity, this study, will assume that the fifth wheel is above the supporting axle, although legally it has to be in front of it.

Load transfer occurs between the edges of fifth wheel, shifting load from the right to the left edge to the right (or vice versa). The load transfer is resisted by the fifth-wheel due to its roll stiffness. The two masses do not roll about the same roll center and, as the fifth wheel has to compensate for the difference in their motion, it results in roll angle at fifth wheel given by.

$$\phi_{fw} = \phi_{2,tl} - \phi_{2,tr} \quad (59)$$

ϕ_{fw} – fifth wheel roll angle [rad]

$\phi_{2,tr}$ – roll angle of tractor at the drive axle [rad]

$\phi_{2,tl}$ – roll angle of trailer considering total sprung mass [rad]

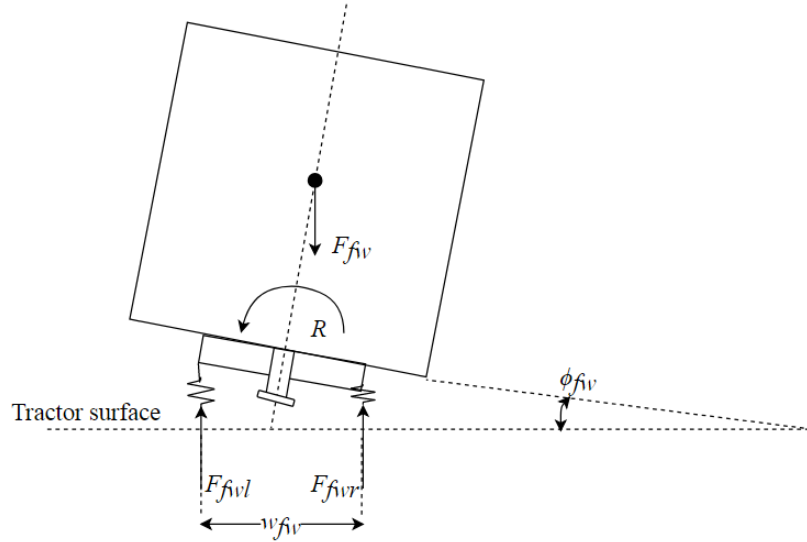


Figure 32 FBD For Stage 1 Load Transfer

The moment applied at the fifth-wheel M_{fw} is given by:

$$M_{fw} = (F_{fvl} - F_{fvr}) \frac{w_{fw}}{2} \quad (60)$$

If the roll stiffness of the fifth wheel is K_{fw} . The resisting moment R is given by:

$$R = K_{fw} \phi_{fw} \quad (61)$$

where,

w_{fw} -width of fifth wheel [m]

Under equilibrium : $M_{fw} = R$

solving for ϕ_{fw}

$$\phi_{fw} = \frac{w_{fw}}{2K_{fw}} (F_{fvl} - F_{fvr}) \quad (62)$$

At trailer separation: $F_{fvl} = 0$, $F_{fvr} = F_{fw}$, using (58), (62)

$$\phi_s = \frac{w_{fw} F_{fw}}{2k_{fw}} \quad (63)$$

Stage 2: After Separation before Bump Stop Contact

At trailer separation, trailer lifts-off from fifth-wheel left edge. After this point, if the roll moment M_{fw} is further increased. The trailer starts to roll freely w.r.t. to fifth-wheel. This continues until all the fifth-wheel is used up and the bump stop makes contact. The roll resistance remains constant as given by (63).

The fifth-wheel lash depends on design of fifth-wheel, and, since it is a design parameter it will be known beforehand and will be used to calculate the limiting roll angle at which bump-stop makes contact.

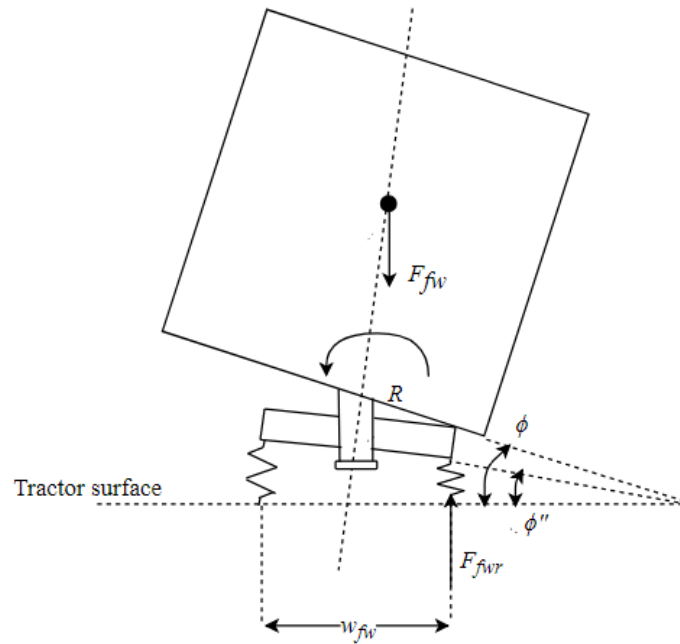


Figure 33 FBD in Roll Plane for after Trailer Separation

At bump-stop contact:

$$\phi_{lash} = \phi_s + \Delta\phi_{lash} \quad (64)$$

$\Delta\phi_{lash}$ -fifth wheel lash [rad],

Stage 3: After bump stop contact

Once the lash is taken up, the tractor and trailer move together as one unit. If the applied roll moment is increased, the connection becomes rigid and the combination behaves as one unit lumped together with the roll resistance defined as:

$$R = K_{fw}(\phi_{fw} - \phi_{lash}) + \frac{w_{fw}F_{fw}}{2} \quad (65)$$

8. Validation

For the purpose of validating the fifth-wheel model a representative vehicle model was developed in Chapter 5. This model is not only used for validation but also for generalization of fifth-wheel model's applicability. Therefore, the validation is divided in two steps:

1. Validation of RVM.
2. Validation of fifth-wheel friction model.

8.1 Validation of RVM

RVM is a simplified representative vehicle model and will be validated using:

1. Static Validation
2. Dynamic Validation

8.1.1 Static Validation

For static validation of the model, the static loads on the axles and fifth-wheel load of the vehicle combination are compared against those obtained from VTM. Three loading conditions are under considerations in the current study, the results for scenario 2/scenario 6 are given in Table 3.

Axle	RVM (kg)	VTM (kg)	Error*(%)
1	7914.447	7915	-0.0070
2	11500.351	11500	0.0031
3	6585.201	6585	0.0031
4	6953.373	6953.409	-0.0005
5	6953.373	6953.409	-0.0005
6	7647.75	7674.72	-0.3514
7	7647.75	7674.72	-0.3514
8	7647.75	7674.72	-0.3514
fifth-wheel	11506.747	11506.81	-0.0005

Table 3 Static Load

(* - relative to VTM)

As the error is extremely low (mean error=0.117%), the model is considered to be statically validated.

8.1.2 Dynamic Validation

For dynamic validation both the vehicle models, RVM and VTM, are given the same constant longitudinal velocity and sinusoidal steering input and the yaw rate at the truck is compared.

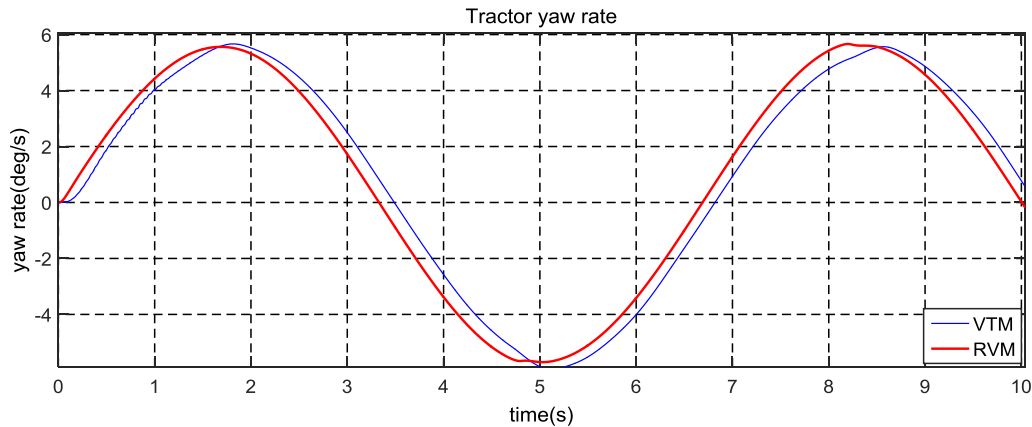


Figure 34 Tractor yaw rate RVM vs. VTM for Scenario-2

From figure 34, RVM shows the same amplitude of yaw rate as compared to VTM but also displays a phase lead which increases at high speeds. This is attributed to the absence of steering and suspension compliance in RVM. Since the phase lead is minimalistic in nature and the peak amplitude error is <1% (from Table 4), the model is accepted.

Table 4 Peak Yaw Rate RVM vs. VTM

	VTM (deg/s)	RVM (deg/s)	Error*(%)
Yaw Rate peak	5.665	5.707	0.741

(* - relative to VTM)

8.2 Fifth-wheel Model Validation

When developing the friction model and estimating its parameters, the influence of vehicle model was not considered (with the exception of normal load on fifth-wheel). In principle for validation, the friction model should not depend on the vehicle model and give same results, if given the same inputs, irrespective of the vehicle model being used.

The same cannot be said for the bushing compliance, as it is an inherent part of the vehicle. Therefore, in order to generalize the fifth-wheel the influence of bushing compliance on vehicle behavior will be analyzed first.

8.2.1 Influence of Bushing compliance on Vehicle behavior

A null hypothesis is established as shown below:

H_0 : Bushing compliance has significant influence on overall vehicle behavior

H_1 : Bushing compliance does not have significant influence on overall vehicle behavior

Explanation:

The null hypothesis states that the bushing compliance needs to be considered when implementing the fifth-wheel model as it significantly influences the overall vehicle

behavior. While the alternate hypothesis states that it does not have significant influence and can be considered as a rigid connection.

To accept or reject the null hypothesis, the fitted parameters derived previously and a bushing with 2.5 times more compliance than that derived in 7.2.2 are implemented on a fifth-wheel in a tractor-semi-trailer. The vehicle combination is subjected to two tests: a 'J-turn' and 'sinusoidal' steering input at vehicle speed of 30 km/hr. **If no significant difference is found, the null hypothesis is rejected.** Consequently, only the friction model is implemented in the fifth-wheel.

Test Signals:

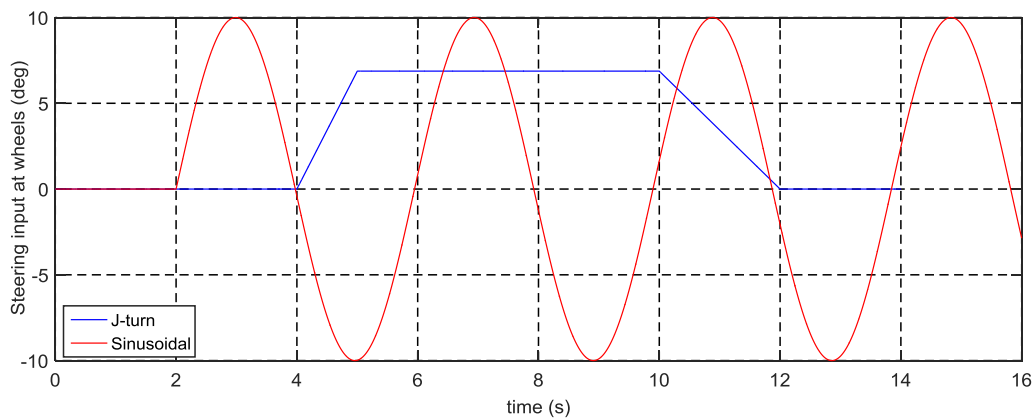


Figure 35 Steering Inputs for tests

Results:

Lateral Acceleration:

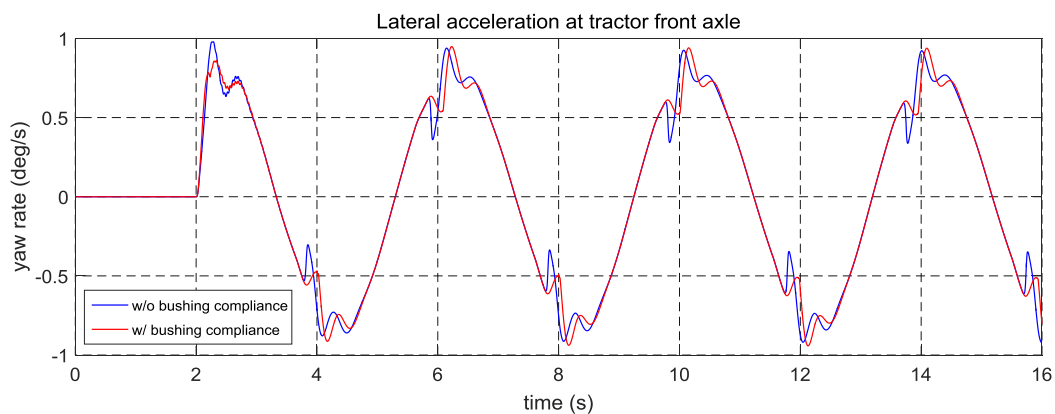


Figure 36 Lateral acceleration under sinusoidal input

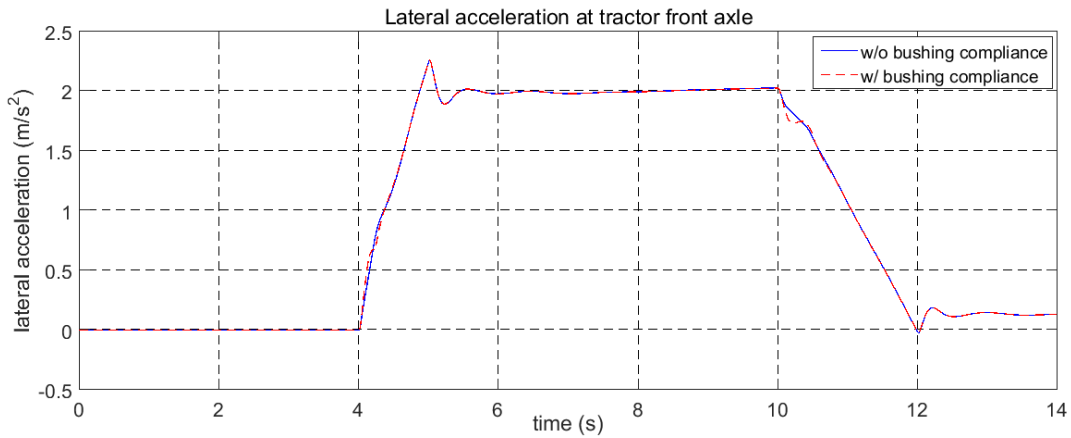


Figure 37 Lateral acceleration under J-turn

Observations: As, seen from Figure 32, the lateral acceleration shows less reduction in the presence of bushing and consequently has a smoother transition from stick phase to slip phase. The peak values obtained are as shown Table 5:

Table 5 Peak Lateral Acceleration (m/s²)

Test	w/ bushing compliance	w/o bushing compliance	% Error
Sinusoidal	0.98	0.95	3.1 %
J-turn	2.261	2.261	0 %

Articulation Angle:

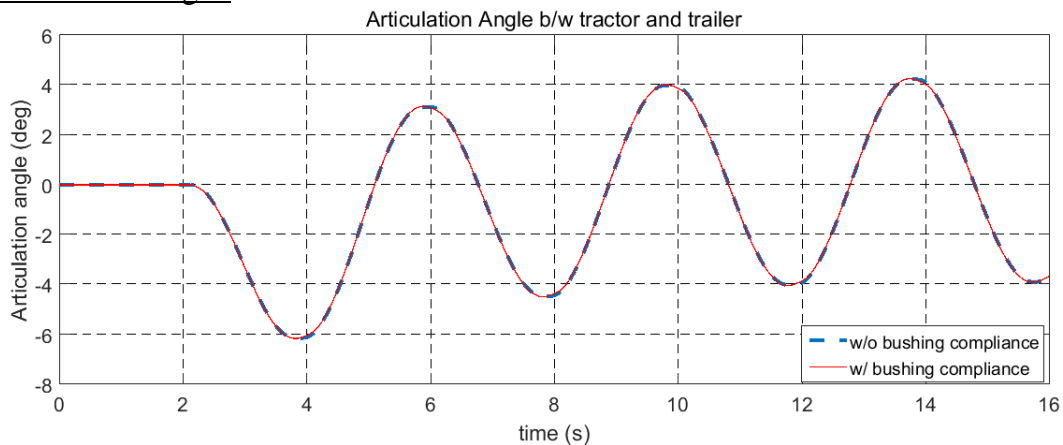


Figure 38 Articulation Angle under Sinusoidal Input

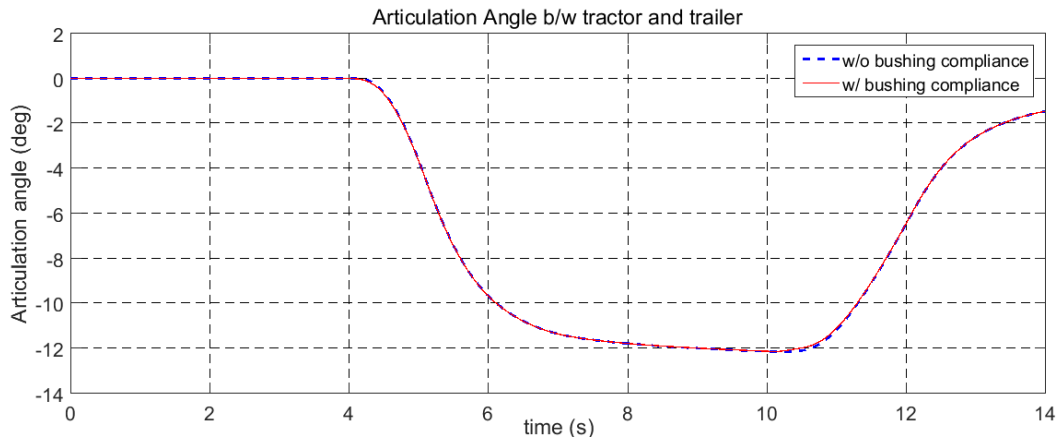


Figure 39 Articulation Angle under J-turn

Observations: The articulation angle under both the tests shows virtually no difference, when operated with and without bushing compliance. The peak values obtained are shown in Table 6.

Test	w/ bushing compliance	w/o bushing compliance	% Error
Sinusoidal	4.23	4.24	-0.23 %
J-turn	12.14	12.12	0.16 %

Figure 40 Maximum Articulation Angle (deg)

Additional Observations:

- a.) **Need for stiff solver:** The fifth-wheel model w/ bushing compliance could not be implemented using ode45, as the solver is not built to handle the transition from stick to slip phase resulting and slowed the simulation to the extent that every millisecond of simulation time took more than a second in real time. Hence, a stiff solver **ode23tb** was implemented which is capable of handling singularities [36]. Even then, the simulation was only possible with very strict tolerance limits (10^{-5}).
- b.) The memory employed by the model w/ bushing compliance showed an increase of 33.8% when compared to the model w/o bushing compliance. This affects the maximum buffer available for the simulation and will hamper longer simulations and subsequent transfer to VR environment.

Conclusion: The inclusion of bushing compliance. The trade-off for a smoother transition from stick to slip phase is heavily outweighed by the increase in simulation time and little to negligible differences in the overall vehicle behavior. Hence, **H_0 is rejected** and fifth-wheel with only the friction model will be considered for validation and simulation studies.

8.2.2 Procedure

As stated earlier, the friction model should not depend on the vehicle model and give same results, if given the same inputs. Using this principle, the fifth-wheel model, developed in Chapter 7, will be implemented in VTM, which is a 3-D model, as well as in RVM. If same results are obtained upon implementation in both these vehicle models, the fifth-wheel model can be considered validated and generalized at the same time.

The test scenarios, used previously, were simulated to validate the friction model. The parameters obtained in 7.4.2 were used for simulations. The result for Scenario-2 is given below, for case-by-case validation see Appendix C.

Scenario 2: Normal force=11 tons, longitudinal velocity=10 km/hr, lubricant=new, surface wear=worn

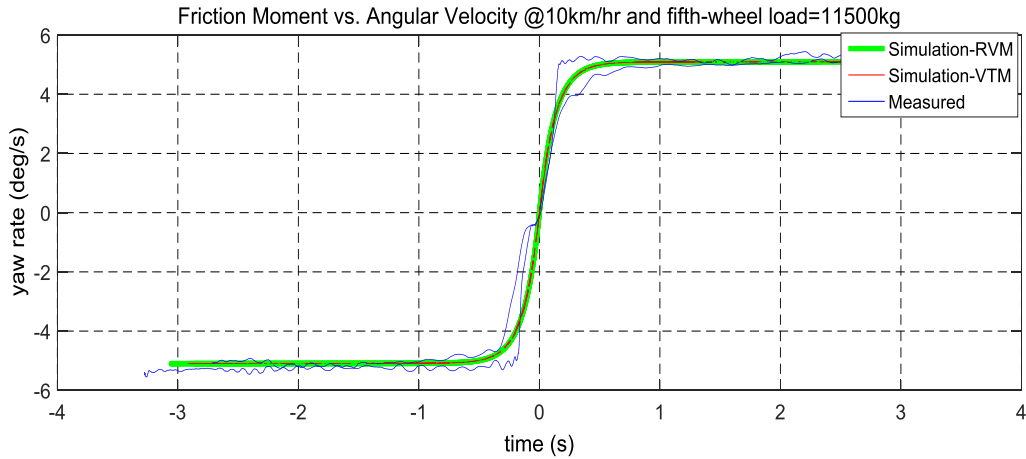
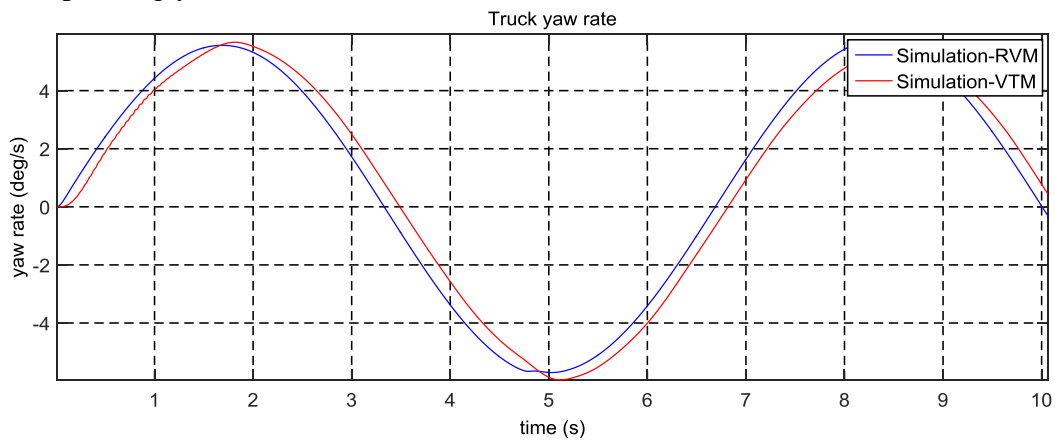


Figure 41 Friction moment vs. Angular velocity (Measured and Simulated)

Corresponding yaw rate at the truck:



	VTM (deg/s)	RVM (deg/s)	Error*(%)
Yaw Rate peak	5.955	5.928	-0.453

(*- relative to VTM)

9. Case Studies

To understand the influence of fifth-wheel model, the following cases were studied:

1. Different fifth-wheel friction level (Sensitivity Analysis)
2. Different road friction level with constant fifth-wheel friction (Sensitivity Analysis)
3. Slow ramp steer (up and down) @70 km/hr
 - With fifth-wheel load=11.5 tons and 16.5 tons
4. J-turn in slow speed @ 30 km/hr
 - With fifth-wheel load=11.5 tons and 16.5 tons
5. Lane change @ 50 km/hr and @80 km/hr
 - Steering frequency (0.4 Hz)
 - With fifth-wheel load=11.5 tons and 16.5 tons

9.1 Different Fifth-wheel friction level

- Test Conditions:
 - Vehicle: Tractor-semitrailer (with 2- and 3-axles respectively).
 - Longitudinal vehicle velocity=10 km/hr.
 - Steering input=10° sinusoidal input at the wheels (slalom test)
 - Fifth-wheel load=11500 kg
- Fifth-wheel friction Levels:
 1. No friction ($\mu_c=0$)
 2. Low friction($\mu_c=0.117$)
 3. High friction($\mu_c=0.26$)
 4. Extreme friction /No lubrication ($\mu_c=0.41$)
- Variable/Measures of interest:
 - Lateral acceleration
 - Articulation angle

Results:



Figure 42 Articulation Angle for different levels of fifth-wheel friction

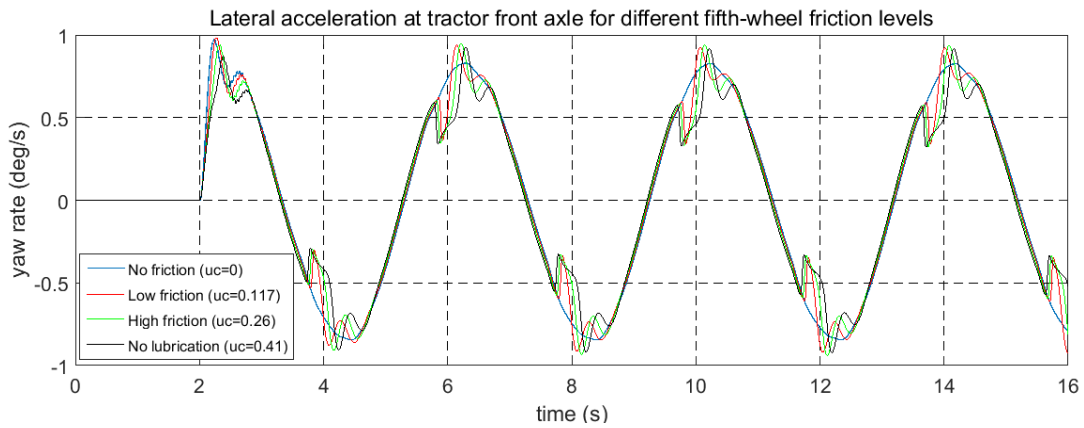


Figure 43 Lateral Acceleration for different levels of fifth-wheel friction

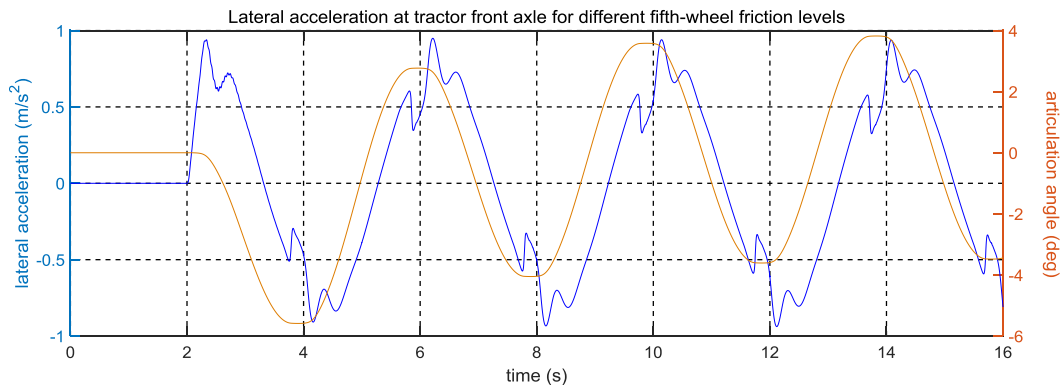


Figure 44 Lateral acceleration and articulation angle for $\mu_c=0.26$

With the increase in friction co-efficient the peak articulation angle achieved decreases, the reduction reaching a maximum of 24%, in case of 'No Lubrication'. With the implementation of fifth-wheel model, the articulation angle shows saturation at the peaks, indicating the advent of stick phase and subsequent transition into slip phase. As expected, the duration of stick phase also increases with friction co-efficient, as more resistive moment has to be overcome before sliding.

The sudden change in the articulation upon entry into the stick phase reduces the instantaneous acceleration, due to increased friction moment and the exit from the stick phase results in an increase in the acceleration, as the friction moment begins to drop. This can be seen in the minor peaks in the acceleration plot.

9.2 Different road friction level with constant fifth-wheel friction

- Test Conditions:
 - Vehicle: Tractor-semitrailer (with 2- and 3-axles respectively).
 - Longitudinal vehicle velocity=10 km/hr.
 - Steering input=10° sinusoidal input at the wheels(slalom test)
 - Fifth-wheel load=11500 kg
- Road friction Levels:
 - Concrete road ($\mu=0.9$)
 - Asphalt ($\mu=0.8$)
 - Snow ($\mu=0.2$)
 - Ice ($\mu=0.05$)
- Variable/Measures of interest:
 - Lateral acceleration
 - Articulation angle

Results:

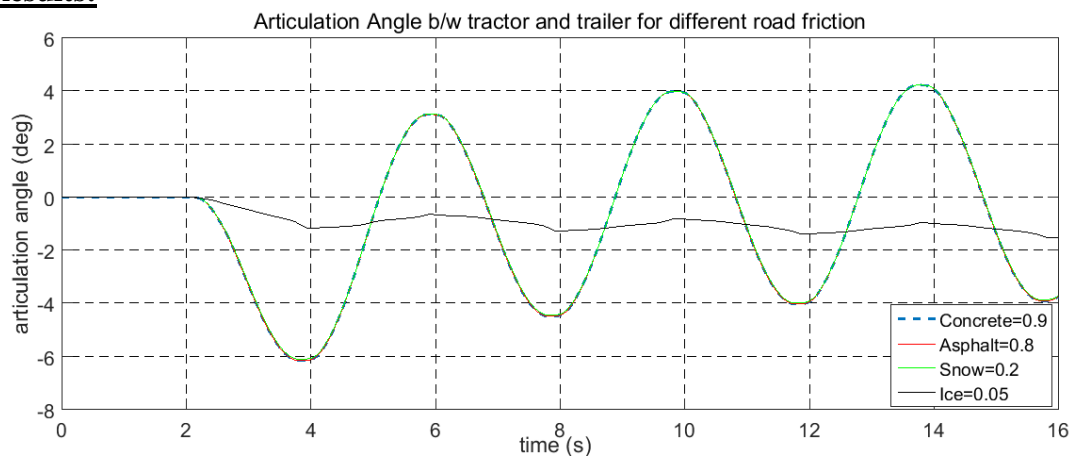


Figure 45 Articulation Angle as a function of time for different levels of road friction

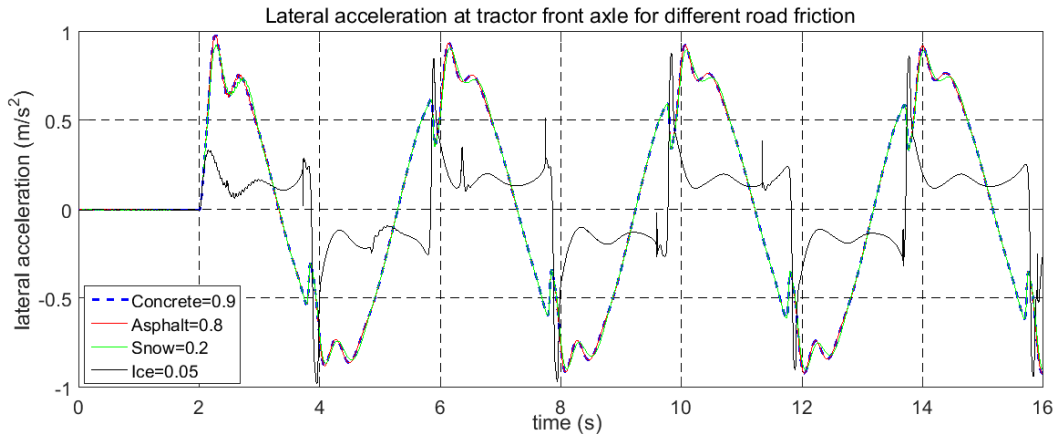


Figure 46 Lateral Acceleration as a function of time for different levels of road friction

The change in road friction does not show any effect on the vehicle behavior, except when driving on ice, which has been dealt separately in section 9.6.

9.3 Slow ramp steer

- Test Conditions:
 - Vehicle: Tractor-semitrailer (with 2- and 3-axes respectively).
 - Longitudinal vehicle velocity=70 km/hr.
 - Fifth-wheel load=11500 kg/16500 kg
- Fifth-wheel friction Level:
 - High friction($\mu_c=0.26$)
- Variable/Measures of interest:
 - Path of tractor front axle and trailer rearmost axle.
 - Lateral acceleration
 - Articulation angle

Results:

For fifth-wheel load=11500 kg

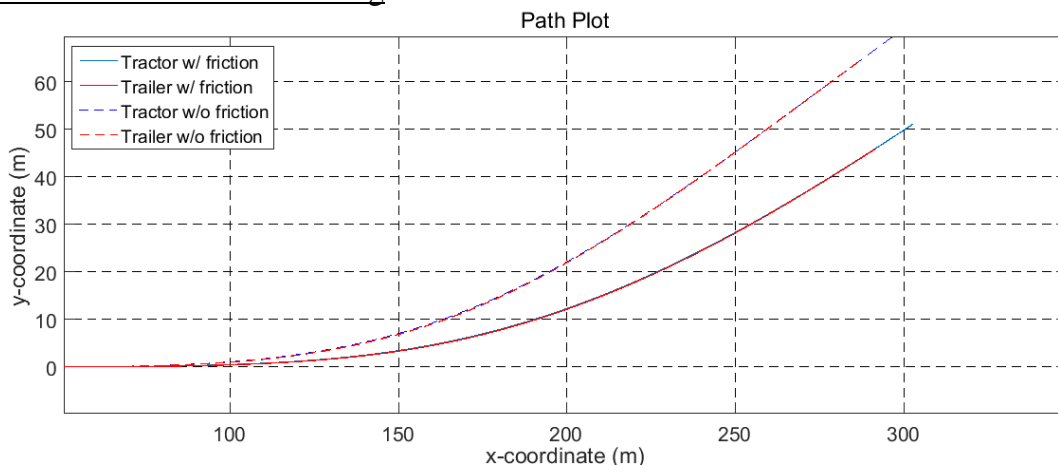


Figure 47 Tractor and trailer path under ramp steer

For fifth-wheel load=16500 kg

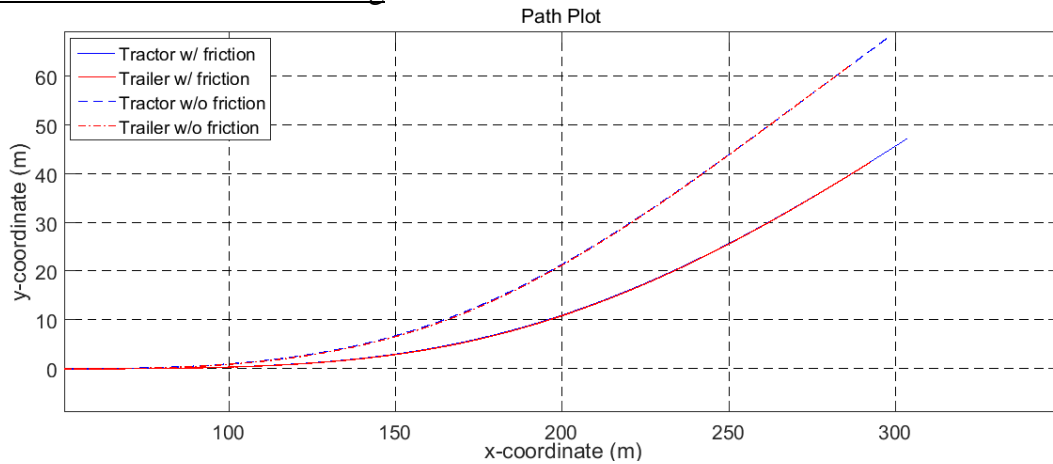


Figure 48 Tractor and trailer path under ramp steer

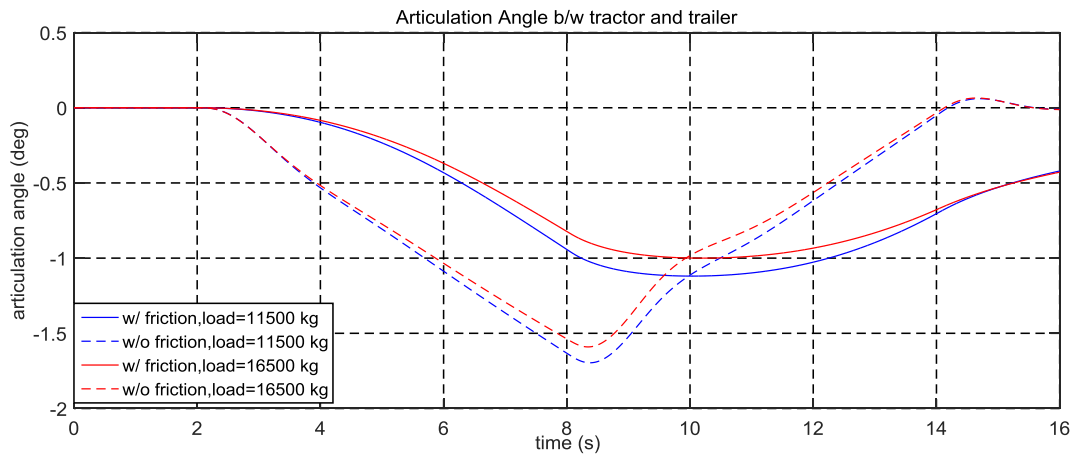


Figure 49 Articulation Angle as a function of time for ramp steer

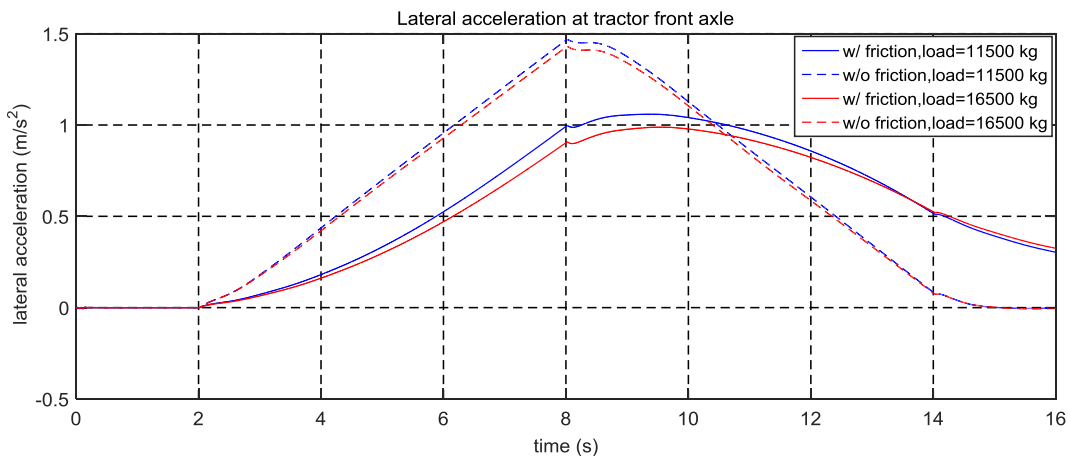


Figure 50 Lateral Acceleration as a function of time for ramp steer

The articulation angle achieved is reduced with the implementation of friction model and also shows a delay when compared to its counterpart. The amount of reduction, as seen previously, is influenced by the friction coefficient while the delay is attributed to the relaxation factor k , with increasing delay observed for higher values of relaxation factor. The effects of relaxation factor and friction coefficient are also reflected in acceleration and trajectory followed.

The acceleration at the end ($t=16$ s) is non-zero, this follows from the articulation angle ~ 0.5 deg, indicating that the vehicle needs to drive more in order to align itself.

Parameters (Peak Values)	load=11500 kg		load=16500 kg	
	w/ friction	w/o friction	w/ friction	w/o friction
y-position (tractor) [m]	51.175	69.798	47.385	67.988
articulation angle [deg]	-1.12	-1.696	-1	-1.590
lateral acceleration [m/s^2]	1.065	1.468	0.989	1.429

9.4 J-turn

- Test Conditions:
 - Vehicle: Tractor-semitrailer (with 2- and 3-axles respectively).
 - Longitudinal vehicle velocity=30 km/hr.
 - Fifth-wheel load=11500 kg/16500 kg
- Fifth-wheel friction Level:
 - High friction($\mu_c=0.26$)
- Variable/Measures of interest:
 - Path of tractor front axle and trailer rearmost axle.
 - Lateral acceleration
 - Articulation angle

Results:

For fifth-wheel load=11500 kg

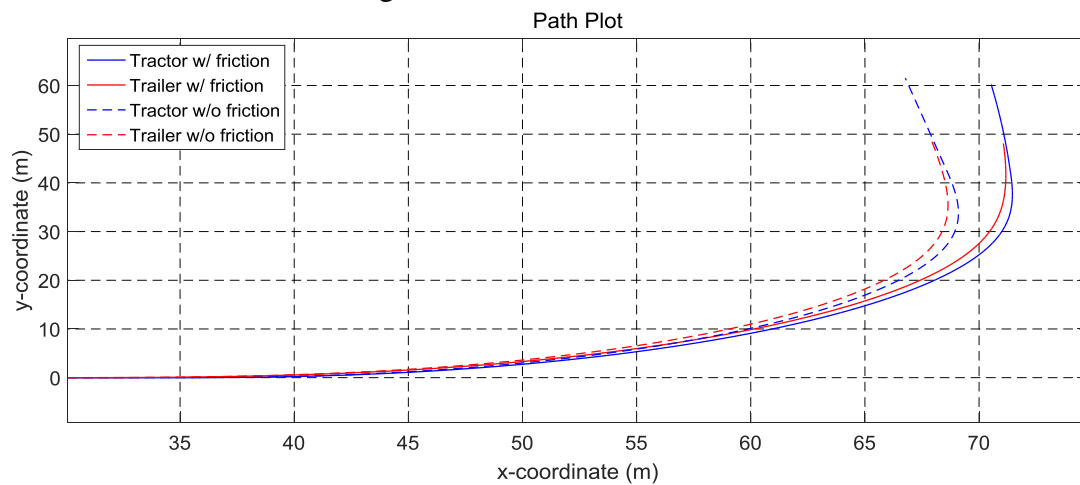


Figure 51 Tractor and trailer path under J-turn

For fifth-wheel load=16500 kg

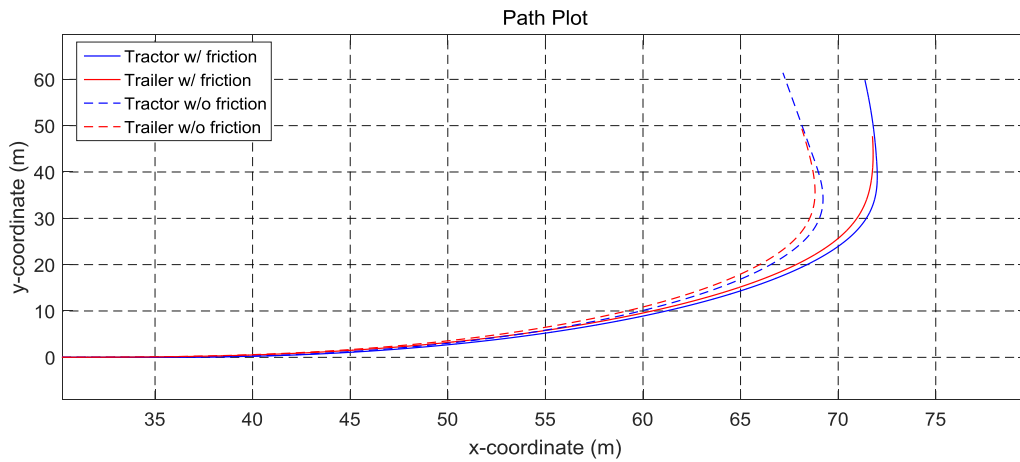


Figure 52 Tractor and trailer path under J-turn

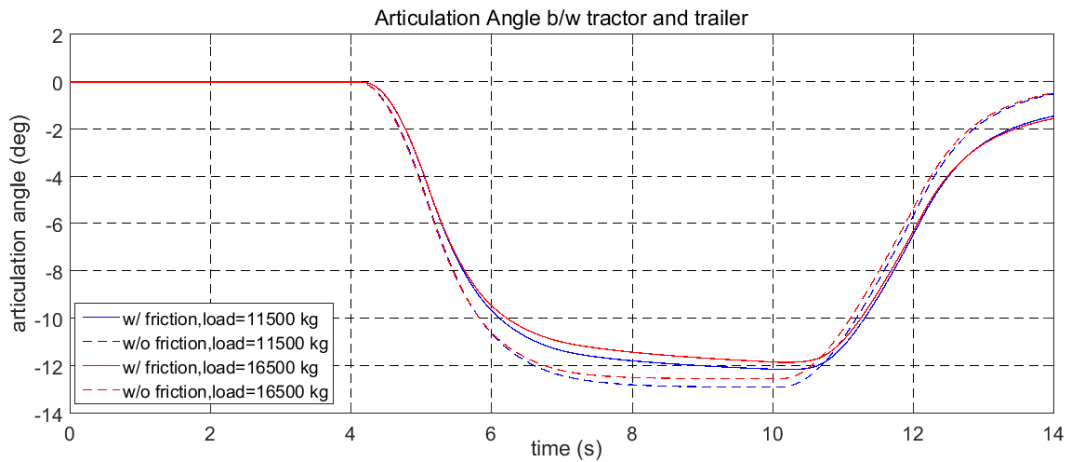


Figure 53 Articulation Angle as a function of time for J-turn

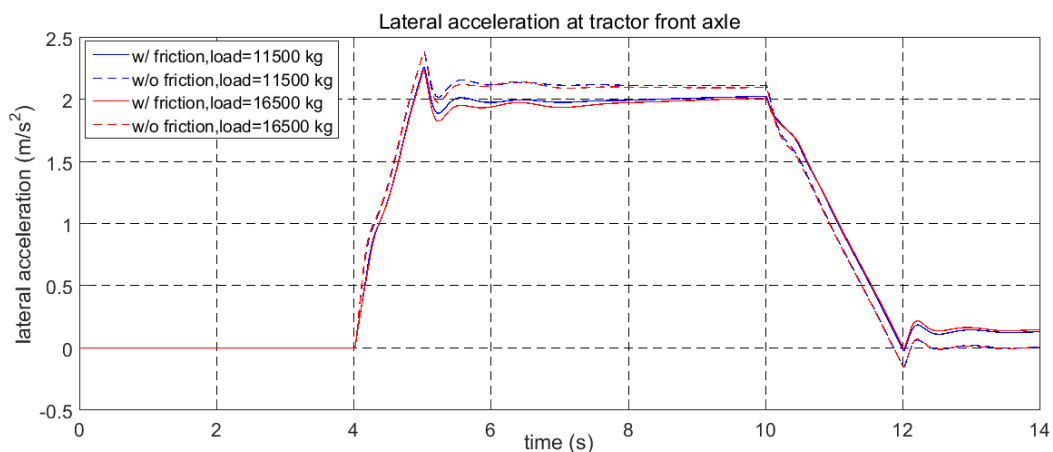


Figure 54 Lateral Acceleration as a function of time for J-turn

The articulation angle achieved is reduced with the implementation of friction model and also shows a delay when compared to its counterpart. The amount of reduction, as seen previously, is influenced by the friction coefficient while the delay is attributed to the relaxation factor k , with increasing delay observed for higher values of relaxation factor. The effects of relaxation factor and friction coefficient are also reflected in acceleration and trajectory followed.

The acceleration at the end ($t=14$ s) is non-zero, this follows from the articulation angle ~ 2 deg, indicating that the vehicle needs to drive more in order to align itself, i.e. articulation angle = 0 deg. The overshoot of acceleration shows improvement which increases for heavier loads.

Parameters (Peak Values)	load=11500 kg		load=16500 kg	
	w/ friction	w/o friction	w/ friction	w/o friction
y-position (tractor)	60.204	61.504	59.841	61.419
articulation angle (deg)	12.143	12.886	11.839	12.533
lateral acceleration (m/s^2)	2.261	2.386	2.236	2.382
Overshoot (%)	11.483	12.49	10.96	13.536

9.5 Lane change

- Test Conditions:
 - Vehicle: Tractor-semitrailer (with 2- and 3-axles respectively).
 - Longitudinal vehicle velocity=50 kmph/80 kmph
 - Fifth-wheel load=11500 kg/16500 kg
 - Steering input= sinusoidal for one time period
- Fifth-wheel friction Level:
 - High friction($\mu_c=0.26$)
- Variable/Measures of interest:
 - Path of tractor front axle and trailer rearmost axle.
 - Lateral acceleration
 - Articulation angle

Lane change@50 kmph

For fifth-wheel load=11500 kg

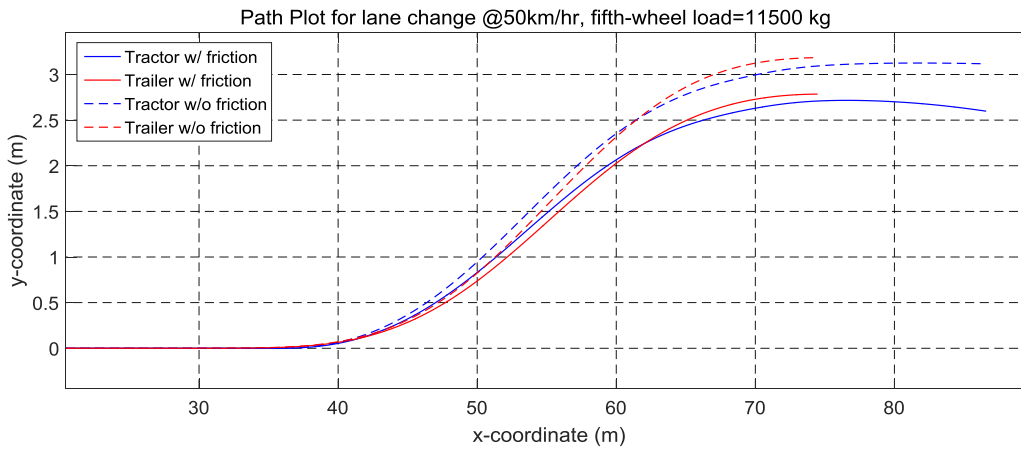


Figure 55 Tractor and trailer path under lane change for fifth-wheel load=11500 kg

For fifth-wheel load=16500 kg

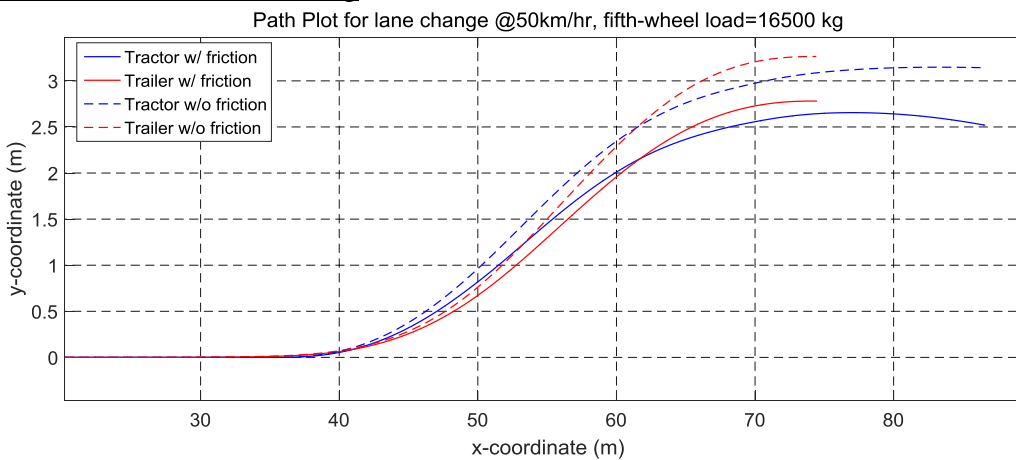


Figure 56 Tractor and trailer path under lane change for fifth-wheel load=16500 kg

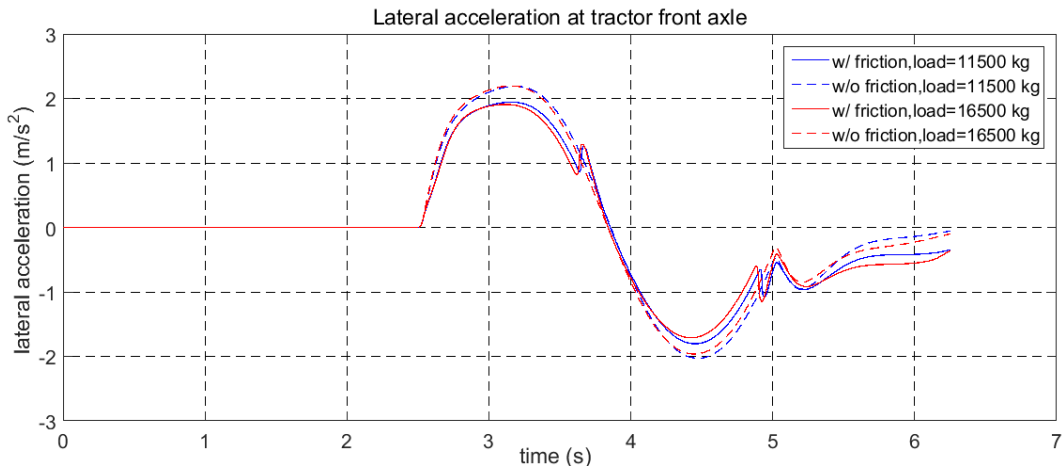


Figure 57 Lateral Acceleration as a function of time for lane change @ 50 kmph

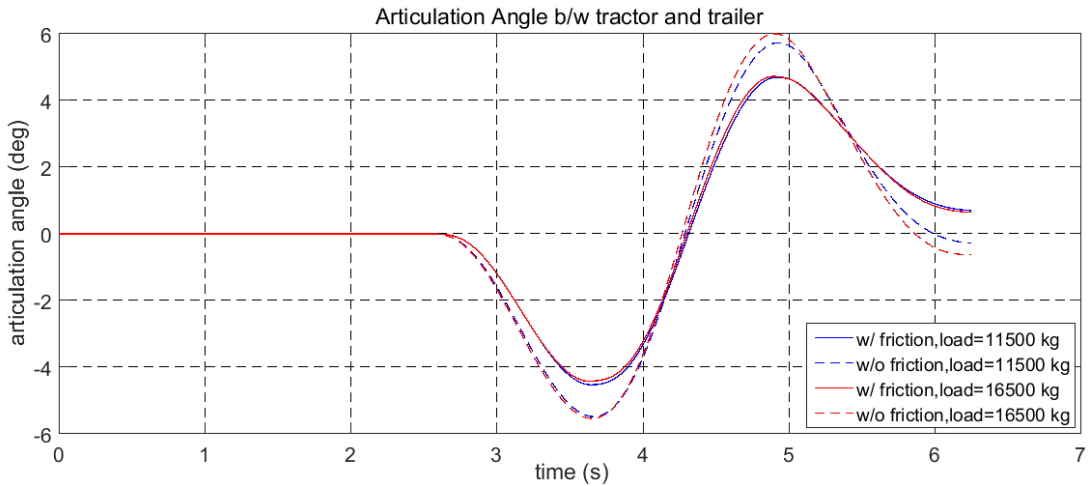


Figure 58 Articulation Angle as a function of time for lane change @ 50 kmph

The articulation angle achieved is reduced with the implementation of friction model and also shows a delay when compared to its counterpart. The acceleration at the end ($t=14$ s) is non-zero, this follows from the articulation angle = 0.8 deg, indicating that the vehicle needs to drive more in order to align itself, i.e. articulation angle = 0 deg. The increase in acceleration seen at $t=3.63$, is due to the stick-slip behavior.

Lane change @ 50 kmph (Peak Values)	load=11500 kg		load=16500 kg	
	w/ friction	w/o friction	w/ friction	w/o friction
y-position (tractor)	2.716	3.125	2.655	3.148
articulation angle (deg)	4.699	5.733	4.724	5.999
lateral acceleration (m/s ²)	1.942	2.188	1.907	4.729

Lane change @80 kmph

For fifth-wheel load=11500 kg

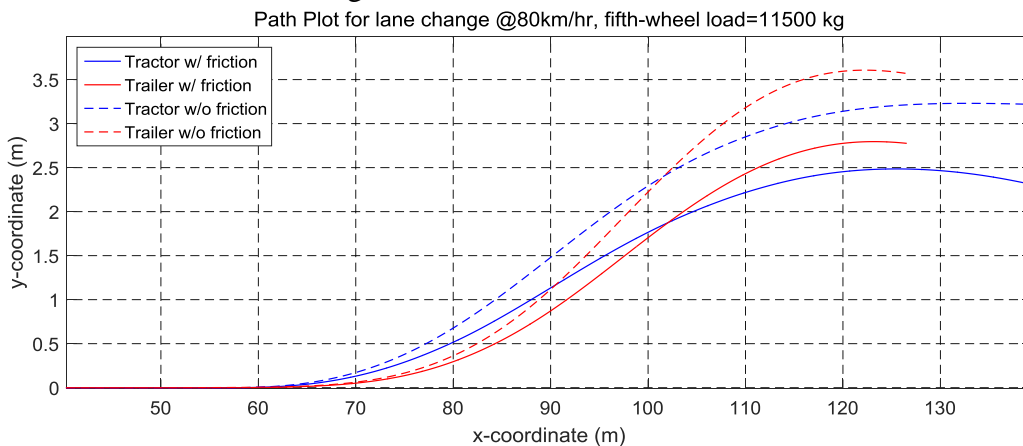


Figure 59 Tractor and trailer path under lane change for fifth-wheel load=11500 kg

For fifth-wheel load=16500 kg

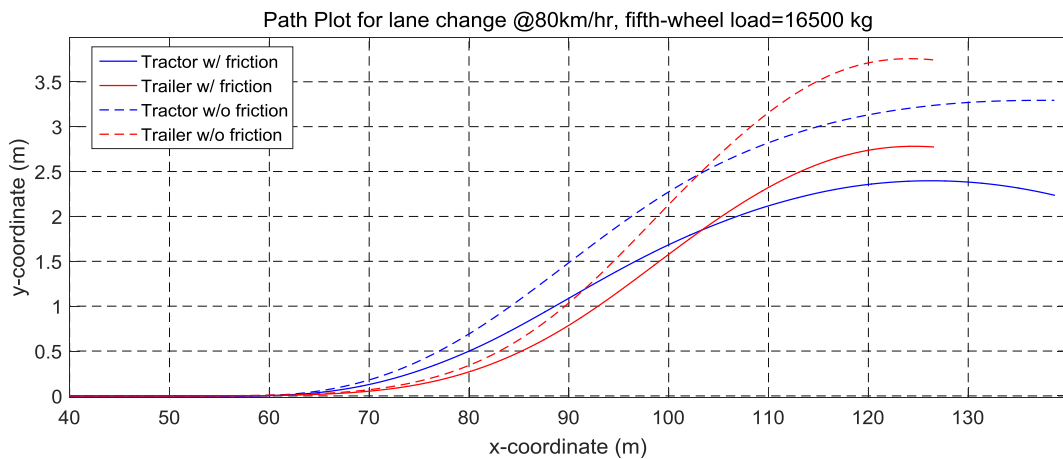


Figure 60 Tractor and trailer path under lane change for fifth-wheel load=16500 kg

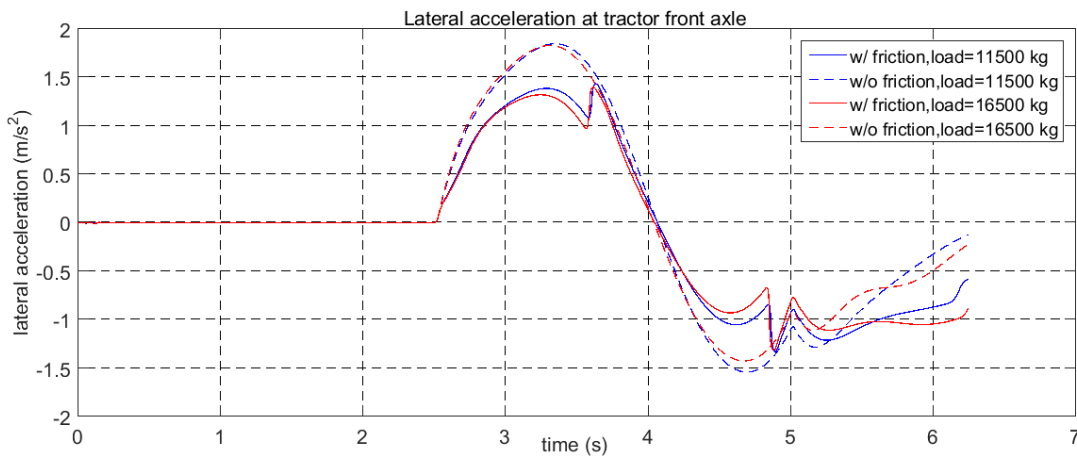


Figure 61 Lateral Acceleration as a function of time for lane change @ 80 kmph

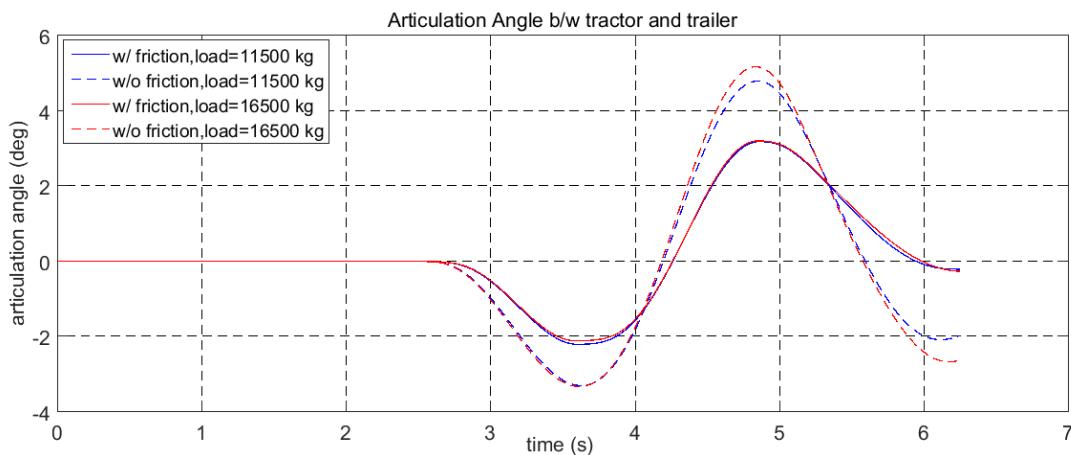


Figure 62 Articulation Angle as a function of time for lane change @ 80 kmph

The effects are amplified as the load and velocity increases.

Lane change @80kmph (Peak Values)	load=11500 kg		load=16500 kg	
	w/ friction	w/o friction	w/ friction	w/o friction
y-position (tractor)	2.485	3.230	2.397	3.293
articulation angle (deg)	3.185	4.792	3.203	5.171
lateral acceleration (m/s ²)	1.436	1.847	1.397	1.829

9.6 Driving on ice

High friction at the fifth-wheel reduces the free movement of trailer resulting in a stabilized motion at slow speeds. (Even when friction is considered, jackknifing occurs at 23km/hr)

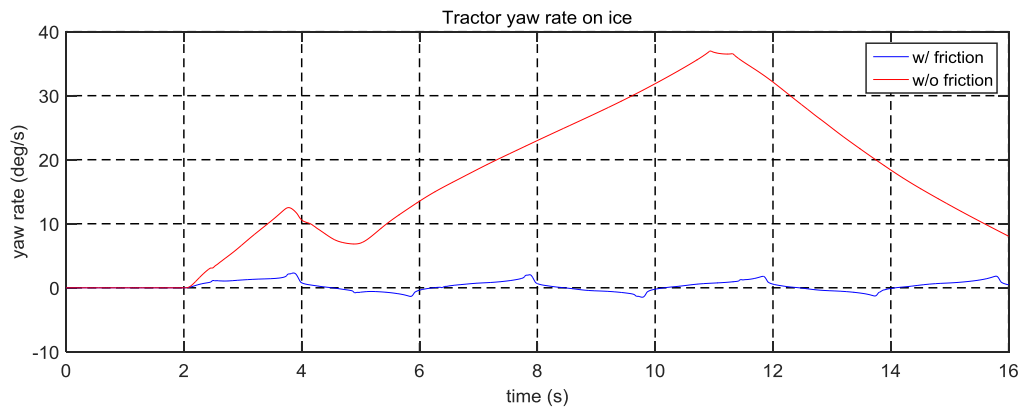


Figure 63 Tractor and yaw rate driving over ice

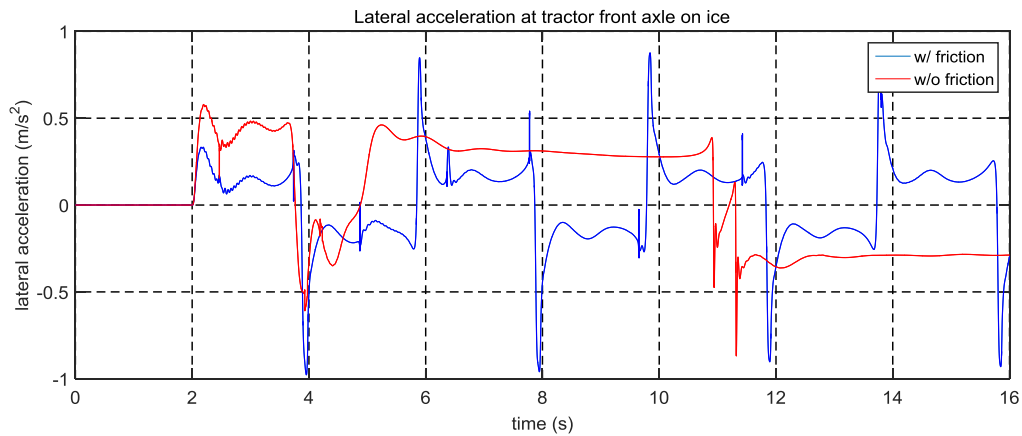


Figure 64 Lateral Acceleration as a function of time driving over ice

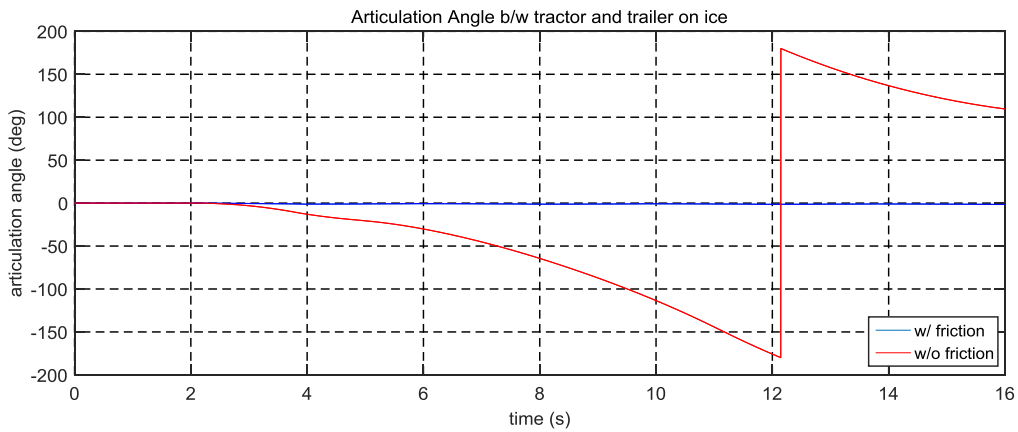


Figure 65 Articulation Angle as a function of time driving over ice

The frictional resistance

9.7 Roll Behavior

The influence of fifth-wheel roll compliance was studied for the following two cases:

1. Medium Load Height (platform laden height=3.5m)
2. High Load Height (platform laden height=4.0m)

This changes the height of C.o.G of the trailer. The vehicle combination of tractor-semitrailer was steered until all the inner wheels lift-off. The load on the fifth-wheel is kept constant at 11500 kg.

9.7.1 Medium Load Height

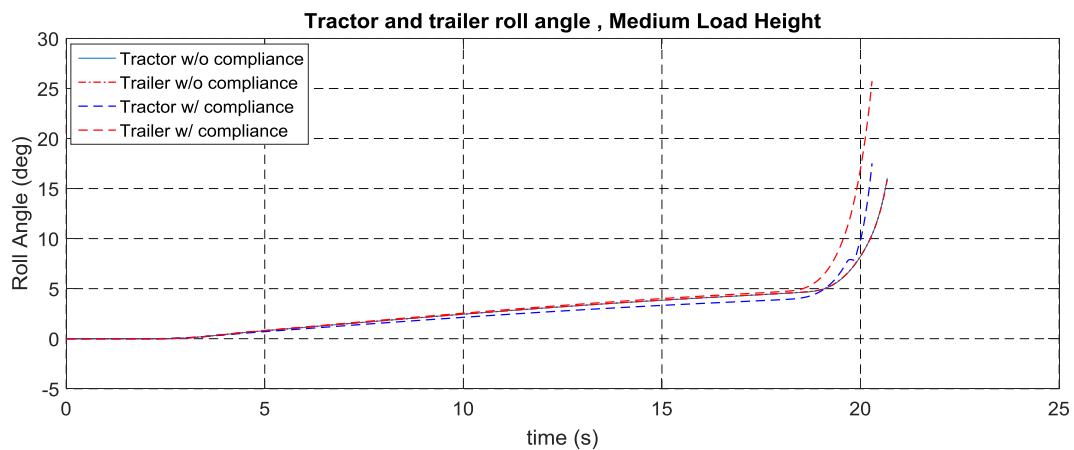


Figure 66 Tractor and Trailer roll behavior, medium load height

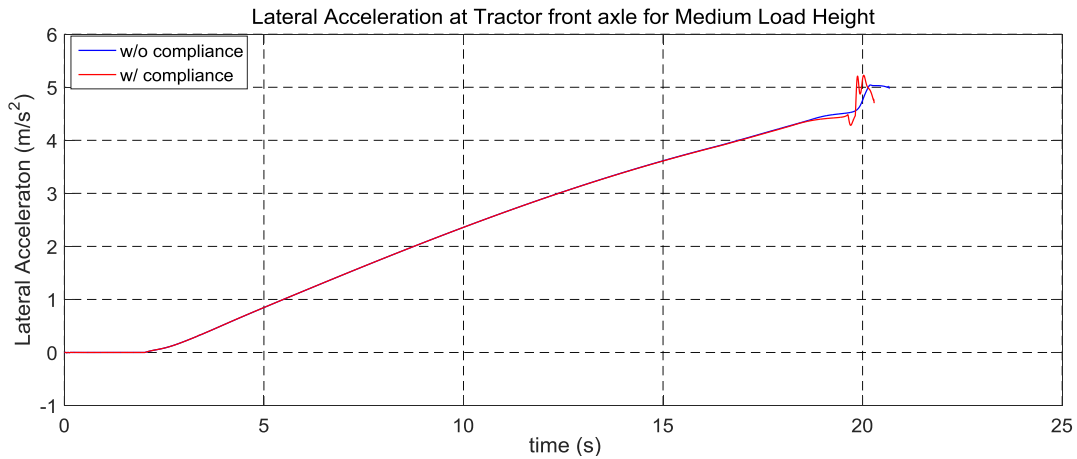


Figure 67 Lateral Acceleration at Tractor front axle for Medium Load Height

In the absence of fifth-wheel roll compliance the roll angle of the trailer increase together and to the same values before roll over. In comparison, with the introduction of fifth-wheel compliance the roll motion of the trailer shows larger roll angle than the tractor, which is expected on account of its higher C.o.G. During fifth-wheel lash the tractor roll angle remains nearly constant, increasing once the lash is consumed and the bump stop makes contact.

The corresponding effect is seen on lateral acceleration as it decreases during the lash period. As explained earlier, during this period the trailer is free rolling over the fifth-wheel, reducing the effective mass rolling over the drive axle and consequently reducing the lateral acceleration.

At the end of the lash, when the bump stop makes contact the sudden increases in roll resistance result in the small oscillation seen towards the end, before rollover. The limiting acceleration at roll over is lowered by 5.43%

w/o fifth-wheel compliance (m/s ²)	w/ fifth-wheel compliance (m/s ²)	Error*(%)
4.97	4.7	-5.43

9.7.2 High Load Height

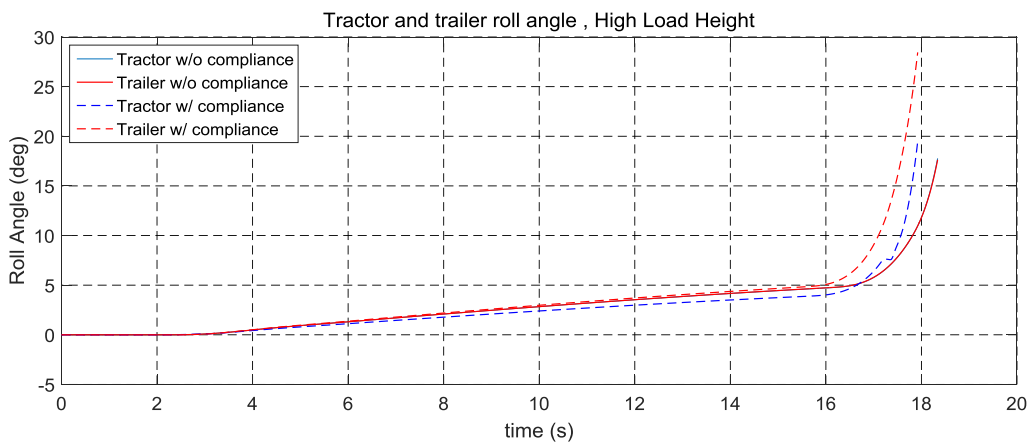


Figure 68 Tractor and Trailer roll behavior, high load height

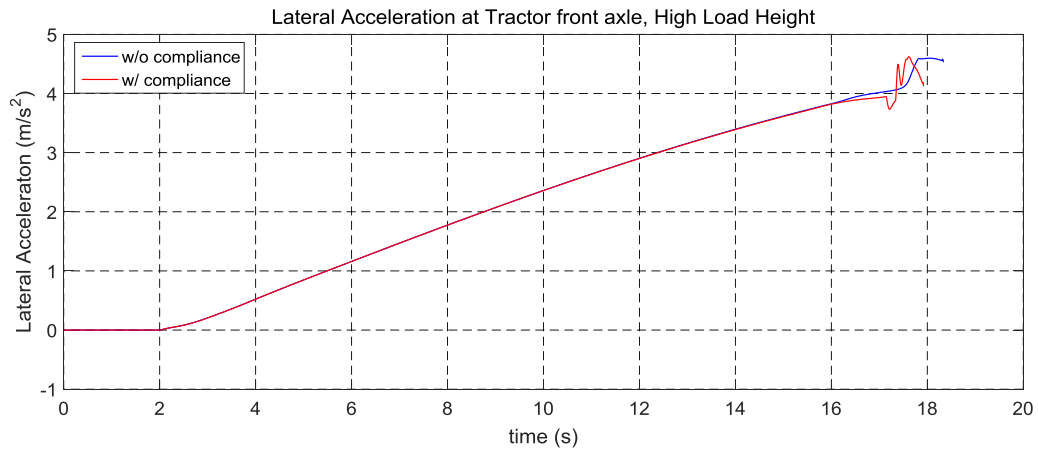


Figure 69 Lateral Acceleration at Tractor front axle for High Load Height

In addition to the earlier observations, with the increase in load height, the rollover occurs earlier and at lower lateral acceleration. The limiting acceleration at roll over is lowered by 6.16% .

w/o fifth-wheel compliance (m/s²)	w/ fifth-wheel compliance (m/s²)	Error*(%)
4.43	4.157	-6.16

10. Conclusion

The thesis work provides a fifth-wheel model based on the physical interaction of the fifth-wheel with the trailer as well as the tractor (or dolly). This is done by taking into account the effects of bushing at the interface with the tractor and in case of trailer by including friction moment along with the coupling forces at the kingpin. In roll plane, a roll stiffness for the fifth-wheel is introduced

For the fifth-wheel under study, it was observed that the bushings did not have any significant influence on the vehicle behavior and were dropped from subsequent analysis. The friction model is developed, which is empirical in nature, i.e. the model is governed by measurement data. The friction interaction is found to have dry friction and viscous governing components. The model makes use of five parameters and can demonstrate the stick-slip phenomena. Out of the five parameters needed, two come from system design, i.e. loading condition and the design of fifth-wheel, while the others depend on the condition of lubrication at the fifth-wheel-trailer interface.

The roll behavior is influenced by the design of the fifth-wheel as the lash, a design parameter, decides the amount of free play of the trailer before rolling along with the tractor (dolly) as one lumped unit. A compromise is made to approximate the roll characteristic, preventing the simulation from being bogged down due to high frequency oscillations, when the bump stop come into contact.

The influence of fifth-wheel model on vehicle behavior is analyzed and shows reduced levels of articulation angle with the change being directly influenced by the friction at play on the interface. The maximum reduction in amplitude of articulation angle is seen when running a dry contact between the trailer and the fifth-wheel (24%).

In comparison to the model without friction, the articulation angle shows an offset or residue, depending on the relaxation factor, indicating that the need of further steering to align itself.

The most interesting behavior is observed when driving on ice, in the absence of fifth-wheel friction jack-knifing occurs even at low vehicle speeds (10 km/hr) whereas, with the introduction of friction an additional resistance is provided and the motion is stabilized. It should, however, be noted that friction could not prevent from jack-knifing at higher vehicle speed (~25 km/hr and above).

The influence on roll behavior is as predicted, the tractor and trailer shown different roll angle which are compensated by the fifth-wheel. The magnitude of tractor roll angle is always lower when compared to the trailer, on account of its lower center of gravity height. The decrease in limiting acceleration, with roll compliance, is consistent with the findings of Law [35]. Their analysis predicts an 11.62 % reduction in the limiting acceleration, under similar loading conditions, against 10.8% reduction obtained above with an error of less than (1%).

References

- [1] H. Backman and R. Nordström, "Improved Performance of European Long Haulage Vehicles," TFK-Transport Research Institute, 2002.
- [2] J. Woodrooffe and L. Ash, "Economic Efficiency of Long Combination Transport Vehicles in Alberta," Woodrooffe & Associates, 2001.
- [3] J. Aurell and T. Wadman, "Vehicle Combination Based on the Modular Concept," Nordiska Vägteknisk Förbundet (Nordic Road Association), 2007.
- [4] I. Åkerman and R. Jonsson, "European Modular System for Road Freight Transport – Experiences and Possibilities," TFK-Transport Research Institute, Report 2007:2E, 2007.
- [5] G. Svenson and C. Lofroth, "ETT – Modulsystem för skogstransporter (One More Stack - Modular Combination for Timber Transport)," Skogforsk, Report NR 723, 2010.
- [6] R. D. Ervin, P. Fancher and T. Gillespie, "An overview of the dynamic performance properties of long truck combinations," The University of Michigan, Ann Arbor, Transportation Research Institute., 1984.
- [7] R. Ervin and Y. Guy, "Influence of Weights and Dimensions on the Stability and Control of Heavy-Duty Trucks in Canada."
- [8] R. Ervin and C. C. MacAdam, "The Dynamic Response of Multiply-Articulated Truck Combinations to Steering Input," *SAE Paper No. 820973*, August 1982.
- [9] P. Fancher, "The Transient Directional Response of Full Trailers," *SAE Paper No. 821259*, November 1982.
- [10] F. Jindra, "Lateral Oscillations of Trailer Trains," *Ingenieur- Archiv*, no. XXXIII, 1964.
- [11] F. Jindra, "Off tracking of Tractor-Trailer Combinations," *Automobile Engineer*, pp. 96-101, March 1963,.
- [12] J. P. Pauwelussen, *Essentials of Vehicle Dynamics*, Elsevier Ltd, 2015.
- [13] S. Monsma, *MAS AVD 1617 7 Handling Behavior part 1*, 2016.
- [14] H. Pacejka, *Tire and Vehicle Dynamics*, Oxford: Elsevier Butterworth-Heinmann, 2004.
- [15] U. Kiencke, *Automotive control systems*, Berlin: Springer, 2005.
- [16] A. Andersson, S. Söderberg and S. Björklund, "Friction models for sliding dry, boundary and mixed lubricated contacts," *Tribol Int*, no. 40, p. 580–587, 2007.

- [17] P. Dahl, A solid friction model, El Segundo, California: The Aerospace Corporation, 1968.
- [18] F. B. Haessig D.A., On the modeling and simulation of friction, 113 ed., Journal of Dynamics System Measurement and Control, 1991, pp. 352-364.
- [19] C. Canudas de Wit, H. Olsson, K. Åström and P. Lischinsky, A new model for control of systems with friction, 40 ed., IEEE Trans Autom Control, 1995, pp. 419-425.
- [20] H. Olsson, K. Åström, C. Canudas deWit, M. Gäfvert and P. Lischinsky, Friction models and friction compensation, Eur J Control 4, 1998, pp. 176-195.
- [21] R. Stribeck, Die wesentlichen Eigenschaften der Gleitund Rollenlager, 46 ed., Die wesentlichen Eigenschaften der Gleitund Rollenlager, 1902, pp. 1342-1348.
- [22] L. Bo and D. Pavelescu, The friction-speed relation and its influence on the critical velocity of stick-slip motion., Wear 82, 1982, p. 277-289.
- [23] B. Armstrong-Hélouvry, Control of machines with friction, Norwell: Kluwer Academic Publishers, 1991.
- [24] D. Karnopp, Computer simulation of stick-slip friction in mechanical dynamic systems, J Dyn Syst Meas Control 107, 1985, pp. 100-103.
- [25] D. Threlfall, "The inclusion of Coulomb friction in mechanisms programs with particular reference to DRAM," *Mechanism and Machine Theory*, vol. 13, pp. 475-483, 1978.
- [26] M. Bengisu and A. Akay, "Stability of friction-induced vibrations in multi-degree-of-freedom systems," *Journal of Sound and Vibration*, vol. 4, no. 171, pp. 557-570, 1994.
- [27] J. Awrejcewicz, D. Grzelczyk and Y. Pyryev, "A novel dry friction modeling and its impact on differential equations computation and Lyapunov exponents estimation," *Journal Vibroengineering*, no. 10, pp. 475-482, 2008.
- [28] I. Adamiec-Wójcik, J. Awrejcewicz, W. Grzegózek and S. Wojciech, Dynamical Systems - Mathematical and Numerical Approaches, TU of Lodz, 2015, pp. 11-20.
- [29] E. Mikulcik, "The Dynamics of Tractor-Semitrailer vehicle: The Jackknifing Problem," *SAE*, 1971.
- [30] R. Hibbeler, Engineering Mechanics-Statics and Dynamics, 6 ed., Toronto, Canada: Maxwell Macmillian, 1992.
- [31] P. Fancher and et.al., "Tracking and Stability of Multi-Unit Truck Combinations," Ann Arbor, MI, 1984.
- [32] P. Fancher, "Directional Dynamics Considerations for Multi-Articulated, multi-Axled Heavy Vehicles," *SAE International*, pp. 19-29, 1989.

- [33] American Society for Testing and Materials, Annual Book of ASTM Standards, vol. 14.02., 2015.
- [34] I. Ibrahim, "Design of a compensating fifth-wheel for improving the roll dynamic behavior of the tractor semi-trailers," SAE Technical Paper, 2002.
- [35] E. Law, "Effects of tire and vehicle design characteristics on rollover of tractor semi-trailers," Department of Mechanical Engineering, Clemson University, 2003.
- [36] Mathworks Inc., [Online]. Available:
<https://se.mathworks.com/help/matlab/ref/ode23tb.html>.

Appendix A

Representative Vehicle Model Static Load Calculation

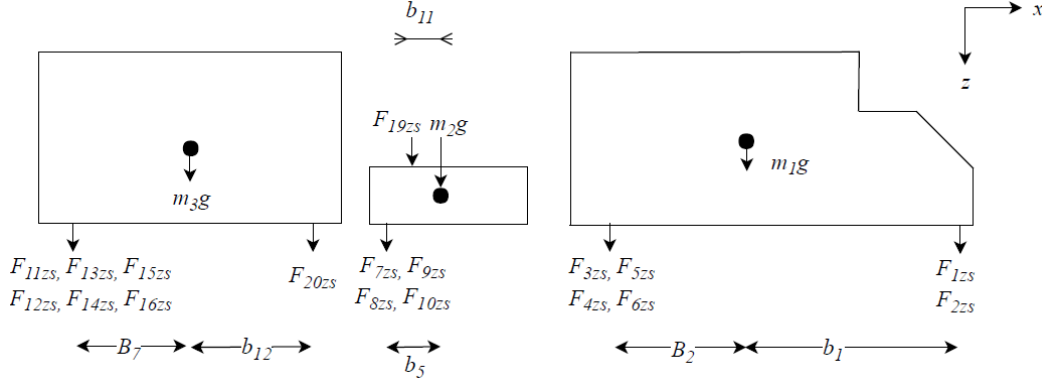


Figure A. 1 Static Loading

where, B_7 and B_2 are the distances of equivalent axle from respective C.o.G for the axle groups.

$$B_2 = b_2 + (b_3 - b_2) * (1 - \text{load ratio}) \quad (\text{A.1})$$

$$B_7 = (b_6 + b_7 + b_8)/3 \quad (\text{A.2})$$

Applying force and moment balancing on the forces as shown in the figure above.

The following relations can be derived:

$$F_1 = F_{1zs} + F_{2zs} \quad (\text{A.3})$$

$$F_3 = F_{3zs} + F_{4zs} + F_{5zs} + F_{6zs} \quad (\text{A.4})$$

$$F_7 = F_{7zs} + F_{8zs} + F_{9zs} + F_{10zs} \quad (\text{A.5})$$

$$F_{11} = F_{11zs} + F_{12zs} + F_{13zs} + F_{14zs} + F_{15zs} + F_{16zs} \quad (\text{A.6})$$

For semi-trailer:

$$F_{11} + F_{20zs} + m_3g = 0 \quad (\text{A.7})$$

$$F_{11}B_7 = F_{20zs}b_{12} \quad (\text{A.8})$$

For dolly:

$$F_7 + F_{19zs} + m_2g = 0 \quad (\text{A.9})$$

$$F_7b_5 + F_{19zs}b_{11} = 0 \quad (\text{A.10})$$

$$F_{19zs} = -F_{20zs} \quad (\text{A.11})$$

For truck:

$$F_1 + F_3 + m_1g = 0 \quad (\text{A.12})$$

$$F_3B_2 = F_1b_1 \quad (\text{A.13})$$

The equations (A.1)-(A.13) can be solved to give the following expressions for the static loads, F_{izs} is the static load on the i^{th} tire.

Appendix B

The details case-by-case analysis of the scenarios mentioned in Chapter 6 are discussed and then the result of parameter determination are presented.

Scenario 1

Normal force=9 tons, longitudinal velocity=10km/hr, lubricant=base, surface wear=base

The test was conducted with kingpin pressure/normal load at fifth wheel =9050 kg, at low longitudinal velocity of 10 km/hr while giving small sinusoidal input. The lubrication at the fifth-wheel was estimated to be between fresh lubrication and dry lubrication, the state in which it remains for most of the time (Subjective impression by Niklas).

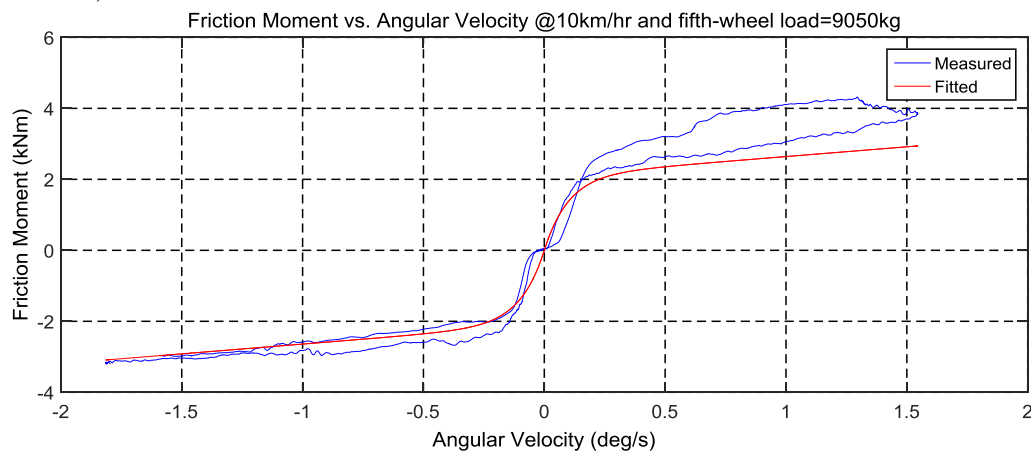


Figure B. 1 Friction moment vs. Angular velocity, fifth-wheel load=9050 kg

Observations:

From the figure, it can be seen that, the friction moment increases with angular velocity reaching the maximum values of ± 3.5 kNm. The increase has two components. The first part is an exponential rise with velocity and the second part is a linear increment with velocity.

The increase in friction moment when velocity reverses at the $+1.5$ deg/s, is not observed in any other case and is concluded to be an outlier and neglected from analysis.

Fitted parameters:

μ_{sat}	0.0612
b	55
k	10

Scenario 3

Normal force=16 tons, longitudinal velocity=10 km/hr, lubricant=new, surface wear=worn

The test was conducted with kingpin pressure/normal load at fifth wheel =16500 kg, at low longitudinal velocity of 10 km/hr while giving small sinusoidal input. The existing lubrication at the fifth-wheel was removed and fresh lubrication was applied.

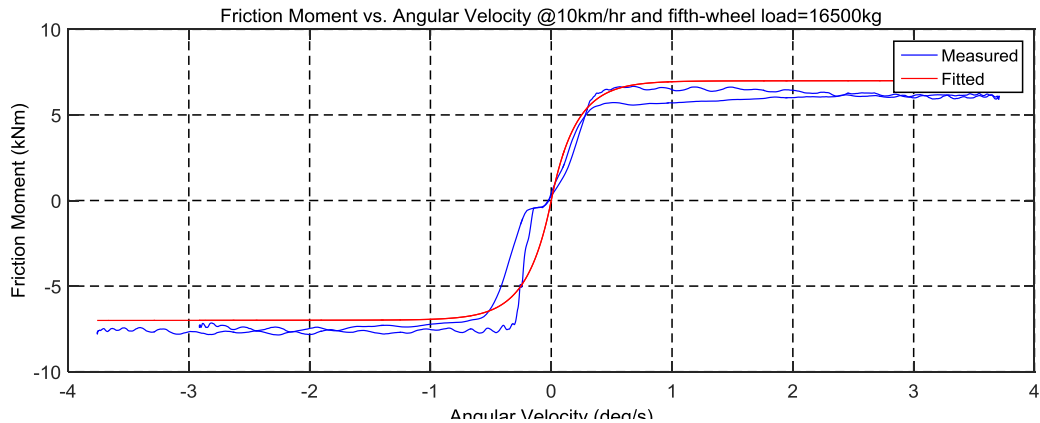


Figure B. 2 Friction moment vs. Angular velocity, fifth-wheel load=16500 kg

Observations:

From the figure, it can be seen that, the friction moment increases with velocity, reaching the maximum values of ± 6.5 kNm. The increase is not linear and has two components.

Fitted parameters:

μ_{sat}	0.117
b	5
k	5

Scenario 4

Normal force=9 tons, longitudinal velocity=10km/hr, lubricant=dry, surface wear=base

The test was conducted with kingpin pressure/normal load at fifth wheel =9050 kg, at low longitudinal velocity of 10 km/hr while giving small sinusoidal input. The existing lubrication at the fifth-wheel was removed and test was conducted without any lubrication at the fifth-wheel.

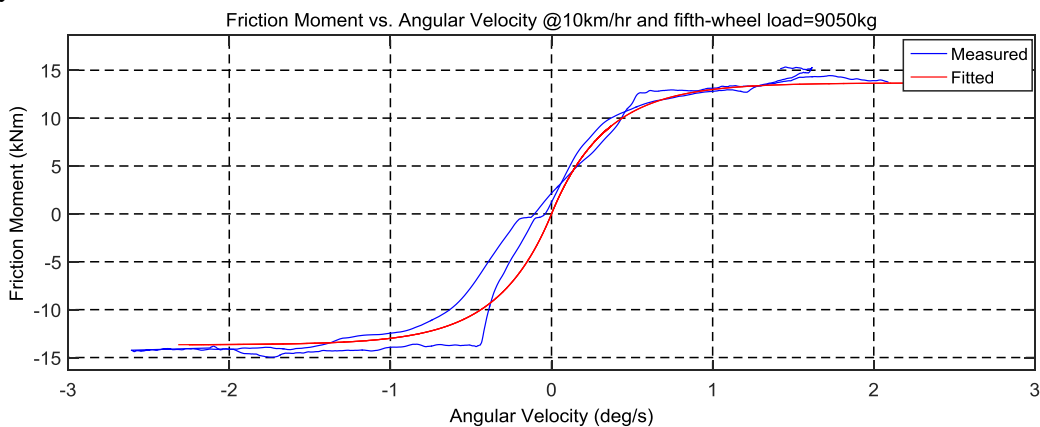


Figure B. 3 Friction moment vs. Angular velocity, fifth-wheel load=9050 kg, no lubrication

Observations:

From the figure, it can be seen that, the friction moment increases with velocity, reaching the maximum values of ± 14 kNm. The increase is exponential with velocity. The rate of increase is lower as compared to other cases.

Fitted parameters:

μ_{sat}	0.41
b	0
k	3

Scenario 5

Normal force=9 tons, longitudinal velocity=80km/hr, lubricant=base, surface wear=base

The test was conducted with kingpin pressure/normal load at fifth wheel =9050 kg, at longitudinal velocity of 80 km/hr while giving small sinusoidal input. The lubrication is the same as in Scenario 1.

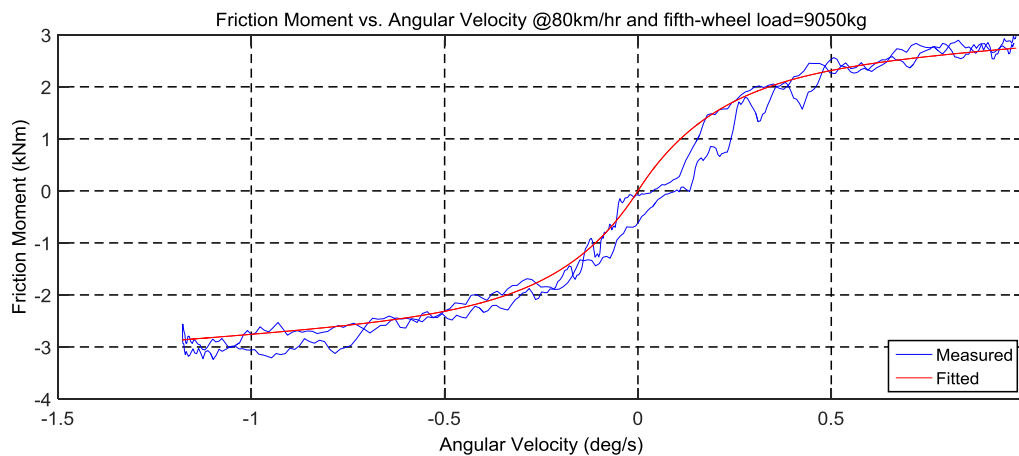


Figure B. 4 Friction moment vs. Angular velocity, fifth-wheel load=9050 kg

Observations:

From the figure, it can be seen that, the friction moment increases with velocity, reaching the maximum values of ± 3 kNm. The increase is not linear, it has two distinct components. The rate of increase is lower as compared to Scenario 1.

Fitted parameters:

μ_{sat}	0.065
b	55
k	5

Scenario 6

Normal force=11 tons, longitudinal velocity=80 km/hr, lubricant=new, surface wear=worn

The test was conducted with kingpin pressure/normal load at fifth wheel =11500 kg, at longitudinal velocity of 80 km/hr while giving small sinusoidal input. The lubrication is the same as in Scenario 2.

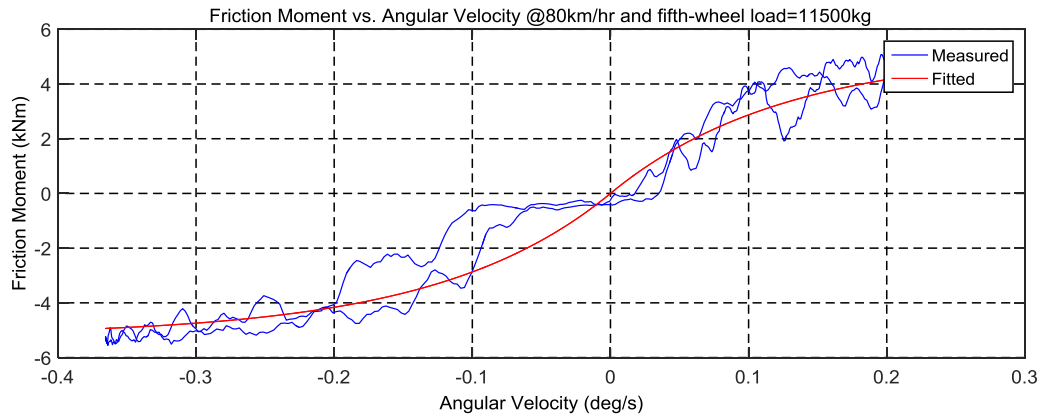


Figure B. 5 Friction moment vs. Angular velocity, fifth-wheel load=11500 kg

Observations:

From the figure, it can be seen that, the friction moment increases with velocity, reaching the maximum values of ± 5 kNm. The rate of increase is higher as compared to Scenario 2.

Fitted parameters:

μ_{sat}	0.117
b	5
k	8

Scenario 7

Normal force=16 tons, longitudinal velocity=80 km/hr, lubricant=new, surface wear=worn

The test was conducted with kingpin pressure/normal load at fifth wheel =16500 kg, at longitudinal velocity of 80 km/hr while giving small sinusoidal input. The lubrication is the same as in Scenario 3.

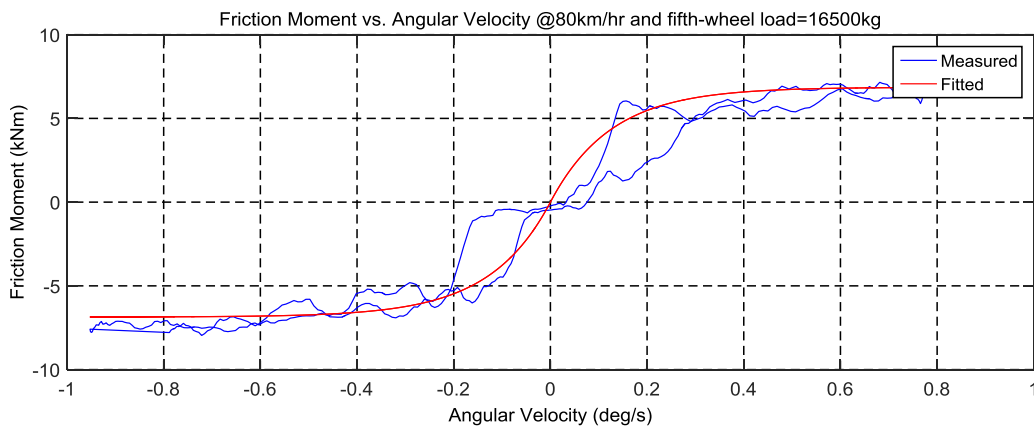


Figure B. 6 Friction moment vs. Angular velocity, fifth-wheel load=16500 kg

Observations:

From the figures, the friction moment increases with velocity, reaching the maximum values of ± 7 kNm. The increase is not linear, it has two distinct components. The first part is an exponential rise with velocity and the second part is a linear increment with velocity. The rate of increase is higher as compared to Scenario 3.

Fitted parameters:

μ_{sat}	0.12
-------------	------

b	5
k	8

Appendix C

Scenario 1

Normal force=9 tons, longitudinal velocity=10km/hr, lubricant=base, surface wear=base

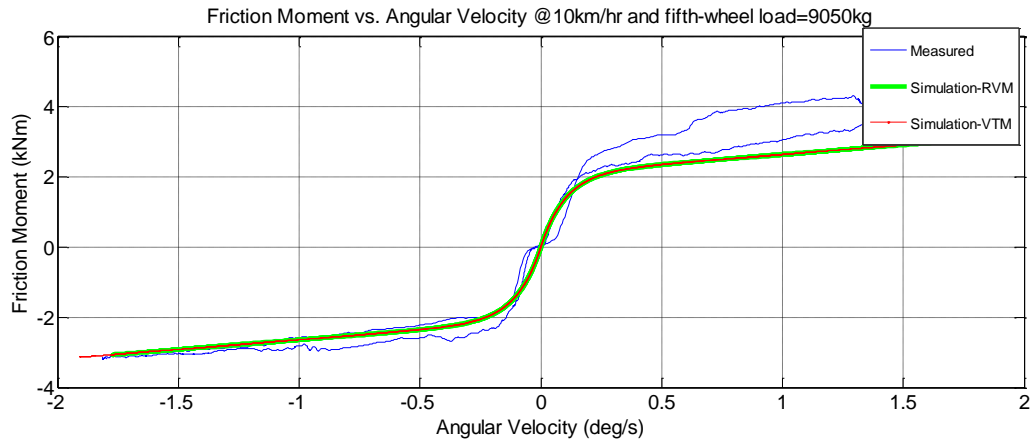


Figure C. 1 Friction moment vs. Angular velocity, fifth-wheel load=9050 kg

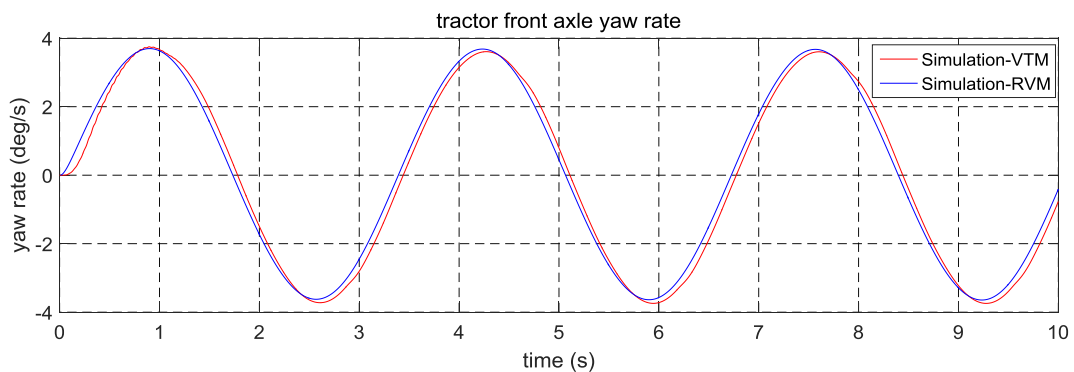


Figure C. 2 Tractor yaw rate, fifth-wheel load=9050

Scenario 3

Normal force=16 tons, longitudinal velocity=10 km/hr, lubricant=new, surface wear=worn

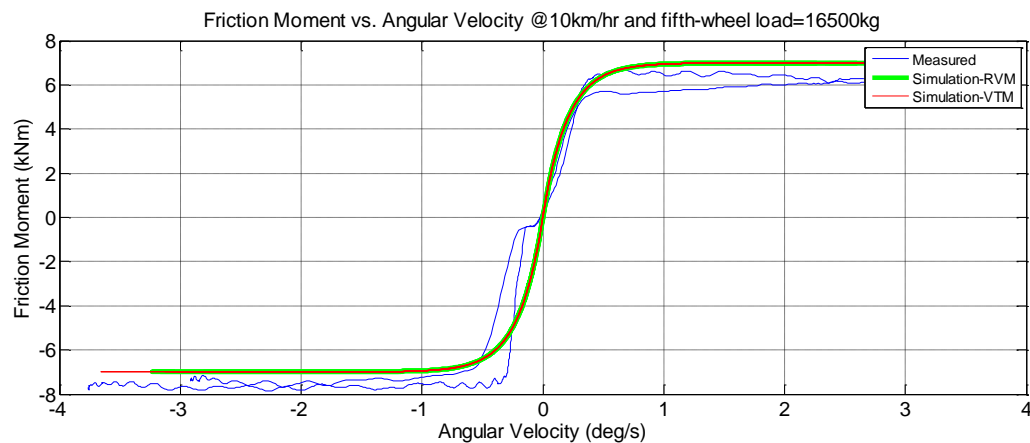


Figure C. 3 Friction moment vs. Angular velocity, fifth-wheel load=16500 kg

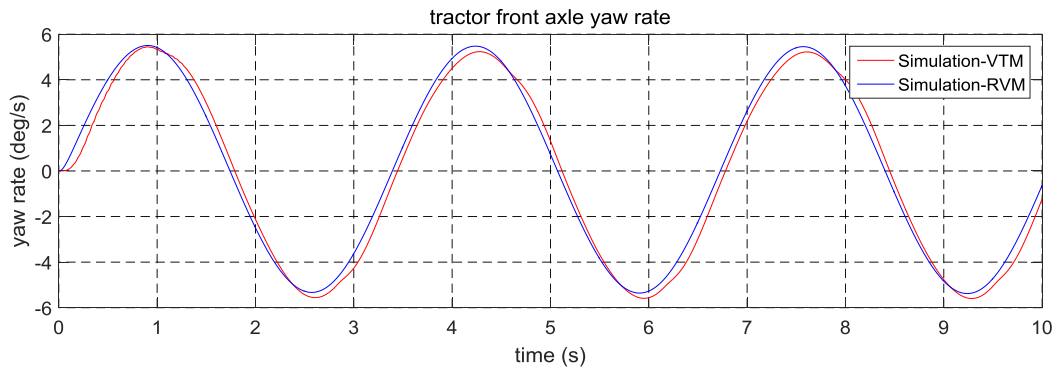


Figure C. 4 Tractor yaw rate, fifth-wheel load=16500 kg

Scenario 4

Normal force=9 tons, longitudinal velocity=10km/hr, lubricant=dry, surface wear=base

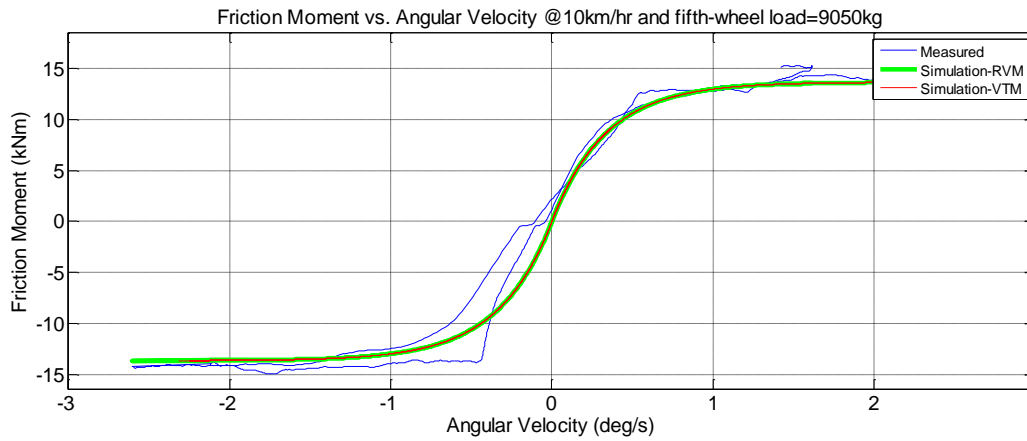


Figure C. 5 Friction moment vs. Angular velocity, fifth-wheel load=9050 kg, no lubrication

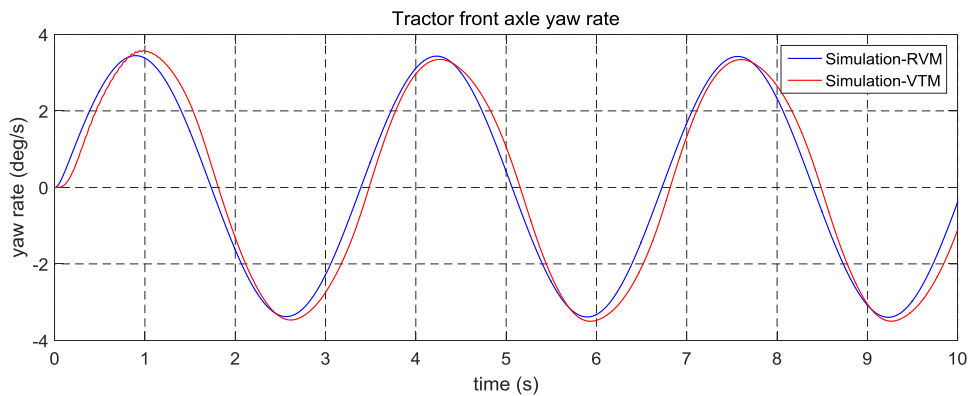


Figure C. 6 Tractor yaw rate, fifth-wheel load=9050 kg, no lubrication

Scenario 5

Normal force=9 tons, longitudinal velocity=80km/hr, lubricant=base, surface wear=base

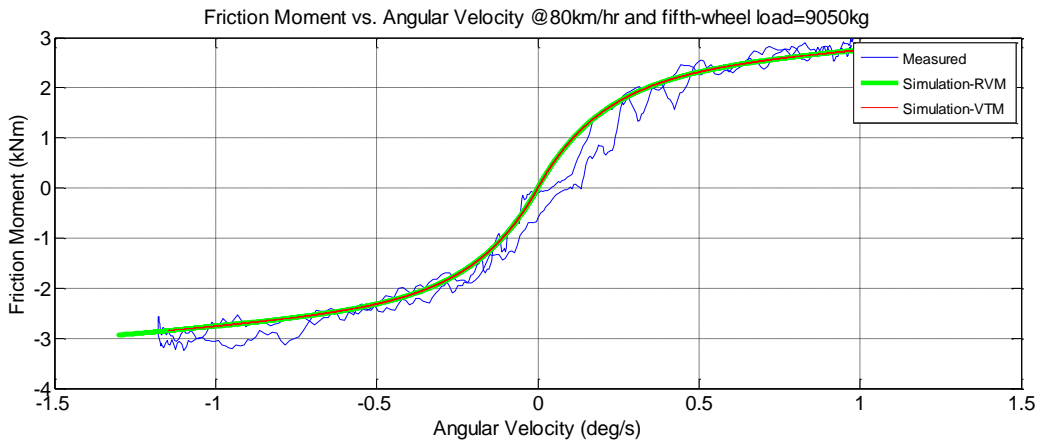


Figure C. 7 Friction moment vs. Angular velocity, fifth-wheel load=9050 kg

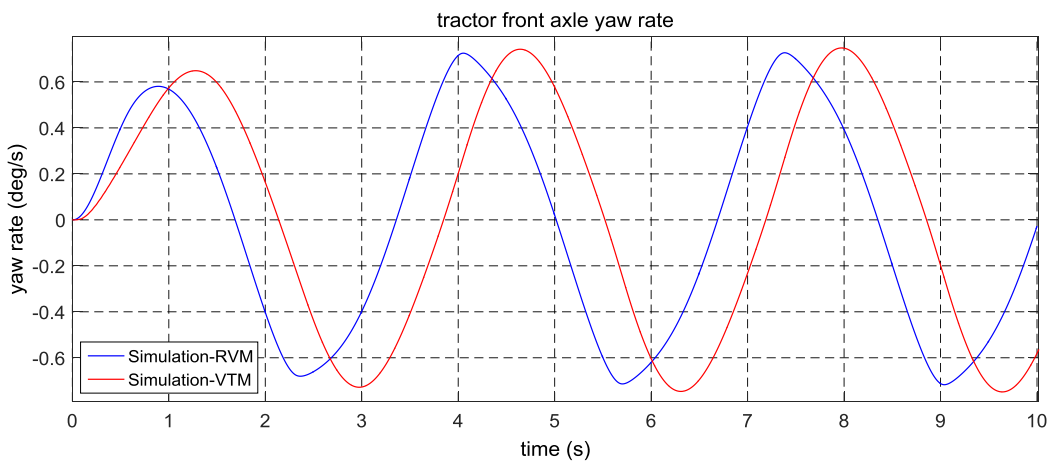


Figure C. 8 Tractor yaw rate, fifth-wheel load=16500 kg

Scenario 6

Normal force=11 tons, longitudinal velocity=80 km/hr, lubricant=new, surface wear=worn

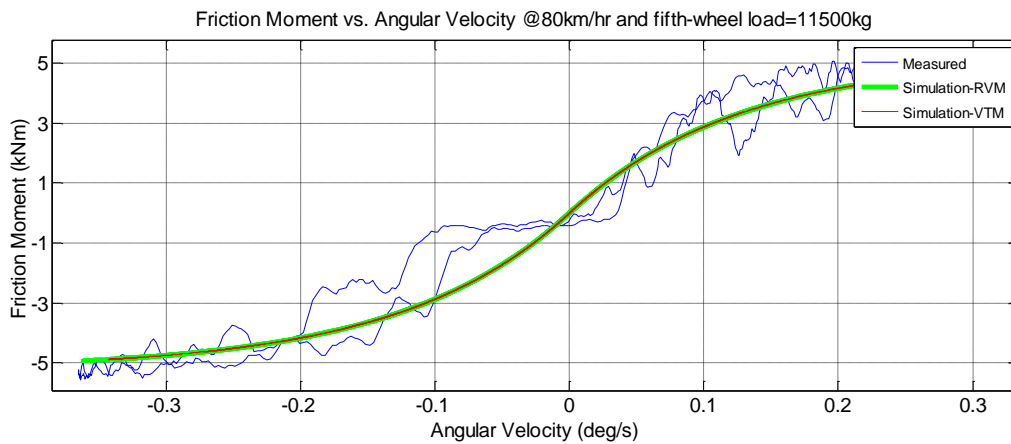
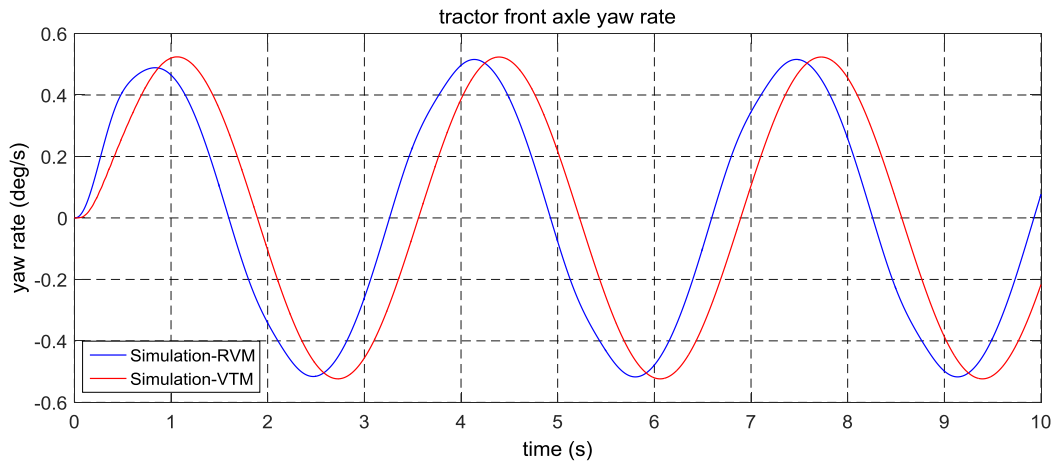


Figure C. 9 Friction moment vs. Angular velocity, fifth-wheel load=11500 kg



Scenario 7

Normal force=16 tons, longitudinal velocity=80 km/hr, lubricant=new, surface wear=worn

